Scattering Phase Shift of Electrons and Its Applications in Mesoscopic Systems

Thesis submitted for the degree of

Doctor of Philosophy (Sc.)

in **Physics (Theoretical)**

by

Kanchan Meena

Department of Physics

University of Calcutta

2024

Abstract

In this thesis, we studied important features of the quantum mechanical scattering phase shift of electrons in low-dimensional mesoscopic systems. The functional derivatives of the scattering phase shift define local objects in the hierarchy of density of states in quantum systems. Some recent experiments have made the subject very topical. A lot of information can be obtained from such measured phase shifts that can have wide-scale applications.

The theoretical concept of local partial density of states has been given a firm physical foundation. It is revealed that local partial density of states appear in several experimental situations of a three-terminal mesoscopic setup. In this three-terminal setup, two of the leads are current carrying leads, while the third could be a lossy lead like an earthed lead or a voltage probe. Furthermore, the local partial density of states results in higher objects like injectivity and emissivity, which also have experimental signatures in these setups. Besides this, we cleared the conceptual issues associated with the negativity of the local partial density of states. We revealed that this negativity is physical as well and a consequence of processes in reverse time, which can also be revealed in the associated experiments. In establishing these, we coined the idea of a theoretical experiment in the sense that we can get the relevant quantum mechanical objects without using the axioms of quantum mechanics.

To further strengthen our philosophy, we took up a problem of tunneling current or time, which cannot be solved within the framework of quantum mechanics. For this problem, one uses the analyticity of the wave functions, completely ignoring the fact that such an analytic continuity does not respect the structure of Hilbert space. We exhibited that such tunneling currents can be again derived from the analyticity of wave functions without using the axioms of quantum mechanics, and this in fact agrees with the current of analytical continuation. The scattering phase shift and its universal behaviour are exploited for this purpose. The setup, 1D open Aharonov-Bohm ring in equilibrium, considered for this work has the added benefit that one can also conduct a practical experiment on it to confirm our results further. This setup bypasses the issues of quantum measurements under the barrier that has bogged this problem since the inception of quantum mechanics.

List of publications

This theis is based on following publications:

1. **Kanchan Meena** and P. Singha Deo,"Time-reversed states in barrier tunneling", Physica E, **149**, 115680 (2023).

2. **Kanchan Meena** and P. Singha Deo, "A Mechanism to attract Electrons", Adv Theo Comp Phy, **52**, 458 (2022).

3. **Kanchan Meena** and P. Singha Deo, "Multiple manifestations of negative local partial density states", AIP Proceedings, DAE Symposium (2023) (Accepted).

4. P. Singha Deo and **Kanchan Meena**, "A Reality: Time Travel in Mesoscopic Physics", Springer (in press).

5. **Kanchan Meena**, P. Singha Deo, and A. M. Jayannvar "Mesoscopic response: semi-classical versus quantum mechanics", Submitted to ArXiv (2021).

To My Family

Acknowledgements

Embarking on a PhD journey proved to be an exceptionally challenging and demanding endeavor for me. It demanded a substantial investment of time and effort, with a journey spanning from inception to completion, characterised by numerous obstacles and setbacks. The duration of this pursuit is notably extensive and arduous, involving rigorous academic research, the intricacies of writing, and defending one's work or dissertation. These components collectively contribute to the complexity and difficulty inherent in the process.

I am profoundly grateful to my eldest brother, Gajendra Singh, whose insistence persuaded me to pursue my M.Sc. in physics. My parents have been unwavering pillars of support, consistently acknowledging even my smallest achievements. My mother, Heera Devi, inspires me every day with her dedication to our family, serving as a constant motivation for my research and responsibilities. My father, Ramkaran Meena, supports and motivates me in every decision, always encouraging me to strive for success.

My siblings, Dimpi Bhaiya, Lalita Di, Baby Di, and Pintu (my younger brother), each provided their unique form of support, always standing by me in their individual ways. Completing my thesis would have been impossible without the nurturing support of my parents, siblings, friends, teachers and guide. Their collective encouragement propelled me forward during the most challenging phases of my academic journey.

During my higher secondary schooling, Bhawani Sharma, my physics teacher, sparked my interest in the subject of physics. Among my classmates were Rachana, the sisters Kavita and Savita, Shivani Sharma, Diksha, Tanisha, Rakashanda, Anjali, Rekha, Jyoti, and Nidhi. We had a supportive environment where we appreciated each other's successes in various exams.

During my post-graduation, Rakesh Dhaka Sir and Poonam Chaudhary Ma'am played a pivotal role by guiding us and motivating us to pursue a PhD degree.

I am immensely grateful to my M.Sc. friends: Madhu Yadav, Kiran, Himani, Hemant Dhaka, Parag Jain, Veerpal, Ankita Jangid, Jyoti Saini, Shweta, and Shivani Kumawat. Our time together was truly wonderful. They were always there for me throughout my PhD journey whenever I needed them. I especially want to express my heartfelt gratitude to Jyoti Saini, Shivani, Himani and Ankita who stood by me through thick and thin. Their presence made a significant difference, and I am deeply thankful for them friendship and kindness.

I began my PhD program in August 2019 and continued my research under the guidance of Prof. Prosenjit Singha Deo. I would like to express my sincere gratitude and utmost respect to my supervisor. His ongoing discussions expanded my thinking in various directions on different problems. His consistent availability also instilled punctuality in me.

I want to express my gratitude to Prof. Sanjay Chaudhary for granting me another interview opportunity in condensed matter theory after my initial interview in theoretical physics. Additionally, I would like to thank Prof. Priya Mahadevan for her friendly demeanor and encouragement during the interview and after joining the institute in the condensed matter theory. Her support helped me overcome nervousness and present myself effectively in interviews.

Prof. Manoranjan Kumar was happy to see someone from Rajasthan in West Bengal.

However, I couldn't shake off feelings of anxiety and loneliness in this new environment. Everything seemed unfamiliar – the food, the language, and the culture. Being a pure vegetarian and not knowing Bangla added to my discomfort.

Fortunately, the companionship of two fellow IPhD students from Rajasthan, Varsha Jangid and Ankita, helped ease my transition. With their guidance, I gradually adapted to my surroundings. Varsha, in particular, provided invaluable assistance in navigating the local cuisine and language barriers. Additionally, Ishita Jana, another batchmate of theirs, was always ready to lend a helping hand.

I wish to extend my heartfelt gratitude to my dissertation committee members, Prof. Prasanta Panigrahi, Prof. Priya Mahadevan, and Prof. Manoranjan Kumar. Their invaluable insights, thoughtful suggestions, and scholarly contributions have greatly enhanced the quality and depth of my dissertation.

I would like to express my sincere gratitude to the S. N. Bose National Centre for Basic Sciences, including the academic administration, ground staff, and canteen members. Their collective efforts provided me with an environment conducive to completing my PhD.

After the first wave of COVID-19, I had the pleasure of meeting more people at the institute. Sumanti Patra, a senior, along with Ishita Jana and Shinjini Paul, juniors, made my PhD journey incredibly enjoyable. Unfortunately, during my third year of the PhD, I encountered an accident which caused me to overlook a significant phase. However, during this challenging time, all of them extended their support and care towards me. They took great care of my medications, dressings, and food requirements, ensuring my well-being was prioritized. Their kindness and assistance during that period were truly invaluable.

I am deeply grateful to the campus security and Imadul Bhaiya (senior) for their assistance during my COVID-19 quarantine period. When my RT-PCR report came positive, they ensured I had access to medications and other essentials, which was immensely helpful during that challenging time. In particular, I want to extend my heartfelt thanks to Imadul Bhaiya for providing me with meals throughout the days of quarantine. I am truly thankful for his generosity.

I would also like to express my gratitude to my friends, including juniors Sakshi Chaudhary and Ajay Sharma, as well as seniors Sumona Di and Atul Bhaiya, for their presence with me during PhD. I am grateful to Sumona Di for sharing her own PhD journey experiences, which provided invaluable mental strength during my final years in the program. I also want to thank Atul Bhaiya for his valuable knowledge and assistance, which greatly helped with tasks like writing documentation.

I am deeply thankful to Prof. Parongama Sen for their invaluable assistance in completing the paper work for my Pre-Thesis talk and thesis submission. I would like to extend my gratitude to Prof. Guruprasad Kar and Debnarayan Jana for their recognition and appreciation of my work in Pre-Thesis Talk.

I would also like to thanks to my batchmate, Sreya Pal, for her assistance in completing the paperwork procedures at Calcutta University and within the institute.

I would like to express my gratitude to the CSIR-JRF fellowship and the financial assistance provided by the institute. Their support has been instrumental in facilitating my research experiences, and I am deeply appreciative of the opportunities they have afforded me.

I would like to extend my thanks to all the organizing committees of conferences and seminars, which are listed below, that have provided me with opportunities to present

my work. I am thankful for the platforms they have offered me to share my research findings and engage with fellow scholars.

1. **International Conference on Advances in Chemical and Material Sciences (ACMS-2022)**, Indian Institute of Chemical Engineers, Kolkata, 700032, India, April 14 - 16, (Virtual mode).

2. **Annual Conference on Quantum Condensed Matter (QMAT- 2022)**, Indian Institute of Technology, Kanpur, India, September 18 - 22, (in person).

3. **PRL Conference on Condensed Matter Physics (PRL CCMP - 2023)**, PRL, Ahemdabad, India, February 06 - 08, (in person).

4. **67th DAE Solid State Physics Symposium (DAE SSMP - 2023)**, GITAM University, Visakhapatnam, India, AIP Proceedings: "Multiple manifestations of negative local partial density of states, December 20 - 24, (in person).

IN MESOSCOPIC PHYSICS, YOU REALLY NEED TO BUILD UP INTITUTION BECAUSE IT IS NOT THE WORLD YOU KNOW

–CARLO BEENAKKER

CONTENTS

CHAPTER 1

INTRODUCTION

Around 1960s, new technologies were being developed and specially the chip fabrication industries were highly focused on making smaller and smaller devices with high accuracy and control. In 1965, Gordon Moore noticed that the number of transistors on a microchip doubles approximately every two years which is known as Moore's law [1]. Naturally, it means that at some point, devices will go into the quantum regime. In that regime, currently used classical techniques and methods will break down. As devices became smaller and approached the nanoscale, the behaviour of electrons exhibited wave-particle duality and quantum interference effects. In material physics, new sample fabrication techniques (Section 2.1) [2] within the quantum regime and low temperature cryogenics have evolved to such an extent, that with their help, one can conduct physics experiments [3, 4] with samples like quantum rings, quantum dots, point contacts, etc. that are as small as 10 to 100 microns. Such samples have novel features that lead to the development of the subject of mesoscopic physics [5, 6]. Firstly, the equation of motion for electrons in these systems is the Schrödinger equation. This essentially requires that the inelastic mean free path or phase-breaking length of the electrons be comparable with the sample size [2]. At low temperatures, typically milli Kelvin, the inelastic mean free path is greatly increased. Secondly, the relevant length scales that determine the physics of these systems, like the elastic mean free path, or field penetration length, or any correlation length, etc., become comparable to the sample dimensions. As a result of this, the artificially created competing length scales lead to new and novel phenomena in these systems. This has opened up renewed interest in addressing two central questions in physics. First, how can we make sense of quantum mechanics, and how does it cross over to classical behaviour as the sample size grows? Second, is it possible to control the quantum fluctuations and use the novel properties of these systems to build devices? One very intriguing feature of quantum systems is the linear superposition of states, which is often stated in the form of Schrödinger's cat paradox. It essentially means that a

quantum cat can be dead and alive at the same time, which is difficult to accept in reality. Another intriguing feature is that quantum mechanics can allow non-local behaviour, a good example for which is the Aharonov-Bohm (AB) effect [7] that will be discussed in Section 3.1. In this regard, this thesis will firmly establish a local object in quantum mechanics, namely the local partial density of states (LPDOS) [8, 9], which will appear in present-day mesoscopic experiments [10, 11, 12] although the axiomatic framework of quantum mechanics denies its existence. These local objects can also be summed up in the classical sense to lead to the correct density of states that can be obtained from quantum mechanics, and hence the notion of these local states can co-exist with the rest of quantum mechanics. There is a well defined unique time spent by electrons in these local states and not that the electron is partly in a local state and partly somewhere else at the same time. Time spent at local states can be summed up in the classical sense to find the total time spent. This total time spent is also consistent with relativity and can co-exist with it, opening up the possibility of uniting quantum mechanics and relativity at low energies rather than the usual notion that one should try for this unification at high energies [9].

Devices like the present-day computer, mobile phone, or any device that requires an electronic circuit use the law of large numbers. This essentially means that current, magnetisation, or any response of a sample is due to a statistically large number of carriers, say electrons, typically of the order of the Avogadro number. So resistance, capacitance, or magnetisation is an average response produced by the carriers, the fluctuations are of the order $\frac{1}{\sqrt{N}}$, as we have seen in statistical mechanics text books [13], and they can be ignored. This creates an upper limit on what we can achieve technologically. We can break this barrier by using mesoscopic principles wherein a few electrons can be used to create currents and responses that will make the devices fast and easy to manage because of low energy dissipation [9]. Thus, we will not use averages but fluctuations will be quantum in nature, which will make our devices very unreliable. In this thesis, we will show how evanescent modes can be used to solve this problem for which one has to address the question of what exactly is current and magnetisation due to evanescent modes [12].

The primary development in fabrication technique that has enabled the initial quantum transport experiments [3, 4] was the two-dimensional electron gas (2DEG) which is described in the book by S. Datta [2]. One can apply lithography or etching techniques on this 2D film to curve out geometries like an isolated ring or a sample connected to electron reservoirs. The equation of motion for electrons in such systems is just the single particle Schrödinger equation wherein the bare mass of the electrons are replaced by an effective mass. This effective mass incorporates the effect of other interactions that may be present in the system. Through out this thesis, we will focus on such realistic

samples and hence when we talk of time travel or local density of states in these systems, then all these effects can be realized in the laboratory. It is to be noted that one can also make such samples with metals and crystalline semiconductors, but the physics of those systems will be different in terms of theory. For example, in gold and copper rings the electrons are mostly diffusive and may not be studied using the effective mass single particle Schrödinger equation. The book by S. Datta, 1995 [2] is mainly written for engineering students intended to numerically apply Landauer's two probe, three probe and four probe conductance formulas wherein one starts from a Hermitian Hamiltonian or a scattering matrix. Such an application oriented book will rely on representing the Hamiltonian in the form of a matrix and apply recursive techniques [14]. So this approach will not lead to fundamental aspects of quantum mechanics in a straight forward approach. One has to look for clever ways of modeling and incorporating the related effects.

Modern day science is driven by giants of the past. Many people enriched physics thinking independently from different points of view. The theory of quantum mechanics gives abstract quantities that are difficult to relate to the nature (or real world). These abstract quantities are Hilbert space, wave function, density matrix etc. Question is how to extract information from quantum mechanics, in order to define probability, position, momentum, energy, current density etc. These physical obervables are well defined in quantum mechanics with expectation value of operators. Thereby, in quanum mechanics, to extract information from these observables locally is not possible. There were some more queries about observables like resistance, capacitance, inductance, time in quantum mechanics, etc. The correct theory for quantum mechanics was developed by von Neumann and others and beautifully explained in the YouTube lecture series by Frederic Schuller. Operators in quantum mechanics are not supposed to be Hermitian but are supposed to be self-adjoint. Throughout this thesis, we will stick to first quantisation, or, in other words, we will solve for the continuous energy or wave-vector of a scattered electron that is consistent with the von Neumann approach. It is known that for large crystalline systems the Hermitian Hamiltonian and diagonalization approaches are valid but at no point we are talking of such large systems with a periodic potential. It is possible that in some cases the continuum model can be mapped to a discrete model with a Hermitian Hamiltonian. For example, the effects of evanescent modes in a single channel quantum wire can be mapped to a tight binding stub [15] to give some aspects of the physics involved but this inspection is never done in the community. Thermodynamic properties of mesoscopic systems has been particularly ignored in Datta's book and so is the role of evanescent modes, that we believe leads to many new phenomena and will attract a lot of attention in the future. Like S. Datta, we will restrict to electronic properties only because phononic properties in mesoscopic systems are mostly done in analogy with electronic properties and have not yet reached a level of maturity to be presented

here in our opinion. Of course the role of phonons on electronic properties has been presented to some extent by S. Datta but that is again an alternate view to what will be also discussed here.

In quantum mechanics, time is regarded as a parameter unlike any other observables which are defined through expectation values of some operator in abstract Hilber-space. Then defficulty arrises, how to define time in quantum mechanics. For that, Wigner [16, 17] and Smith [18] approached delay time and dwell time respectively. Wigner was a pioneer to provide an approximate notion of delay time in quantum mechanics i.e., Wigner Delay Time (WDT). Wigner time is defined as the derivative of the phase of the electron's wave function with respect to the electron's energy. WDT is obtained from the behaviour of a time dependent wave packet analysed in terms of Fourier components which are the stationary state solutions of the time independent Schrödinger equation. It therefore has an explicit reference to propagation of wave packet in time. Smith gave an average time spent in a region by an ensemble of quantum particles i.e., Smith Dwell Time (SDT). SDT can be defined in quantum regime as well as in semi-classical regime as it relies on the undisputable fact that $|\psi|^2$ is Copenhagen probability. Recently, another theory got attention to address the problem of time in quantum mechanics through the idea of precession of spin. This time is Larmor Precession Time (LPT) which is given by Larmor clock theory [19, 20, 21, 22]. Details of Larmor clock is discussed in Chapter 4. LPT is obtained from stationary states or monochromatic plane waves without any reference to the time dependent Schrödinger equation. LPT and WDT are interpreted as traversal time because both can be consistent with the number of intermediate states through which a quantum particle is traversed or propagated in time [23].

Consistency among all these theories is the touchstone of their correctness. However, there are inconsistencies among SDT, WDT and LPT. SDT and WDT consistencies could be seen in semi-classical regime but not in quantum or low energy regime. LPT is consistent with SDT in all regimes but not with WDT. WDT can be calculated for undispersed wave packet using stationary phase approximations in semi-classical regime that will automatically fail in quantum regime. One sometimes encounter negative WDT in quantum regime and it is not clear wheather it is because of dispersion of wave packet or failure of stationary phase approximations [9]. SDT is not related to individual electron's delay time. LPT uses a picture of the precession of spin of electron like a classical precession. Quantum angular momentum has its classical counterpart but quantum spin does not. In [22], the expectation value of angular displacement of spin divided by classical Larmor frequency is LPT that agrees numerically with SDT in all regimes but not with WDT in quantum regime. Thus, "Johny come lately" LPT also does not solve the problem of time in quantum mechanics. Altough it is mathematically very sound but difficult to interpret physically, because there is no physical picture of precession of

quantum spin. It comes from time independent Schrödinger equation with no reference to propagation and can become negative too. For these reasons, none of the above time candidates could solve the problem of time in quantum mechanics. Larmor clock classifies these local objects in the hierarchy of density of states, among them LPT is the lowest in hierarchy [8, 9, 24, 25, 26]. Thereby, another conceptual problem with LPT is that it gives the possibility of local variables in quantum mechanics. Thus, neither negative time problem was solved nor interpretation of local objects was given.

Local objects of the hierarchy are determined by functional derivatives of scattering matrix elements or phase shift [8, 9, 24, 25, 26]. As we had raised question that how to extract information from abstract quantities in quantum mechanics. Similarly, one may ask that how does this phase of an electron help to extract information in mesoscopic [5, 6] systems. However, conductance measurements are sufficient to characterise the electronic transport properties in devices wherein transport occurs incoherently. Mesoscopic systems are the systems with the dimensions of less than inelastic scattering length. Thereby, electron's wave behaviour does matter in these systems as the phase of electron's wave function changes as it passes through the system. Mesoscopic systems behave quantum mechanically because they preserve coherence, which gives them intriguing and unique physical properties. For low-dimensional systems with conductance measurements, phase measurements are also required to characterise the electronic transport properties completely. Electrons quantum mechanical phase changes can be measured from Aharonov-Bohm oscillations [7] etc. But Aharonov-Bohm oscillations restrict to phase of oscillations to be either 0 or π. While [27] reports that abrupt jumps are possible in between allowed phase values of an electron [7]. These abrupt jumps are the results of the measurement of the phase shift of an electron. Phase changes leads to various phenomena like Aharonov-Bohm oscillations [7], conductance quantisation [28], and others, and has significant implications on transport properties. Thus, phase coherence plays an significant role in characterising the electronic transport properties of mesoscopic systems. With this new result of measuring phase shift in laboratory [27, 29], we have revived the Larmor clock theory in mesoscopic systems. Markus Buttiker [8] elaborated a hierarchy of DOS using Larmor clock formalism that builds upto the DOS and applied to mesoscopic systems. Larmor clock theory uses purely the concept of spin precession of an electron and provides this hierarchy. This hierarchy is novel and different from what we study in condensed matter systems. Local version of DOS hierarchy's is given by [21]. We will express all these local objects in terms of scattering phase shift of an electron in Chapter 4.

Both times WDT and LPT are defined in terms of scattering phase shift of electron. Traversal time in quantum mechanics like WDT and LPT is analogous to traversal time in classical mechanics. Classically, one has to go from initial point to final point through

intermediate points while in quantum mechanics one has to go from initial state to final state through the intermediate states [23]. Most adverse factor in the analysis of WDT is the fact that in low energy or quantum regime wave packets vigorously disperse. Our predecessors have shown that Fano resonance [30, 31, 32] can be obtained in quantum regime and can be used to create a non-dispersive wave packet in low energy regime [9, 33] . Such non-dispersive wave packet will satisfy stationary phase approximation in semi-classical regime as well as in quantum regime. So using this paradigm one can extend the analysis of WDT to low energy regime. LPT can be justified by using Burgers circuit on the Fourier components of these non-dispersive wave packets without any reference to spin precession. Thereby, WDT and LPT become consistent in quantum regime. Thus, SDT becomes also consistent with WDT. Consistency of all these three times confirm intermediate states or local partial density of states (LPDOS) through which an electron traverses. Negative time is physically interpreted as non-dispersive wave packet propagating in time carrying a signal back in time [9, 33, 34]. My thesis targets individual object of the hierarchy of density of states (DOS) and make experimental predictions for it [10, 11, 12]. In some cases, it can be verified against parallel theories and first principles.

We take the view that mesoscopic physics is an intermediate regime between microscopic and macroscopic physics. The term "mesoscopic" does indeed come from the Greek word "meso", which means "intermediate" or "middle". Underlying assumption is that quantum theory is the fundamental theory of nature and classicality emerges. Kubo formula [35] provides quantum resistance as quantum corrections over classical formula. One should not usually see a quantum formula as correction over a classical formula. For instance, a quantum particle trajectory can not be considered as a correction over the classical trajectory. And hence, one can not consider quantum electrodynamics as a correction over classical electrodynamics. Because fundamentaly classical and quantum mechanics are at loggerheads.

Mesoscopic physics establishes a sharp demarcation of classical and quantum mechanics. Macroscopic physics widely covers classical electrodynamics, classical thermodynamics, classical statistical mechanics, Newtonian mechanics, STR, GTR etc. which comes under the banner of classical physics. Microscopic physics covers systems that follow from quantum electrodynamics, quantum mechanics, quantum field theory etc. that comes under quantum mechanics. The phenomena of mesoscopic regime can be understood with quantum theory that says equation of motion is Schrödinger equation. However, in mesoscopic systems, fields are classical and electrons are quantum particles. The size of these mesoscopic systems ($\approx$ 10-100 nm) is larger than the atomic size (.1 - .5 nm). This length scale is significantly influenced by temperature and magnetic field. The world of mesoscopic physics has emerged as a frontier research area. Mesoscopic

physics not only upgrade our fundamental understanding of science but plays an efficient role in novel technological developments as well. Discoveries and results in mesoscopic physics got attention of scientific community by the fact that the results go beyond our intuitive thinking. Mesoscopic phenomena such as leads, FSR (Friedel Sum Rule) [36] and especially the hierarchy of density of states (DOS) consists local partial density of states (LPDOS), local density of states (LDOS), partial density of states (PDOS), injectivity, etc. introduce us to local objects in quantum mechanics [9, 10, 11]. All these physical phenomena is elaborated in terms of scattering phase shift. With non-interacting systems new phenomena like quenching Hall resistance [37, 38], $\frac{\Phi_0}{2}$ oscillations [39], persistent current [2, 40, 41, 42], magnetisation of a Aharonov-Bohm systems, breakdown the even-odd parity effect, π phase slip [9], universal conductance fluctuations [28], etc. are found. One can generate equilibrium current in mesoscopic systems [41, 42] called persistent current, perpetual electric current, which does not require any external power source or battery. In 1980s, one of the most prominent experiment was done within nano scale i.e., quantum Hall effect [37, 43]. Details of this experiment can be found in [2]. At high magnetic fields the Hall resistance has been observed to be quantised in units of $\frac{h}{2e_0^2}$ with an accuracy in parts per billion. In quantum Hall regime, conductors with the dimensions of millimetre show quantum behaviour.

Rolf Landauer in 1957 [44, 45, 46] thought purely from quantum mechanical point of view in terms of the behaviour of electrons in small-scale systems. For instance, Landauer formula [2, 44] can be derived for an isolated atom or molecule and it can be probed in the laboratory. Landauer theory predictions have been verified to an accuracy of one part in a billion, far more accurate than solving any other quantum Hamiltonian systems except the phenomena of Lamb shift. Landauer recognised that the transmission probabilities of electronic states played a crucial role in determining conductance. He established a connection between quantum transmission probability and the resistance of a pure quantum ensemble. Landauer and others developed a theoretical framework that can accurately describe electronic transport in mesoscopic systems. His work led to the formulation of the Landauer-Büttiker formalism [44, 45, 46, 47, 48, 49] developed in 1980s which provides a quantum mechanical description of electronic transport and has been influential in developing the field of mesoscopic physics. Thus, Landauer conductance, Smith dwell time (SDT) and Wigner delay time (WDT) often provide the basic structure that allows to probe into transport properties of electrons in mesoscopic regime. For mesoscopic systems one can not give material specific entities like resistivity, permeability, susceptibility and dielectric constant etc. which can be defined by quantum statistical mechanics with ensemble averaging. Classically analogous variables are viscosity, tension, elasticity, and friction etc. This thesis is restricted to scale determined by single particle coherence length of electrons and in-elastic coherence destroys coher-

ence. The single-particle coherence length is a measure of how far a quantum particle can propagate coherently without undergoing significant phase changes or decoherence.

The density of states (DOS) is a physical variable that plays a fundamental and crucial role to understand condensed matter systems [50, 51]. One can understand DOS, physically and mathematically, from the definition of Green's function. The imaginary part of the Green's function [2] yields the density of states (DOS) and contributes to the time-dependent component, linking it to the system's evolution via Fourier transforms. Larmor clock theory provides us a series of local objects called as hierarchy of density of states (DOS) [9]. Quite counter-intitutively local partial density of states (LPDOS) or ρ_{lpd} is a local object defined with respect to the leads and help us derive a hierarchy of density of states (DOS) like partial density of states (PDOS) or ρ_{pd}, local density of states (LDOS) or ρ_{ld}, injectivity (ρ_i), emissivity (ρ_e), etc., see Chapter 4. By adding and integrating partial DOS over lead indices and sample region, one can get DOS which suggests presence of local variables in quantum mechanics. To calculate these quantities we need to solve a quantum mechanical electron scattering problem [52] for the scattering amplitude and the phase shift. Larmor clock uses the analyticity of scattering matrix elements. We put LPDOS on firm mathematical ground from which a clear understanding of time travel emerges that is consistent with quantum mechanics as well as relativity. These local entities with negativity are further analysed with Burgers circuit, Argand diagram, loops, sub loops and Fano resonance in [9, 33, 34]. It is known that the resonances in the mesoscopic systems connected to leads will be mostly Fano resonances and scattering phase shifts at Fano resonances is very special leading to these rich diversity of physical phenomena [53, 54, 55, 56, 57]. And as we discussed that in 1997, R. Schuter [27] and in 2004, K. Kobayashi [29] measurred phase of an electron wave function with the interference effects which is an important achievement in order to define negativity of local variables in quantum systems like mesoscopic systems. Before these experiments, PSD [9] also showed that a particular kind of phase slips in closed quantum ring that breaks parity effect emplying its physical manifestation. Following Legget's conjucture he showed that this phase is different from Aharonov-Bohm phase, phase due to fermion anti-symmetry or due to change of propagation [9, 15].

One of the most mysterious aspects of quantum physics is the existence of evanescent modes, states under the barrier, in tunnling problem. There are issues about whether propagation occurs under the barrier at all, as evidenced by the Hartman effect-like phenomena [58, 59, 60], which reveals that a tunneling particle can exit the barrier before entering it. Evanescent states do not form wave packet and therefore group velocity is not defined. This raises questions about whether propagation occurs under the barrier at all. Also, wheather the hyperbolic wave functions under the barrier are elements of Hilbert space is an unsolved problem. One can address this problem with the help of

physical clocks like Larmor clock and Wigner delay time. Larmor clock theory helps us to establish theoretical validity of tunneling current and freedom to go beyond the axioms of quantum mechanics for the verification of propagation of current under the barrier as well as density of states. In this work [12], we target current under the barrier and theoretically settle its existence. We also propose a experimental mesoscopic setup for it varification, see Chapter 7.

In this thesis, we primarily focus on studying non-interacting open mesoscopic systems that are connected to the leads. With the help of the Larmor clock theory, we make experimental predictions for local objects of hierarchy [10, 11, 12]. In order to describe these objets, we find the scattering amplitude and scattering phase shift in a quantum mechanical electron scattering problem. We further verify the negativity of local partial density of states (LPDOS) in presence of Fano resonance, determined by π phase shift. These negative local partial density of states (NLPDOS) shows the possibility of going electrons back in time [9, 10, 11, 33, 34]. The theoretical validity of tunneling current, confirmation of the propagation of current under the barrier and DOS for evanescent states are established by asymptotic theory by surpassing the axioms of quantum mechanics. Thus, one can establish local objects in quantum systems without using quantum mechanical theory which can be seen as a theoretical experiment. This thesis seeks to observe negative local partial density of states (NLPDOS), tunneling current, DOS for evanescent states through experiments [11] and thereby indirect evidence of time travel [10, 12].

Plan of the thesis

The thesis is organized as follows:

- In Chapter 2, the principles and procedure for sample fabrication of two-dimensional electron gas (2DEG) are presented. This chapter will help us to gain the fundamental concepts such as free electron theory of 2DEG, Landauer formula, etc. in small-structured devices.

- In Chapter 3, the open mesoscopic systems will be thoroughly discussed. There will be a detailed discussion on the Aharonov-Bohm effect, transport current, magnetisation of mesoscopic systems, and inclusion of magnetic field in the electron wave function of mesoscopic systems, etc.

- In Chapter 4, the Larmor clock theory will be used to elaborate all local objects in terms of scattering phase shift of the density of states (DOS) hierarchy.

- In Chapter 5, I will discuss Fano resonance in realistic mesoscopic systems. A detailed calculation of scattering in quasi-1D will also be discussed. A brief discussion on Burgers circuit will also discussed. The square well potential in 1D will discussed as well. Together, a multichannel case of delta function potential will covered in quasi-1D.

- In Chapter 6, I will take into consideration a few experimental configurations that will enable us to establish the local objects of the hierarchy of DOS, confirm the negativity of local partial DOS, and thereby time travel.

- In Chapter 7, I shall demonstrate a mesoscopic setup that clarifies the issue of existence of tunneling current under the barrier. The Larmor clock approach will be validated in this setup with quantum mechanical theory which can be seen as a theoretical experiment. Experimentally, magnetodevices can also be used to measure the magnetisation in the laboratory.

- In Chapter 8, I will be concluding my work and chapters of the thesis at the end.

- Additional calculations given in a Appendix A.

CHAPTER 2

MESOSCOPIC DEVICES

Since the 1980s, semiconductor technology has advanced, enabling the creation of miniature heterostructures. One of the essential structures that enabled the initial quantum transport experiments [3, 4] was the two-dimensional electron gas (2DEG) that develops at the interface between an intrinsic i-GaAs substrate and a doped or extrinsic n-AlGaAs barrier. One can apply lithography or etching techniques on this 2D film to curve out geometries like an isolated ring or a sample connected to electron reservoirs. The equation of motion for electrons in such systems is the single particle Schrödinger equation wherein the bare mass of the electrons are replaced by an effective mass. This effective mass incorporates the effect of other interactions that may be present in the system [2].

A detailed explanation of the two-dimensional electron gas (2DEG) sample fabrication technique is provided in Section 2.1. I cover an effective mass equation for a single band, an effective mass approximation, the E-k dispersion relation, bands and sub-bands, etc. within free electron theory in Section 2.2. I comment on the Landauer approach for mesoscopic systems with the effects of reservoir and also discussed axioms of quantum statistical ensemble in Section 2.3.

2.1 Fabrication of two-dimensional electron gas

During 1980s, physicist were able to fabricate artificial samples or structures with dimensions as small as a few hundred angstroms. Many experiments were conducted in mesoscopic physics with heterojunctions of group III-V semiconductors such as intrinsic i-GaAs and extrinsic n-AlGaAs. The first experiment was done by B. J. van Wees in 1988 [3] and later D. A. Wharam [4] with the heterostructure of 2DEG of GaAs-AlGaAs which is a low-dimensional system. This low-dimensional system is referred as mesoscopic

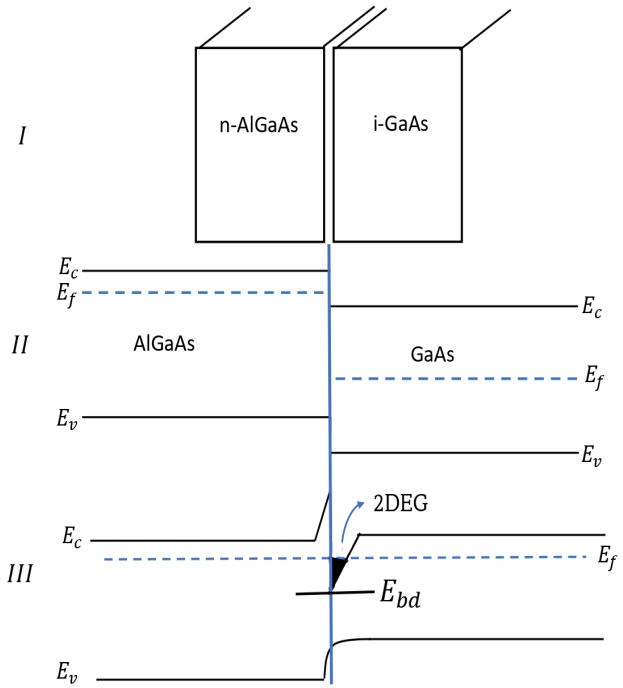

Figure 2.1: Mechanism of 2DEG formation. I: Heterojunction of AlGaAs and GaAs. AlGaAs is n-type semiconductor doped with positive dopant ions. GaAs has equal number of holes and electrons. II: Band structure before charge transfer. III: Band structure after lattice matching and charge transfer. A deep rift is formed towards intrinsic semiconductor where the Fermi level is within the band gap. This well is filled with electrons that are trapped, thus forming a 2DEG. E_{bd} is the band bottom energy or band discontinuity energy.

system. It has been discussed in the textbook [2].

Both GaAs and AlGaAs are direct band gap semiconductors. This specific heterostructure has used an intrinsic (i) semiconductor, i-GaAs, and an extrinsic (n/p) semiconductor, n-AlGaAs. In n-type semiconductors, a group V element is added as an impurity to the pure or intrinsic semiconductor. Group V elements have an extra electron, making electrons the majority carriers in n-AlGaAs and holes the minority carriers. In intrinsic semiconductors, i-GaAs, the number of holes and electrons are equal. The reason for choosing these two semiconductors is that their lattice constants are the same, meaning that their crystal lattices have a similar arrangement. Lattice matching is crucial for the formation of the 2DEG.

The mechanism of the formation of a two-dimensional electron gas (2DEG) involves creating a heterostructure by bringing two semiconductor layers in contact with each other, as illustrated in figure 2.1. The semiconductor layers have similar electron densities and energy band structures, resulting in an confinement potential in the direction perpendicular to the electron propagation. The lattice matching of semiconductor layers and the energy gap between the conduction and valence bands of both semiconductors cause electrons to start spilling over from the electron-rich layer (n-AlGaAs) into the electron-deficient (i-GaAs) layer. The confinement potential traps the electrons in a nar-

row region and causes the energy bands to bend at the interface between the layers. The electrons are confined within narrow trapping region of confinement potential and can only move in the two directions parallel to the interface, as the transverse direction is restricted. At the interface of these two semiconductors, where electrons become trapped in the band gap of lattice-matching regions, they are referred to as a 2DEG.

The band diagram before and after lattice matching is shown in figure 2.1 I, II and III. In n-type semiconductors, the Fermi energy level, E_f, lies near or below the conduction band, E_c. This Fermi level is also known as the donor energy level. The Fermi energy level E_f in the intrinsic semiconductor lies at the middle of the conduction band, E_c, and the valence band, E_v. When GaAs and AlGaAs are brought into contact with each other, electrons start to move from the higher concentration region, AlGaAs, to the lower concentration region, GaAs. This movement of electrons leaves behind holes or positive dopant ions, which creates an electrostatic energy at the lattice matching sites. As the electrostatic energy increases, it reaches a point where electrons cannot cross over to the other side, and the system reaches an equilibrium. This trapping of electrons at the interface causes the energy bands to bend. A narrow well is developed at the interface wherein Fermi energy level is in the conduction band gap. Trapped electrons are confined by a transverse potential in the z-direction, allowing them to move freely only along the x and y-directions at the interface. This confined electron system is referred to as a 2DEG. It gives very high mobility of 2D conduction channel. 2DEG in GaAs is very special because extremely low scattering rates and high mobility have been achieved.

2.2 Free electron model

The free electron model [50, 51] for a two-dimensional electron gas (2DEG) [2] describes the behaviour of electrons confined to move in 2D plane, typically at the interface between two semiconductor layers. According to this model, electrons are considered as free particles that do not interact with the lattice or with other particles. Electrons in 2DEG behave as though they are free to travel in the other two dimensions while experiencing quantisation in the confinement direction.

Single band effective mass equation

In 2DEG heterostructure, current is carried by the electrons in the conduction band. Electron dynamics can be given by single electron effective mass equation [2]

$$\left[E_{bd} + \frac{p^2}{2m_0^*} + V(x,y,z)\right]\psi(x,y,z) = E\ \psi(x,y,z) \tag{2.1}$$

where, E_{bd} is the discontinuity energy of the band bottom, shown in figure 2.1. The quantity p^2 is the kinetic energy term defined by $(i\hbar\nabla)^2$ in absence of magnetic field. The quantity m_0^* is the effective mass of the electron and $V(x,y,z)$ is confinement potential energy. Electron is free to move in $x-y$ direction but confined in $z-$direction. In presence of magnetic field the same quantity p^2 is given by $(i\hbar\nabla + e_0A)^2$

$$\left[E_{bd} + \frac{(i\hbar\nabla + e_0A)^2}{2m_0^*} + V(x,y,z)\right]\psi(x,y,z) = E\ \psi(x,y,z) \tag{2.2}$$

Here, A is the vector potential. The lattice potential $U(\vec{r})$, which is periodic on atomic scale, does not appear explicitly in Eq.(2.1). Actually, effect of lattice potential is involved through the effective mass (m_0^*), which is spatially constant. Eq.(2.2) is satisfied by the plane waves and not Bloch waves.

Effective mass approximation

This approximation assumes that the behaviour of the charge carriers can be approximated by that of a free particle with a modified mass, known as the effective mass. For convenience, one can solve effective mass equation for 1D. A quantum wire (known as lead in mesoscopic systems) has finite height and width, while the length extends to $\pm\infty$, referred to as a quasi-1D quantum wire. The 1D quantum wire is an idealisation. The energy of a free electron is given by $E = \frac{\hbar^2k^2}{2m_0}$, k is the momentum of the particle and m_0 is the mass of a free electron. An electron moves in a periodic varying potential, $U(x)$, in a solid. Periodicity of varying potential = lattice constant, a. Therefore, $U(x) = U(x+Na)$, for 1D where $N = 0, \pm1, \pm2, \pm3$,... Now Schrödinger equation for periodically varying potential in 1D (Kronny-Penning model [50, 51]).

$$\frac{-\hbar^2}{2m_0}\nabla^2\psi(x)\ +\ U(x)\psi(x) = E\ \psi(x) \tag{2.3}$$

Here, $U(x)$ is periodic potential and E is the incident energy of electron. For 3D;

$$\frac{-\hbar^2}{2m_0}\ \nabla^2\ \psi(\vec{r}) + U(\vec{r})\ \psi(\vec{r}) = E\ \psi(\vec{r}) \tag{2.4}$$

BLOCH THEOREM [50, 51] suggests solution of this equation

$$\psi(\vec{r}) = U_K(\vec{r})\, e^{i\vec{K}\cdot\vec{r}} \tag{2.5}$$

This is similar to a plane wave solution as it is valid for all $\vec{r}$. The dispersion relation as shown in figure 2.3 within a band is also similar to a plane wave. The difference in slope of the dr can be accounted for by $m_0 \to m_0^*$. This m_0^* is known as effective mass. $\vec{K}$ is

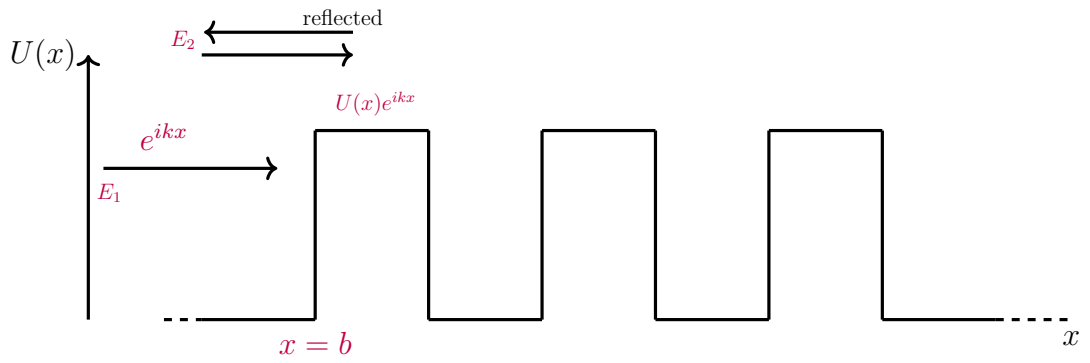

Figure 2.2: Infinitely periodic potential $U(x) = U(x+Na)$ with $N = 0, \pm1, \pm2, \pm3,...$ is shown. The incident wave packet $e^{i\vec{k}\cdot\vec{x}}$ with energy E_1 feels lattice potential, shown with Bloch wave function $U(x)e^{i\vec{k}\cdot\vec{x}}$. Another wave packet with energy E_2 is in forbidden gap. It reflects back without interacting with the lattice potential $U(x)$.

the Bloch momentum. $U_K(\vec{r})$ is Bloch function with the property

$$U_K(\vec{r}) = U_K(\vec{r} + \vec{R}) \tag{2.6}$$

where, $\vec{R}$ is a reciprocal lattice vector. From Eqs.(2.5) and (2.6)

$$\psi(\vec{r} + \vec{R}) = \psi(\vec{r})\, e^{i\vec{K}\cdot\vec{R}} \tag{2.7}$$

For 1D, it takes a simple form: $\psi(\vec{x} + \vec{a}) = \psi(\vec{x})\, e^{i\vec{K}\cdot\vec{a}}$

Dispersion relation

If incident energy E of the electron lies in the wavy region of figure 2.3 then it propagates in conduction band to the right with energy E_1 in figure 2.2. Electron encounters to periodic potential in this regime. Due to mismatch of potential at $x = b$ there can be some reflection at b. Electrons described by the Bloch function $U_K(\vec{x})\, e^{i\vec{K}\cdot\vec{x}}$, its amplitude does not decay or grow with x but oscillates periodically with x. So these electrons can go to any distance in the periodic potential without decay or resistance. This may not be true for electrons incident with an energy E_2 in forbidden gap. They are entirely reflected. They do not find a state inside the periodic potential. So, we may make an approximation here that electrons with energy like E_1 (lying within the conduction band) does not see the periodic potential (or $U(x) = 0$) and obey a Schrödinger equation

$$\frac{-\hbar^2}{2m_0^*}\frac{d^2\psi(x)}{dx^2} = E\psi(x) \tag{2.8}$$

Eq.(2.8) is similar to Eq.(2.4) and E can have two different energies E_1 and E_2. One can solve Eq.(2.4) separately for conduction band in figure 2.1 except intermediate region.

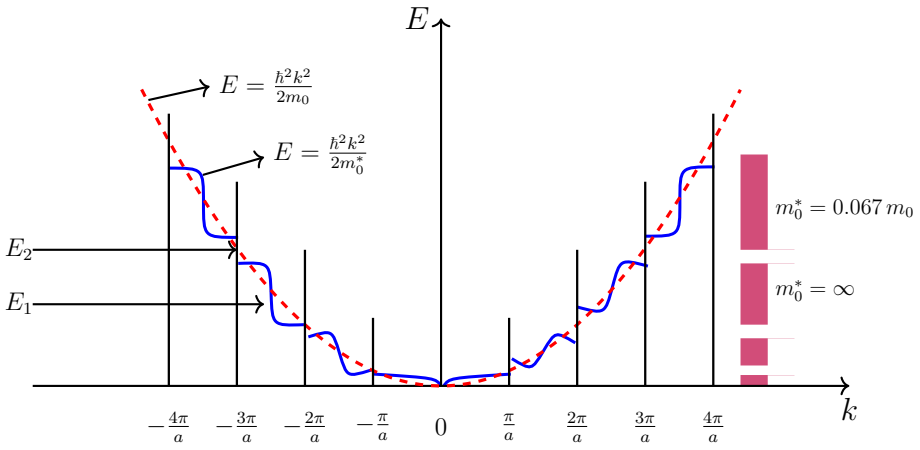

Figure 2.3: **E-k relation**: A dispersion curve E vs k is shown for infinite varying potential in solids. The wavy curve region is conduction band with allowing energy E_1. The discontinuity region is for forbidden gap with energy E_2. The incident energy of parabolic curve is $E = \frac{\hbar^2 k^2}{2m_0}$ and for wavy curve $E = \frac{\hbar^2 k^2}{2m_0^*}$.

From Eq.(2.8), one derive two equations, one involving E_1 with $m_0^* = 0.067m_0$ and the other involving energy E_2 with $m_0^* \to \infty$.

Bands and sub-band diagrams

In these narrow conductors, sub-bands or transverse modes are well separated at a given energy so such conductors are known as electron waveguides [2]. In two-dimensional electron gas (2DEG), electrons are confined in one direction with confinement potential, $V(z)$, and can move freely in remaining two directions x and y. The wave function in the absence of magnetic field can be written as

$$\psi(x, y, z) = \sin\left(\frac{n'\pi}{d}\left(z + \frac{d}{2}\right)\right) e^{ik_x x}\, e^{ik_y y} \tag{2.9}$$

The total energy and the dispersion relation will be

$$E = E_{bd} + \epsilon^{n'} + E_y + E_x \tag{2.10}$$

$$E = E_{bd} + \epsilon^{n'} + \frac{\hbar^2}{2m_0^*}(k_x^2 + k_y^2) \tag{2.11}$$

Where, E is the total energy given by the sum of band bottom E_{bd}, thershold $\epsilon^{n'}$ in z-direction and $x - y$ direction energy. In Eq.(2.10)

$$E_s = E_{bd} + \epsilon^{n'} \tag{2.12}$$

is sub-band energy as shown in figure 2.4. Here, $\epsilon^{n'}$ shows the threshold energies corresponding to different sub-bands with different wave functions ψ_z. At low temperatures

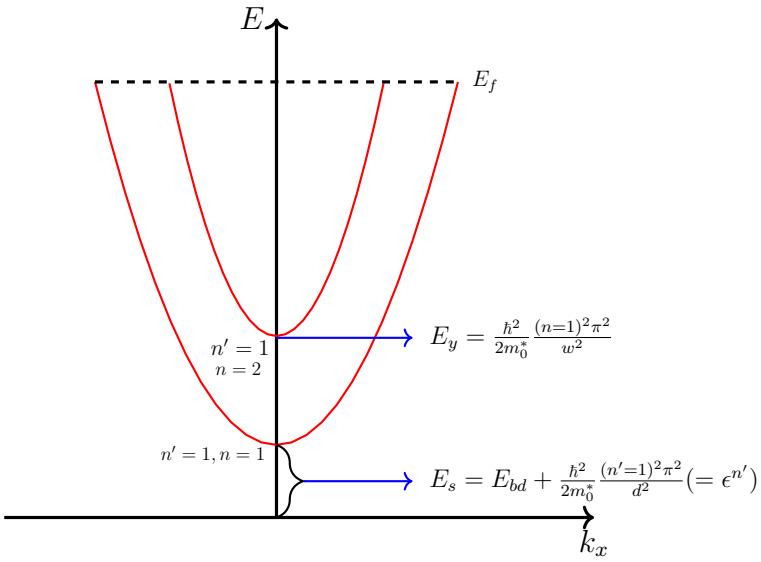

Figure 2.4: A dispersion relation curve is drawn for 1D conduction channel in 2D material. The confining potential is in y-direction and electron propagates in x-direction within transverse modes. The energy, $\epsilon^{n'}$, in z-direction is dropped because it is constant everywhere. E_{bd} is the band discontinuity energy. $\epsilon^{n'}$ is the energy along z-direction which is also known as thershold energy and n' denotes number of modes. Here, n' is taken 1. E_y is the energy in y-direction with n mode. E_f denotes Fermi energy and E_s is sub-band energy which is sum of E_{bd} and $\epsilon^{n'}$. For simplicity, E_{bd} can set to be zero.

only the lowest sub-band $n' = 1$ is occupied in z-direction and higher sub-bands have very low electron/hole densities that do not play any role in conduction.

Suppose a rectangular conductor which is uniform in x-direction and has confinement potential, $V(y)$, in y-direction. It means electrons are confined in y-direction. Wave function can be written as

$$\psi = \sin\left(\frac{n'\pi}{d}\left(z + \frac{d}{2}\right)\right) \sin\left(\frac{n\pi}{w}\left(y + \frac{w}{2}\right)\right) e^{ik_x x} \tag{2.13}$$

for $d >> W$, d is the height in z-direction and W is the width in y-direction. For $n' = 1$, different parabolic curves are shown with different values of n in figure 2.4. The energy in z-direction will be constant so one can drop its corresponding term i.e., $\epsilon^{n'}$ and total energy of an electron will be

$$E = E_{bd} + \frac{\hbar^2}{2m_0^*}\frac{n^2\pi^2}{w^2} + \frac{\hbar^2 k_x^2}{2m_0^*} \tag{2.14}$$

On comparing Eqs.(2.10), (2.11), (2.12) and (2.14),

$$E_s = E_{bd} + \frac{\hbar^2}{2m_0^*}\frac{n'^2\pi^2}{d^2}(= \epsilon^{n'}, \text{ this term has dropped in Eq.(2.14)},$$
$$E_y = \frac{\hbar^2}{2m_0^*}k_y^2 = \frac{\hbar^2}{2m_0^*}\frac{n^2\pi^2}{w^2} \quad \text{and} \quad E_x = \frac{\hbar^2 k_x^2}{2m_0^*}.$$

Lowest sub-band for z-axis is $n' = 1$, with discrete values of $n' = 1, 2, 3, ...$ in y-axis shows transverse modes or sub-bands shown in figures 2.4 and 2.6.

Difference between two-dimensional electron gas (2DEG) & metals

- At low temperatures the current in 2DEG is carried by electrons that have energies more or less equal to Fermi energy. That is why Fermi wavelength is very relevant length for conduction and given by $\lambda_f = \frac{2\pi}{k_f} = \sqrt{\frac{2\pi}{\rho_{e_0}}}$, where, k_f is the Fermi energy and ρ_{e_0} is the electron density. The Fermi wavelength in a 2DEG is generally higher than in a metal. This is because the Fermi wavelength is inversely proportional to the square root of the electron density, i.e $\sqrt{\rho_{e_0}}$. In a metal, the electron density is typically very high due to the large number of electrons ($10^{28}/\text{cm}^3$) in the material. This high electron density results in a smaller Fermi wavelength in metal. On the other hand, in a 2DEG, the electron density ($10^{11}/\text{cm}^2$) is typically lower because the electrons are confined to move in a 2D plane. With a lower electron density, the Fermi wavelength in a 2DEG is larger. The larger Fermi wavelength in a 2DEG has important consequences for the electronic properties of the system. It leads to enhanced quantum effects, such as quantum confinement and quantisation of energy levels, which can give rise to unique phenomena like the quantum Hall effect and ballistic transport [2]. In 2DEG, Fermi wavelength is about 35 nm for electron density $5 * 10^{11}/\text{cm}^2$. In metals, Fermi wavelength is extremely short, of the order of the distance between atoms ($\approx$ .25 nm).

- In-elastic mean free path is a distance, travelled by an electron before loosing its initial momentum, given by $l = v_f\tau$. Here l is the in-elastic mean free path, v_f is the Fermi velocity and τ is the relaxation time of momentum. The Fermi velocity is given by $v_f = \frac{\hbar k_f}{m_0^*} = \frac{\hbar}{m_0^*}\sqrt{2\pi\rho_{e_0}} = 3 * 10^7\text{cm/s}$ with number of electrons $\rho_{e_0} = 5 * 10^{11}/\text{cm}^2$. Thus, one can say Fermi velocity is lower in a 2DEG than a metal because Fermi velocity is directly proportional to the square root of electron density.

2.3 Landauer formula

In condensed matter physics, four probe method is used to separate the contact resistance and sample resistance [61]. In mesoscopic physics, experimental observations can be interpreted as quantum measurements. So, four probe method can not be used to separate sample and contact resistance. A schematic diagram is illustrated in figure 2.5 for Landauer conductance setup. In this figure, a barrier with a certain height connects two electron reservoirs, depicted by wavy lines. These reservoirs are connected via lead 1

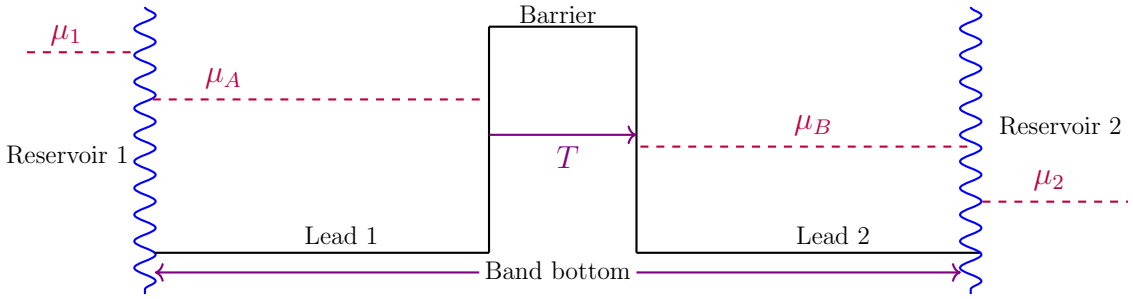

Figure 2.5: A setup of Landauer conductance shown in figure wherein a conductor with a transmission probability T is connected to left reservoir 1 and right reservoir 2 via lead 1 and lead 2 respectively. Reservoirs are classical batteries (current probe) and leads (voltage probes) are quantum wires. The wavy signs are shown for a sharp demarcation of classical (reservoir) and quantum (lead) regime. Reservoirs have chemical potential μ_1 for left reservoir and μ_2 for right reservoir. Leads also have with their own chemical potentials like μ_A for left lead and μ_B for right lead. Current is going from left reservoir 1 to right reservoir 2.

and lead 2, respectively. Each reservoir and lead has its own chemical potential denoted as μ_1 and μ_2 for reservoirs, and μ_A and μ_B for leads. T is the transmission probability. At zero temperature, the energy distribution of electrons are shown in figure 2.6 with transverse modes in left and right leads. One can find derivation in [2].

In figure 2.5, if the barrier height is infinite then $\mu_A = \mu_1$ and $\mu_B = \mu_2$. But, if there is transparency of barriers then $\mu_1 > \mu_A > \mu_B > \mu_2$. This transparency of barriers does not affect the chemical potential of reservoirs by definition. Below μ_2 the system is in equilibrium. Transport can occur only in this regime $\mu_2 < E < \mu_1$. Current emitted by reservoir 1 is

$$dI_1 = (dn)\, e_0\, v_0 = \frac{dn}{dE}\, e_0\, v_0\, dE = \frac{dn}{dE}\, e_0\, v_0\, (\mu_1 - \mu_2)$$

This is differential current dI_1 which is proportional to the difference of chemical potentials $\mu_1 - \mu_2$ so it is linear response i.e. $(\mu_1 - \mu_2) << 1$. dI_1 is influx current in conductor from left lead 1. $\frac{dn}{dE}$ is 1D DOS given by $\frac{2}{hv_0}$, here 2 stands for spin degeneracy. Therefore,

$$dI_1 = \frac{2}{hv_0}\, e_0\, v_0(\mu_1 - \mu_2) = \frac{2e_0}{h}\, (\mu_1 - \mu_2) \tag{2.15}$$

Current reaches to the other reservoir $dI_{1\to 2}$ is

$$dI_{1\to 2} = \frac{2e_0(\mu_1 - \mu_2)}{h}\, T; \quad \text{where } T = |t|^2 \text{ is the transmission probability.}$$

$dI_{1\to 2}$ current is transmitting from left lead 1 to right lead 2. Now $(\mu_1 - \mu_2)$ corresponds to a differential potential difference $e_0\ dU_{1\to 2}$ i.e., $(\mu_1 - \mu_2) = e_0\ dU_{1\to 2}$. The term $(\mu_1 - \mu_2)$ is other form of energy in terms of chemical potential which is also equal to

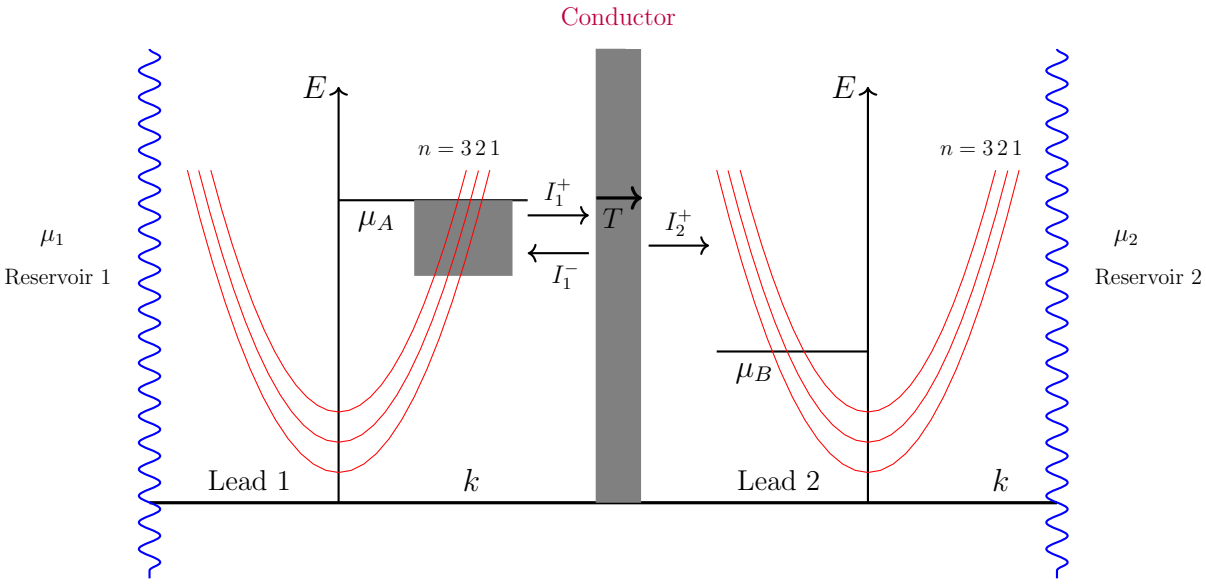

Figure 2.6: A schematic diagram of mechanism of the energy distributions of the incident electrons at zero temperature is supposed to be step functions. μ_1 and μ_2 are the chemical potentials in both reservoirs. T is the transmission probbability. I_1^+ is the current going from reservoir 1 to conductor. I_1^- is the reflected current from conductor before reaching reservoir 2. I_2^+ is the current going from conductor to reservoir 2. We have shown only three sub-bands in leads with integer values $n = 1, 2, 3$ in y-direction corresponding $n' = 1$ sub-band in z-direction.

energy $e_0\ dU_{1\to 2}$ in terms of electrostatic potential. Since,

$$\begin{aligned} dI_{1\to 2} =& \frac{2e_0^2}{h}\ dU_{1\to 2}\ T \\ \mathtt{G}_{1\to 2}\ (\text{or}\ \mathtt{G}) =& \frac{dI_{1\to 2}}{dU_{1\to 2}} = \frac{2e_0^2}{h} T \end{aligned} \tag{2.16}$$

The conductance of small sized conductors introduces two modifications to Ohm's law. First, contact resistance is independent of the length L of the sample. Second, conductance does not decrease linearly with the width W but varies with the transverse modes and goes down in discrete steps of $\frac{2e_0^2}{h}$. Voltage probes are attached to reservoirs. This expression is celebrated as two probe conductance formula. Voltage probes are analogous to voltmeter so no current in the lead. If $T = 1$, then $\mathtt{G} = \frac{2e_0^2}{h} \approx \frac{1}{25} k\Omega^{-1}$; $R = 25k\Omega$. The measured conductance is shown in figure 2.7 wherein plateaus exhibit that is corresponding to constant number of propagating modes, discussed in [2].

We consider the left lead for the same figure 2.5 and write number of states in between chemical potentials. Number of occupied states above μ_A are equal to number of unoccupied states below μ_A. Again, we write number of occupied states between μ_A and μ_1 is given by $\frac{dn}{dE}(\mu_1 - \mu_A)(1 + R)$, where R means all the left moving or $-k$ states are not occupied. Similarly, number of unoccupied states between μ_2 and μ_A is given by $2\frac{dn}{dE}(\mu_A - \mu_2) - \frac{dn}{dE}(\mu_A - \mu_2)(1 + R)$.

Similarly, we consider right lead in figure 2.5 and write number of states between

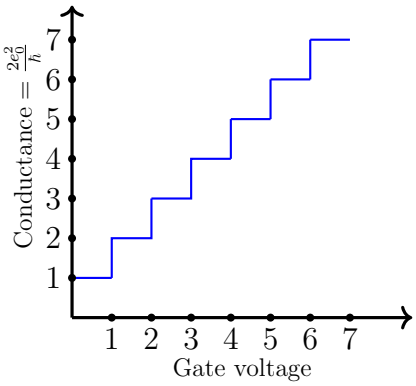

Figure 2.7: A schematic figure of discretized conductance versus gate voltage is shown. Conductance is discrete in terms of $\frac{2e_0^2}{h}$ from Landauer's formula.

different chemical potentials. Number of occupied states above μ_B are equal to number of unoccupied states below μ_B. Number of occupied states between μ_B and μ_1 is given by $\frac{dn}{dE}(\mu_1 - \mu_B)T$. Similarly, number of unoccupied states between μ_2 and μ_B is given by $2\frac{dn}{dE}(\mu_B - \mu_2) - \frac{dn}{dE}(\mu_B - \mu_2)T$. First term $2\frac{dn}{dE}(\mu_B - \mu_2)$ represents total number of states in this energy range. Factor 2 because $\pm$ states are degenerate. In second term, $\frac{dn}{dE}(\mu_B - \mu_2)T$, T is the probability with which $+k$ states are filled. $-k$ states cannot be filled because reservoir 2 cannot eject electrons above μ_2. Solving all these one can get,

$$e_0\, dU = \mu_A - \mu_B = R(\mu_1 - \mu_2)$$

Current from lead 1 to lead 2 can be written as

$$dI_{1\to 2} = \frac{2e_0}{h}(\mu_1 - \mu_2)T = \frac{2e_0}{h}\frac{e_0 dU_{1\to 2}}{R}T$$

$$\text{or,} \qquad \mathtt{G}_{1\to 2} = \frac{dI_{1\to 2}}{dU_{1\to 2}} = \frac{2e_0^2}{h}\frac{T}{R}$$

This should be observed for four probe measurement if objective reality exists like condensed matter physics. But in mesoscopic case this is not observed because of quantum measurements. Theoretically, in this thesis, we focus on three probe setup rather than four probe (Chapter 6). We are considering finite temperature in figure 2.5. At absolute zero temperature, we do not differentiate in states and electrons as each electron occupies single state. Number of electrons in left lead with the Fermi function is written as

$$\frac{dn}{dE}f(E,\mu_1) \tag{2.17}$$

Similarly, number of electrons in right lead is

$$\frac{dn}{dE}f(E,\mu_2) \tag{2.18}$$

where, $f(E,\mu_1)$ and $f(E,\mu_2)$ are Fermi-Dirac distribution functions. This function gives energy distributions of electrons in leads as

$$f(E,\mu_1) = \left[\frac{1}{e^{\frac{(E-\mu_1)}{k_BT}}+1}\right]_{\mu_1=E_f}$$

Number of electrons on the left that wants to cross to the right of the sample is

$$\frac{dn}{dE}\left[f(E,\mu_1), f(E,\mu_2)\right]$$

Again, $\frac{dn}{dE}$ is the density of states. In actual, number of electrons of them that cross to the right of the sample is given by difference of Eqs.(2.17) and (2.18) with transmission probability T

$$\frac{dn}{dE}\left[f(E,\mu_1) - f(E,\mu_2)\right]T$$

Current can be given by

$$\begin{aligned} dI_{1\to2} &= \frac{2}{hv_0}\left[f(E,\mu_1) - f(E,\mu_2)\right]Te_0v_0 \\ \text{or,}\qquad dI_{1\to2} &= \frac{2e_0}{h}\left[f(E,\mu_1) - f(E,\mu_2)\right]T \end{aligned} \tag{2.19}$$

If both potentials are held at the same temperature or potential then $\mu_1 = \mu_2$ and Eq.(2.19) predicts zero current. As one would expect $f_1(E) = f_2(E) \to I_{1\to2} = 0$. But at different temperatures or chemical potentials of leads, current will be

$$dI_{1\to2} = \frac{2e_0}{h}\frac{\partial f}{\partial \mu}\,d\mu\,T(E) = \frac{2e_0}{h}(-1)\frac{\partial f}{\partial E}(\mu_1-\mu_2)$$

$I_{1\to2}$ will be non zero as $\frac{\partial f}{\partial \mu} = -\frac{\partial f}{\partial E}$. This fraction shows differential change of Fermi function with respect to chmical potential or energy. Total current is expressed as

$$\begin{aligned} I_{1\to2} &= \int_0^\infty \frac{2e_0}{h}\left(-\frac{\partial f}{\partial E}\right)T(E)(\mu_1-\mu_2)dE \\ \text{or,}\qquad \frac{I_{1\to2}}{U_{1\to2}} &= \frac{2e_0^2}{h}\int_0^\infty dE\left(-\frac{\partial f}{\partial E}\right)T(E) \end{aligned} \tag{2.20}$$

Eq.(2.20) is linear response formula at non-zero temperature. The fraction, $\frac{\partial f}{\partial E} \approx \delta(E_f - E)$ as $f(E) = \theta(E_f - E)$ which shows step function.

$$\mathtt{G}_{1\to2} = \frac{2e_0^2}{h}\,T(E_f) \tag{2.21}$$

Where, $T(E_f)$ is transmission probability at Fermi energy of incident electrons E_f with respective reservoir. Eq.(2.21) is famous Landauer conductance formula that relates conductance or resistance to transmission probability of electrons.

Consequences of reservoir in mesoscopic system

The Landauer conductance is provided by mesoscopic systems having an electron reservoir with chemical potential μ and temperature T connected to the sample via leads [9, 44]. In statistical mechanics, thermodynamically large systems are considered. We deal with these systems that connected to electron reservoir(s). One can hypothetically decompose a microcanonical ensemble into a grand canonical ensemble and an environment to define probability distribution. The total Hamiltonian $H(p, q, N)$ of the canonical system with N particles of coordinates and momenta (q, p), in [13],

$$H(p, q, N) = H_s(p_1, q_1, N_1) + H_e(p_2, q_2, N_2)$$

where, $H_s(p_1, q_1, N_1)$ is Hamiltonian of grand canonical system with N_1 particles. Similarly, $H_e(p_2, q_2, N_2)$ is the Hamiltonian of electron reservoir with N_2 particles. We start by saying that the total Hamiltonian of the system and reservoir can be decoupled as $H = H_s + H_e$. Where, H_s is the system Hamiltonian that gives some single particle or many body eigenenergies ϵ_s. The degrees of freedom in H_e, the Hamiltonian of the reservoir, can be integrated out to lead to parameters like chemical potential μ and temperature T. Now from ϵ_s , μ and T one can derive a free energy that determines transport and thermodynamic properties. This will obviously fail as the system size starts becoming smaller. And then, mesoscopic physics helps us understand step by step how it happens. First of all, statistical mechanics ignores a surface term in the Hamiltonian which is of the form say H_{se} that depends on the combined degrees of freedom of the system and that of the reservoir. In mesoscopic physics, the leads take care of such terms and this is the first reason why we need the leads. At one end, it is connected to the ring or the sample and reservoir at the other end. Secondly, the Hamiltonian will only give the electronic states and so where are the electrons? Statistical mechanics tell us that we do not have to be very particular about that. The electrons are anyway there and the only thing that matters is their fluctuations for which the law of large numbers applies (Stirling formula etc). All these ideas break down for mesoscopic systems in the laboratory. Law of large numbers has to be discarded and ensemble averaging does not work. Exchange of electrons takes place between the reservoirs and the system via leads that model the voltage probes, current probes or any other probe like a scanning tunneling microscope (STM) tip etc. We have to consider their specific roles and configurations through the electronic Hamiltonian in the leads. The role of leads can be partially included with the help of a

self energy term in H_s that can account for level broadening as the energy levels of H_s leak out. One has to solve the scattering problem to account for this and thereby understand the effective changes in the eigenenergies and states of the system. These changes cannot be always modeled through parameters as is done via non-equilibrium Green's function techniques [2] because these changes are responsible for mesoscopic phenomena involving resistance, capacitance and inductance. These changes can be explicitly calculated by solving the scattering problem and to setup the scattering problem we need the lead is the third reason. This will further give us concepts like partial states and local states that cannot be defined from the Hamiltonian alone. As a fourth reason, something very drastic happens because of the leads for which so far there is no way to account for by correcting eigenenergies of the system using some parameters. A state in the system can leak out through the leads in multiple ways, some of them being evanescent modes. This leads to bound states in the continuum and very dramatic changes in properties of the system. Without considering their effect mesoscopic systems cannot be properly understood.

Classical and quantum statistical mechanics

Classical and quantum statistical mechanics are two branches of physics that deal with the statistical behaviour of systems consisting of a large number of particles. There are key differences between both approaches which include classical particles being distinguishable with well defined positions and momenta, no uncertainty principle, continuous energy, ensemble with Maxwell-Boltzmann distribution and thermal equilibrium etc. While quantum particles are indistinguishable, exhibit wave-particle duality, quantised energy, ensemble with Bose-Einstein and Fermi-Dirac distributions, exhibit quantum fluctuations etc. [13]. Both statistical systems can be divided in three parts of ensembles the microcanonical ensemble, the canonical ensemble, and the grand canonical ensemble. All these ensembles are used to describe systems in equilibrium. The postulates of quantum statistical mechanics are discussed below.

a. Equal a prior probability : It implies that each state of a system is equally probable. The probability distribution in microcanonical ensemble is given by this axiom, which states that all accessible micro states with the same energy are equally accessible.

$$\overline{\langle a_n|a_n\rangle} = \begin{cases} 1 & E < E_n < E + \delta; \\ 0 & else \end{cases} \tag{2.22}$$

b. Random phase approximation : It implies that state of the system in equilibrium can be written as an incoherent (or mixed states) superposition of eigenstates of H. This

mixed state can be understood by density matrix.

$$\overline{\langle a_n | a_m \rangle} = 0 \tag{2.23}$$

The diagonal elements of the density matrix represent the probabilities of finding the system in the corresponding eigenstates of the system's observable. The off-diagonal elements represent the coherence between different states, indicating the presence of quantum correlations or interference effects.

This chapter thereby clarifies fundamental physics of new a branch of condensed matter physics. The two-dimensional electron gas (2DEG) is formed at the interface of a heterojunction, usually of GaAs-AlGaAs. Small-structured devices such as quantum ring, quantum dot, quantum point contacts etc. can be fabricated from 2DEG. Sub-bands quantisation (consequences will be discussed in Chapter 5 of the thesis) is very specific feature in mesoscopic samples which are created due to confinement potential. From this confinememt potential an electron rich region is created in 2DEG. The electron transport in this regime can be very well explained by using the Landauer formalism. Leads are integral part of Landauer formalism.

NOTE: In the following chapters, we will conveniently utilise m_0 to represent the effective mass and symbolise confinement and electrostatic potential with U.

CHAPTER 3

OPEN MESOSCOPIC SYSTEMS

One of the great achievements in mesoscopic physics is that Landauer-Büttiker formalism [44, 45, 46, 47, 48, 49] considers electrons transport as a transmission problem at Fermi level. Mesoscopic systems behave quantum mechanically because they preserve coherence, which gives them intriguing and unique physical properties. Magnetisation is an essential thermodynamic property of a system that responds to a magnetic field. It is an emergent and equilibrium property that can not be defined for a single atom or molecule. In this chapter, the calculation of magnetisation [9] in mesoscopic systems will be elaborated in detail. Mesoscopic systems connected to reservoir termed as open mesoscopic systems. These systems respond to interference effects like Aharonov-Bohm effect [7] etc.

We introduce the Aharonov-Bohm effect in Section 3.1. We compute the current expression for semi-infinite leads, which is in accordance with the Landauer formula, in Section 3.2. The calculation of the magnetisation of an open Aharonov-Bohm ring using the normalisation constant is discussed in Section 3.3. In Section 3.4, we show the incorporation of the Aharonov-Bohm phase α into the electron wave function in the presence of a magnetic field, using the Feynman path approach.

3.1 Aharonov-Bohm effect

Aharonov-Bohm (AB) effect [7] is a quantum mechanical phenomena, in which any charge particle is affected by the electromagnetic potential in a region where the electromagnetic fields are zero. It can be studied for both open and closed systems. We consider a Hamiltonian for a particle with charge e_0 in magnetic field will be

$$H = \frac{1}{2m_0}\left[\left(\hat{p} - \frac{e_0}{c}\vec{A}\right)^2\right] + e_0\, U \tag{3.1}$$

Here, $\vec{A}$ is the vector potential and U is the scalar potential. The operator $\hat{p} = -i\hbar\vec{\nabla}$ is momentum operator where ∇ is the del operator. The magnetic field is given by $\vec{B} = \vec{\nabla} \times \vec{A}$. The dynamics of the particle will be governed by Schrödinger equation

$$i\hbar\frac{\partial\psi}{\partial t} = H\psi \tag{3.2}$$

Gauge transformations, for mesoscopic systems, which keeps the Schrödinger equation invariant are

$$\vec{A} \to \vec{A} + \vec{\nabla}\lambda = \vec{A}' \tag{3.3a}$$

$$U \to U - \frac{1}{c}\frac{\partial\vec{\lambda}}{\partial t} = U' \tag{3.3b}$$

$$\psi \to w\psi = \psi' \tag{3.3c}$$

$$w = e^{\frac{ie_0\lambda}{\hbar c}} \tag{3.3d}$$

The last two equations (3.3c) and (3.3d) are required conditions only for quantum particles. To understand the significance of gauge transformations, first of all, in Eq.(3.3a) one can see that $\vec{\nabla} \times \vec{\nabla}\lambda = 0$ for any scalar λ. That implies $\vec{A}$ and $\vec{A}'$ both give same magnetic field $\vec{B}$. Schrödinger equations before and after transformations is

$$i\hbar\frac{\partial\psi}{\partial t} = \left[\frac{1}{2m_0}\left(\frac{\hbar}{i}\vec{\nabla} - \frac{e_0}{c}\vec{A}\right)^2 + e_0\,U\right]\psi \tag{3.4}$$

$$i\hbar\frac{\partial\psi'}{\partial t} = \left[\frac{1}{2m_0}\left(\frac{\hbar}{i}\vec{\nabla} - \frac{e_0}{c}\vec{A}'\right)^2 + e_0\,U'\right]\psi' \tag{3.5}$$

Claiming that vector potential $\vec{A}$, scalar potential U and Schrödinger equation are all interchangable before and after transformations. One can continue calculations whichever Eq.(3.4) or (3.5) is comparatively easy. We consider for an electron charge $-e_0$ and for a positron charge $+e_0$. The uniformity of two equations

$$H = \frac{1}{2m_0}\left(\hat{p}^2 - \frac{e_0}{c}\hat{p}\cdot\vec{A} - \frac{e_0}{c}\vec{A}\cdot\hat{p} + \frac{e_0^2}{c^2}\vec{A}^2\right) + e_0\,U \tag{3.6}$$

Classically $\hat{p}$ and $\vec{A}$ commute. In quantum mechanics $\hat{p}$ is a differential operator,

$$\hat{p}\cdot\vec{A} = \frac{h}{i}(\vec{\nabla}\cdot\vec{A}) + \vec{A}\cdot\vec{p} \tag{3.7}$$

The uniformity equation

$$H = \frac{\hat{p}^2}{2m_0} + \frac{i\hbar e_0}{2m_0 c}(\vec{\nabla}\cdot\vec{A}) - \frac{e_0}{m_0 c}\vec{A}\cdot\hat{p} + \frac{e_0^2}{2m_0c^2}\vec{A}^2 + e_0\,U \tag{3.8}$$

Note that Coulomb gauge can be used with $\vec{\nabla}\cdot\vec{A}=0$ but it can be inconvenient when one generalise to rings with finite thickness and width. So better to use following identity

$$\left(\frac{\hbar}{i}\vec{\nabla}-\frac{e_0}{c}\vec{A'}\right)w\,\psi = w\left(\frac{\hbar}{i}\vec{\nabla}-\frac{e_0}{c}\vec{A}\right)\psi \tag{3.9}$$

Here, w is not constant but in identity it almost behaves like a constant except $\vec{A'}\rightarrow\vec{A}+\vec{\nabla}\lambda$. The LHS of identity (Eq.(3.9)) is called gauge covarient derivative. Now prove the identity

$$LHS=\frac{\hbar}{i}\left(\vec{\nabla}w\right)\psi+w\,\frac{\hbar}{i}\,\vec{\nabla}\,\psi-\frac{e_0}{c}\,\vec{A}\,w\,\psi-\frac{e_0}{c}\left(\vec{\nabla}\lambda\right)w\,\psi$$

Eq.(3.5) can be written as

$$i\hbar\frac{\partial\psi'}{\partial t}=\frac{1}{2m_0}\left(\frac{\hbar}{i}\vec{\nabla}-\frac{e_0}{c}\vec{A'}\right)\left(\frac{\hbar}{i}\vec{\nabla}-\frac{e_0}{c}\vec{A'}\right)\psi'+e_0U'\psi'$$

substituting from Eq.(3.3c) $\psi'\rightarrow w\psi$

$$\begin{aligned} i\hbar\frac{\partial}{\partial t}(w\psi) =& \frac{1}{2m_0}\left(\frac{\hbar}{i}\vec{\nabla}-\frac{e_0}{c}\vec{A'}\right)\left(\frac{\hbar}{i}\vec{\nabla}-\frac{e_0}{c}\vec{A'}\right)w\psi+e_0\,U'\,w\,\psi \\ \text{or}\qquad i\hbar\frac{\partial}{\partial t}(w\psi) =& \frac{1}{2m_0}\left(\frac{\hbar}{i}\vec{\nabla}-\frac{e_0}{c}\vec{A'}\right)w\left(\frac{\hbar}{i}\vec{\nabla}-\frac{e_0}{c}\vec{A}\right)\psi+e_0\,U'\,w\,\psi \end{aligned}$$

Use identity from Eq.(3.9)

$$\begin{aligned} \left(\frac{\hbar}{i}\vec{\nabla}-\frac{e_0}{c}\vec{A}\right)\psi =& \psi'' \\ \text{or}\quad i\hbar\frac{\partial}{\partial t}(w\psi) =& \frac{1}{2m_0}\left(\frac{\hbar}{i}\vec{\nabla}-\frac{e_0}{c}\vec{A'}\right)w\psi''+e_0\,U'\,w\,\psi \end{aligned} \tag{3.10}$$

again from Eq.(3.9)

$$\begin{aligned} i\hbar\frac{\partial}{\partial t}(w\psi) =& \frac{1}{2m_0}w\left(\frac{\hbar}{i}\vec{\nabla}-\frac{e_0}{c}\vec{A}\right)\psi''+e_0\,U'\,w\,\psi \\ \text{or}\qquad i\hbar\frac{\partial\psi}{\partial t} =& \frac{1}{2m_0}\left(\frac{\hbar}{i}\vec{\nabla}-\frac{e_0}{c}\vec{A}\right)\psi''+e_0\,U'\,\psi \end{aligned}$$

as w does not depend on t as well as $U'=U$, we find by putting the value of ψ'' from Eq.(3.10)

$$i\hbar\frac{\partial\psi}{\partial t}=\frac{1}{2m_0}\left(\frac{\hbar}{i}\vec{\nabla}-\frac{e_0}{c}\vec{A}\right)^2\psi+e_0\,U\,\psi \tag{3.11}$$

It proves that both Eqs.(3.4) and (3.5) are equivalent to each other. We have freedom to set

$$\vec{A'}=\vec{A}+\vec{\nabla}\lambda=0 \tag{3.12}$$

From Eq.(3.12), λ can be choosen arbitrarily which gives from Eq.(3.5)

$$i\hbar\frac{\partial\psi'}{\partial t} = \frac{1}{2m_0}\left[\left(\frac{\hbar}{i}\vec{\nabla}\right)^2 + e_0\,U'\right]\psi' \tag{3.13}$$

This is same as Schrödinger equation in absence of magnetic field. To be noticed that ψ' has an extra phase, as can be seen from Eqs.(3.12) and (3.13), that plays a role for magnetic field at the center of the ring. Since there is no magnetic field in the ring, that's why no Lorentz force acting on the electrons. Now question arises that an extra phase in electron wave function affect observables at all, specifically in case of Copenhagen probability $|\psi'|^2$? The claim is that it will affect observables only when trajectories are closed. This is a purely quantum interference phenomenon which results in an equilibrium current in the system that is not driven by any classical force. But if the system does not allow any closed trajectory then there will be no observable effect. There is no restriction on the path of the closed trajectory that could be circular, or square, or elliptical or random walk that eventually comes back to the starting point.

Gauge fixing for finite thickness ring

Eqs.(3.3a) and (3.3b) allow λ to be any value; however, we have utilized this freedom to imply a derivative in Eq.(3.12). Therefore, gauge fixing-also referred to as fixing the components of $\vec{\nabla}\lambda$-is required. Gauge fixing is typically used to solve the Schrödinger equation in the presence of a magnetic field. With this one can use a particular choice for vector potentials A_x, A_y and A_z that is known as Coulomb gauge i.e., $\vec{\nabla}\cdot\vec{A} = 0$. This gauge fixing perfectly works for a perfect circular 1D ring lies on 2D plane in polar coordinates. If electron trajectory is restricted on square path then we can use cartesian coordinates. Coulomb gauge in cartesian coordinates will be $\vec{\nabla}\cdot\vec{A} = \partial_x A_x + \partial_y A_y + \partial_z A_z = 0$. It shows

$$A_x = -B_o y, \quad A_y = 0, \quad A_z = 0 \tag{3.14}$$

that in turn leads to a magnetic field that can be applied exactly

$$\vec{B} = \vec{\nabla}\times\vec{A} = \hat{k}B_o$$

$$B_z = \partial_x A_y - \partial_y A_x = B_o; \quad B_x = \partial_y A_z - \partial_z A_y; \quad B_y = \partial_x A_z - \partial_z A_x$$

Thus, Coulomb gauge in cartesian coordinates give rise to the vector potential profile shown in the figure 3.1. However, our choice of coordinate system should not determine the outcome of an observation and so one should be able to solve the situation of a perfectly circular ring with the kind of vector potential distribution shown in figure 3.1 and get the same result as that of gauge fixing in polar coordinates. So gauge fixing may

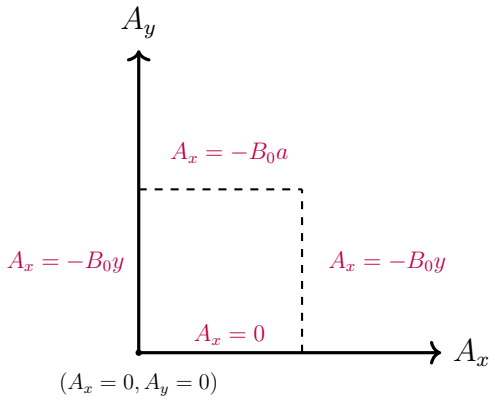

Figure 3.1: Vector potential profile due to Coulomb gauge in Cartesian coordinates along a square path of sides of length "a" as given by Eq.(3.14).

not be at all a good idea in case the ring has a finite thickness or for a disk because in such systems one can imagine all kinds of closed trajectories ranging from circular to square.

Twisted boundary conditions

Twisted periodic boundary condition for a closed trajectory in a finite thickness ring means $\psi(x, y, z) = \psi(x + L_x, y, z)$. It is same for any arbitrary closed trajectory that one can imagine in a finite thickness ring. These trajectories are not directly related to electron motion in the system but effectively related through the concept of Feynman paths that will be further elaborated in Section 3.4. For the special case of a 1D ring one can just drop the y and z degrees of freedom. From Eqs.(3.3c) and (3.3d) using the fact that for electron phase will be with negative sign.

$$\begin{aligned} \psi'(x, y, z) &= e^{-\frac{ie_0}{\hbar c}\lambda}\ \psi(x, y, z) \\ \psi'(x + L_x, y, z) &= e^{-\frac{ie_0}{\hbar c}\int_0^{L_x}\vec{\nabla}\lambda\cdot\vec{dl}}\ \psi(x + L_x, y, z) \\ &= e^{-\frac{ie_0}{\hbar c}\int_0^{L_x}\vec{\nabla}\lambda\cdot\vec{dl}}\ \psi(x, y, z) \end{aligned} \tag{3.15}$$

reason being a closed trajectory implies $\psi(x + L_x, y, z) = \psi(x, y, z)$ for ψ, whereas ψ' satisfies Eq.(3.3c). $\vec{dl}$ is a small change in length along a given trajectory that make a closed path. Total length of the path being L_x. For the special situation of $L_x = 0$ we get

$$\psi'(x, y, z) = e^{-\frac{ie_0}{\hbar c}\oint\vec{\nabla}\lambda\cdot\vec{dl}}\ \psi(x, y, z) = \psi(x, y, z) \tag{3.16}$$

From Eqs.(3.15) and (3.16)

$$\psi'(x + L_x, y, z) = e^{-\frac{ie_0}{\hbar c}\int_0^{L_x}\vec{\nabla}\lambda\cdot\vec{dl}}\ \psi'(x, y, z) \tag{3.17}$$

$$\text{or,} \quad \psi'(x+L_x,y,z) = e^{\frac{ie_0}{\hbar c}\int_0^{L_x}\vec{A}\cdot\vec{dl}}\ \psi'(x,y,z) \tag{3.18}$$

$$\text{or,} \quad \psi'(x+L_x,y,z) = e^{\frac{i2\pi\Phi}{\Phi_o}}\ \psi'(x,y,z) \tag{3.19}$$

where, $\Phi = \int_0^{L_x}\vec{A}\cdot\vec{dl}$ is magnetic flux at the center of the ring and $\Phi_o = \frac{hc}{e_0}$ is defined as flux quantum. Aharonov-Bohm phase α is given by $\frac{2\pi\Phi}{\Phi_o}$ in Eq.(3.19). Note that the only aspect of the ring geometry that has gone into this analysis is the fact that $x + L_x = x$ which means it can be an ellipse or any deformed version of a ring. We want to generalize a ring of finite thickness wherein one can choose from various types of such closed trajectories. So it is important to understand it from the topological point of view that we only need the possibility of trajectories that close on itself. To be mathematically correct the study is done for topology of a ring not for ring geometry.

In the rest of the chapter, we will use the simple system of a one-dimensional ring. It can be solved analytically and the results can be elaborated with respect to the underlying physics in Section 3.3. That the magnetic field affects the phase of the electron wave function in the ring will magnetise the ring as we will show subsequently. This is different from all classical magnetisations and a few Gauss of magnetic field can magnetise the ring due to Aharonov-Bohm effect [7]. Realistic systems like a ring of finite thickness or disk will also get magnetised by a fraction of a single flux quantum based on the same physical principle. For such systems solving and demonstrating explicitly may involve some technical difficulties.

3.2 Transport current

We consider a 1D quantum scattering problem discussed in textbooks and illustrated in figure 3.2. In this scattering problem, either sides of rectangular barrier can be considered as semi-infinite leads likewise in mesoscopic systems [44, 45, 46]. But in quantum mechanics, there is no concept of reservoir. In figure 3.2, one side of leads is connected to quantum scatterer, i.e., rectangular barrier and other side of leads is going upto $\pm\infty$. we will compute current for these semi-infinite leads. The Schrödinger equation for the problem is

$$-\frac{\hbar^2}{2m_0}\frac{d^2\psi}{dx^2} + U(x)\psi(x) = E\psi(x) \tag{3.20}$$

where m_0 is the electron mass and E is the incident energy. In region I and III potential is zero, $U(x) = 0$, whereas region II has some non-zero but finite potential. The solutions of Schrödinger equation in region I and III can be written as.

$$\begin{aligned} \psi_I &= a\ e^{ikx} + b\ e^{-ikx} \\ \psi_{III} &= c\ e^{ikx'} + d\ e^{-ikx'} \end{aligned} \tag{3.21}$$

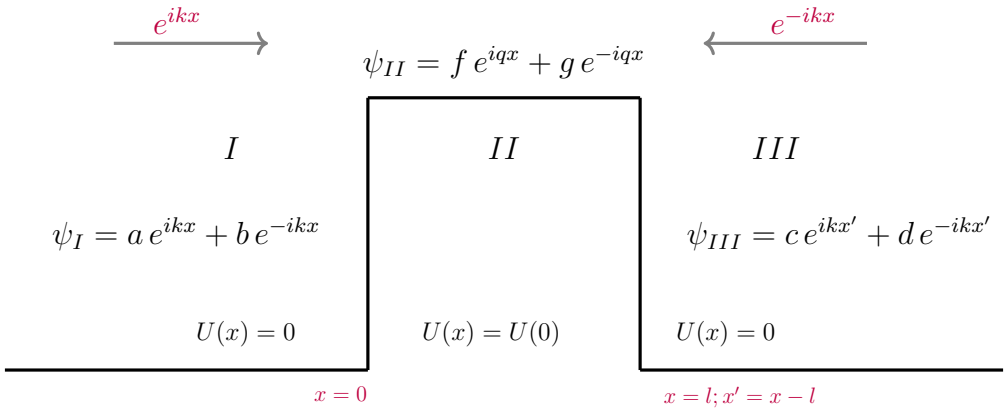

Figure 3.2: A wave (particle) with energy E can incident from left in the region I as well as from right in the region III. Potential barrier and propagation components of the incident, reflected, and transmitted waves are mentioned in all the regions of figure, when energy of incident particle is greater than potential $U(x)$. $U(0)$ is the constant potential in region II. A new coordinate x' is introduced for region III and l is the width of the barrier potential.

where $x' = x - l$ is another coordinate taken zero at $x = l$ for wave function in region III. This kind of scattering problem in 1D is solved by considering that a particle once transmitted never turns back because there is nothing to reflect it back. This problem is solved in textbooks by making $d = 0$ without giving any proper description. In condensed matter systems, we often do not have the freedom to rule out electrons incident simultaneously from the left as well as from the right. We derive current for semi-infinite leads without making $d = 0$ in this section. Leads can go upto $\pm\infty$ but as electrons go far from scatterer then a, b, c and d depend on the the coordinates of the external world with time. This is the time at which electron starts to react with classical world. In this case, we need to use statistical mechanics axioms such as equal a priori probability and random phase (chapter Eight in K. Huang's 2nd edition, Statistical Mechanics [13]) i. e.

$$|\bar{a}|^2 = |\bar{d}|^2 = 1 \tag{3.22}$$

$$\bar{a}b = \bar{c}d = \bar{a}^*b = a\bar{b}^* = c\bar{d}^* = \bar{c}^*d = \bar{d}^*a = \bar{a}^*d = 0 \tag{3.23}$$

Eq.(3.22) demands that the flux of incident particles equally probable from the left as well as the right. Thus, we are avoiding setting $d = 0$ by hand. It also shows that incident flux of electron from left lead is equal to right lead's incident flux. Whereas Eq.(3.23) tells that all cross terms are zero implies symmetry of momentum operator for semi-infinite leads [9, 62]. However, a and d may have some intial phases which do not affect our analysis. c and b is determined with scatterer. In figure 3.2 the amplitude of b can be written as

$$b = a\,r + d\,t'$$

at $x = 0$. Where, b contains the reflected part of a which is $a\,r$ in left lead and in right lead b consists the transmitted part of d which is $d\,t'$. Likewise for amplitude c can be written as

$$c = d\,r' + a\,t$$

at $x' = 0$. Again c has the reflected part of d whch is $d\,r'$ in right lead and in left lead c has the transmitted part of a in left lead. Here, r and t are reflection and transmission amplitude in left lead or region I while r' and t' are reflection and transmission amplitude in right lead or region III in figure 3.2. Thus, the wavefunction in region III can be written as

$$\psi_{III} = d\,r'\,e^{ikx'} + a\,t\,e^{ikx'} + d\,e^{-ikx'} \tag{3.24}$$

Quantum mechanical current is given by for ψ_{III}

$$J = \frac{e_0\hbar}{2m_0 i}\left[\psi^*_{III}\,\nabla\psi_{III} - \psi_{III}\,\nabla\psi^*_{III}\right] \tag{3.25}$$

using Eq.(3.24), conjugation of ψ_{III} can be written as

$$\psi^*_{III} = d^*\,r'^*\,e^{-ikx'} + a^*\,t^*\,e^{-ikx'} + d^*\,e^{ikx'} \tag{3.26}$$

from Eq.(3.25), current density J can be written as

$$\begin{aligned}
J = \frac{e_0\hbar}{2m_0 i}\Big[&(d^*r'^*e^{-ikx'} + a^*t^*e^{-ikx'} + d^*e^{ikx'})\frac{d}{dx}(dr'e^{ikx'} + ate^{ikx'} + de^{-ikx'}) \\
&- (dr'e^{ikx'} + ate^{ikx'} + de^{-ikx'})\frac{d}{dx}(d^*r'^*e^{-ikx'} + a^*t^*e^{-ikx'} + d^*e^{ikx'})\Big] \\
J = \frac{e_0\hbar}{m_0} Im&\left[(ik)(|r'|^2 + |t|^2 - r'^*e^{-2ikx'} + r'e^{2ikx'} - 1)\right] \\
J = \frac{e_0\hbar}{m_0} Im&\left[(ik)(|r'|^2 + |t|^2 - |r'^*|e^{-2ikx'-i\eta} + |r'|e^{2ikx'+i\eta} - 1)\right] \\
J = \frac{e_0\hbar}{m_0} Im&\left[(ik)(|r'|^2 + |t|^2 + (2i)|r'|\sin(2kx' + \eta) - 1)\right]
\end{aligned}$$

here, $r' = |r'|\,e^{i\eta}$. So the current density on the right lead in figure 3.2 at $T = 0K$ for incident wave $e^{\pm ikx}$ is

$$J = \frac{e_0\,\hbar k}{m_0}\left[|r'|^2 + |t|^2 - 1\right] \tag{3.27}$$

The above current is of the form $e_0 v_0 n$. Therefore, differential current dJ_{in}, the current in dE energy interval, is

$$dJ_{in} = e_0\, v_0\, \frac{dn}{dE}\, dE = e_0\, v_0\, \frac{1}{hv_0}\, dE \tag{3.28}$$

Here, $\frac{dn}{dE} = \frac{1}{hv_0}$ is density of states in 1D.

$$dJ = \frac{e_0 \hbar k}{m_0}\, \left(|r'|^2 + |t|^2 - 1\right)\, \frac{dn}{dE}\, dE \tag{3.29}$$

Now instead of unit incoming flux, incident flux of measure $dn(\neq 1)$. As $v_0 = \frac{\hbar k}{m_0}$

$$\begin{aligned} \text{Hence, } \; dJ &= \frac{e_0 \hbar k}{m_0}\, \left(|r'|^2 + |t|^2 - 1\right)\, \frac{1}{hv_0}\, dE \\ &= \frac{e_0}{h}\, \left(|r'|^2 + |t|^2 - 1\right)\, dE \end{aligned} \tag{3.30}$$

This current expression was also derived by Landauer [44]. In Eq.(3.30), $\frac{e_0\hbar k}{m_0}\frac{-1}{hv_0}dE$ is incoming current before scattering and $\frac{e_0\hbar k}{m_0}\frac{|r'|^2+|t|^2}{hv_0}dE$ is current after scttering. At zero temperature, dJ in Eq.(3.30) becomes equal to zero that shows Kirchhoff's low. And sign convention depends on individual's choice. The normalisation constant for the wave functions defined as [9]

$$\sqrt{\frac{1}{hv_0}} = \sqrt{\frac{1}{h \cdot \frac{\hbar k}{m_0}}} = \sqrt{\frac{2\pi m_0}{h^2 k}} \tag{3.31}$$

Normalisation constant takes care itself about current carried states at a given energy which is equal to 1D DOS at zero temperature. The Eq.(3.27) derived for sample current at zero temperature which is equlibrium current. Now at finite temperature [2], a non-equilibrium current can be obtained by taking the temperature on the left different from that on the right

$$dJ = \frac{e_0}{h}[f_r(E)|r'|^2 + f_l(E)|t|^2 - 1 \cdot f_r(E)] \tag{3.32}$$

First term represents reflection of electrons coming from right lead and see the temperature of right reservoir. Similarly, second term shows the transmission of electrons from left lead, so see the temperature of left reservoir. In this equation, $f_r(E)$ and $f_l(E)$ are the Fermi distribution functions for the electrons incident from right and left reservoirs. Fermi distribution function is one at zero temperature. For non-equilibrium system current flows in the sample so sample can have a resistance and that has calculated from Landauer formula.

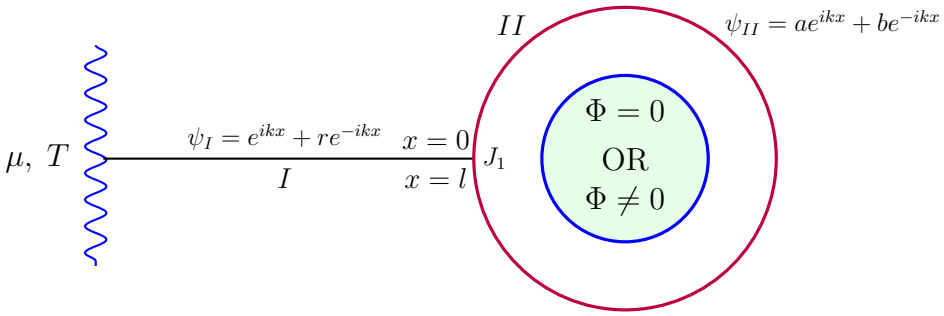

Figure 3.3: A typical mesoscopic grand canonical system is shown. It consists of an open 1D ring pierced by an Aharonov-Bohm (AB) flux Φ at the center of the ring. Potential is zero in the ring i.e., $U(x) = 0$. An 1D thin solid line connects the ring to a reservoir and it is called lead. The lead and ring are shown with region I and region II in the figure. We have taken potential $U(x)$ in the lead to be zero as well. Here, μ and T are the chemical potential and temperature of the reservoir, respectively. Lead connects to the ring at junction J_1 shown in figure.

3.3 Magnetisation of an open Aharonov-Bohm ring

To describe magnetisation of mesoscopic system, an 1D quantum ring [63] is considered in figure 3.3. Mesoscopic samples are made up of semiconductors (GaAs-AlGaAs) or metals etc. with one or multiple 1D channels which can be achieved by lateral confinement potential [2] discussed in Chapter 5. The ring in figure 3.3 is not an isolated but connected to an electron reservoir making it a grand canonical system or an open system. The single reservoir in figure 3.3 have a chemical potential μ and temperature T shown by a wavy line. The electrons in the reservoir are completely thermalized classical particles. With one reservoir we cannot have a chemical potential difference or temperature difference and hence this is a system in equilibrium. The sample (quantum ring) has quantum states while the reservoir has electrons. The 1D thin line connecting the sample and the reservoir is known as the lead. It can be made of the same material as the ring. The lead allows the electrons from the reservoir to populate the states in the ring and also allow the states from the ring to leak out to reservoir as electrons. Lead behaves like voltage probe because net current in lead is zero. Total length of the lead and the circumference of the ring is less than the single particle coherence length of the quantum mechanical electrons at the temperatures at which mesoscopic experiments are conducted. So the electron dynamics in the lead and in the ring is governed by quantum mechanics. The single particle Schrödinger equation with an effective mass works very well for most of these systems. So, we can write down a typical Fourier component of a wave packet, which is also the solution of the 1D Schrödinger equation (as shown in figure 3.3) in the lead and the ring and match them at the junction between the ring and the lead. No wave function is written inside the reservoir and the wave function of an electron coming from the reservoir is taken as $a\ e^{ikx}$ where x represents the coordinate and k the wave vector. The amplitude a is set to 1 as has been described in Eq.(3.22). This

picture as envisaged by Landauer, therefore claims a sharp line of demarcation between the quantum system of the lead and ring with the classical reservoir. While the axiomatic approach presented in Section 3.2 and explicitly stated in Eq.(3.23) does not require such a sharp line of demarcation. Axiomatic approaches lead to an objective theory, while Landauer's claim manifests. The sharp line of demarcation between a classical reservoir and a quantum system results in a contact resistance of 12.9 kilo ohms per sub-band that can be measured in multiple manifestations [2]. In this system the eigenstates of the ring can leak out resulting in level broadening and life time related effects which very accurately models dissipation and decoherence of realistic mesoscopic systems. It is this broadening effect that is captured quantitatively by scattering theory while all approaches starting from Hamiltonian try to parametrize this broadening in terms of a self energy. The non-equilibrium Green's function method discussed in the book [2] is very suited to do this parametrization. However, many physical phenomenon may be overlooked by this parametrization and it is the scattering problem solved quantum mechanically that correctly incorporates evanescent modes and the presence of Fano resonances due to bound states in the continuum. The two reservoirs in figure 3.2 (not shown) model the two battery terminals that drive the current through the system. Voltage probes (mesoscopic analogues of a voltmeter) and current probes (mesoscopic analogues of ammeters) also effectively act as additional electron reservoirs. Each has its own chemical potential and temperature and each can induce dephasing and decoherence [2]. It makes a lot of sense to study mesoscopic systems coupled to an arbitrary number of reservoirs including one and two and all of them correspond to some physical situation that is experimentally relevant. At the temperatures at which mesoscopic experiments are done, the experiments are mostly understood in terms of zero temperature calculations. So we will all along try to understand the zero temperature limit that we get from quantum mechanics. Also many body effects will not be considered in this thesis essentially. Many body effects have been mostly studied through numerical techniques [64]. However, according to Eq.(3.23), we cannot write down any cross terms in the leads, so we cannot write a Slater determinant in the leads. But we can definitely write a Slater determinant in the sample (which in this case is the ring). So electron-electron interactions will give a correlated environment in the sample, with states in the leads being free electron states. [64] shows that the main formalism discussed here, that of the Larmor clock, allows us to include many body effects in such a situation.

We will now proceed to show that the system described in figure 3.3 will carry an equilibrium current called persistent current [40] that does not require a power source. It is a purely mesoscopic phenomenon and very ideal to get insights into mesoscopic physics [41]. This current magnetises the ring and has been observed in rings made of gold or semiconductors [65]. Details of the results can be seen in the 1985 paper by Buttiker

[63]. Here we will provide an exact and hence easy to understand quantum mechanical treatment of the problem as compared to the adhoc theoretical treatment in the original paper by Buttiker. The reservoir injects electrons into the lead which is denoted as region I in the figure. These electrons populate the states inside the ring which is denoted as region II in the figure. The lead and the ring are connected at a point say J_1. The equation of motion in region I (or lead) and region II(or ring or system) is therefore the Schrödinger equation and the wave functions in the two regions in absence of magnetic field can be written as

$$\psi_I = \frac{1}{\sqrt{k}} \ (e^{ikx} + r \ e^{-ikx}) \tag{3.33}$$

$$\psi_{II} = \frac{1}{\sqrt{q}} \ (a \ e^{iqx} + b \ e^{-iqx}) \tag{3.34}$$

Where,

$$q = \left[\frac{2m_0(E-U)}{\hbar^2}\right]^{\frac{1}{2}} \text{ and } \quad k = \left[\frac{2m_0}{\hbar^2}E\right]^{\frac{1}{2}} \tag{3.35}$$

Here, k and q are wave vectors in region I with zero potential and region II with non-zero potential, respectively. One can solve this problem either considering normalisation constant or without normalisation constant. Here, normalisation constants are $\frac{1}{\sqrt{k}}$ and $\frac{1}{\sqrt{q}}$ which are consistent with the Eq.(3.31). The difference in the interpretation of incident wave packet will be incident electron is e^{ikx} with considering normalisation constant. The density of states (DOS) of the 1D lead will be $\frac{1}{\hbar v_0}$ which is equal to DOS in the infinite 1D lead. Aharonov-Bohm (AB) flux Φ is applied at the centre of the ring. There is no magnetic field on the electrons of quantum ring. AB phase α in Eq.(3.19) is incorporated by applying boundary conditions in Eqs.(3.40) and (3.41) in the presence of magnetic field which will be discussed in Section 3.4.

Current conservation boundary conditions

To derive current conserving boundary conditions, for an open system shown in figure 3.3, need time independent Schrödinger equation corresponding to (3.13). In Eq.(3.13), U' is considered time independence i.e. $U' = U$, ψ' also taken no time dependance i.e. $\psi' = \psi$ and $e_0 = 1$ for simplifying

$$-\frac{\hbar^2}{2m_0}\nabla^2\,\psi(\vec{r}) + U(\vec{r})\ \psi(\vec{r}) = E\,\psi(\vec{r}) \tag{3.36}$$

Integrate with volume V_0 around the point of junction over the both sides, we get

$$-\frac{\hbar^2}{2m_0}\int_{V_o}\nabla^2\psi(\vec{r})dV_o + \int_{V_o}U(\vec{r})\psi(\vec{r})dV_o = \int_{V_o}E\psi(\vec{r})dV_o \tag{3.37}$$

$$-\frac{\hbar^2}{2m_0}\int_{V_o}\vec{\nabla}\cdot(\nabla\psi(\vec{r}))dV_o+\int_{V_o}U(\vec{r})\psi(\vec{r})dV_o=\int_{V_o}E\psi(\vec{r})dV_o \tag{3.38}$$

Suppose S is surface enclosing the volume V_o.

$$-\frac{\hbar^2}{2m_0}\lim_{V_o\to 0}\int_S(\nabla\psi(\vec{r}))\cdot d\vec{S}+\lim_{V_o\to 0}\int_{V_o}U(\vec{r})\psi(\vec{r})dV_o=\lim_{V_o\to 0}\int_{V_o}E\psi(\vec{r})dV_o$$

V_o shrinks to 0

$$\int_S(\vec{\nabla}\psi(\vec{r}))\cdot d\vec{S}=0$$

For partial wave integration becomes sum,

$$\sum\vec{\nabla}\psi(\vec{r})=\sum_i\frac{d\psi_i}{dx_i}=0 \tag{3.39}$$

This equation is current conservation boundary condition. Now apply the boundary conditions at the junction of figure 3.3

$$\begin{aligned}&\psi_I|_{x=0^-}=\psi_{II}|_{x=0^+}=\psi_{III}|_{x=l^-}\\&\frac{1}{\sqrt{k}}(1+R)=\frac{1}{\sqrt{q}}(a+be^{-i\alpha})=\frac{1}{\sqrt{q}}(ae^{iql+i\alpha}+be^{-iql})\end{aligned} \tag{3.40}$$

and Eq.(3.39) implies

$$\begin{aligned}\frac{d\psi_I}{dx}|_{x=0^-}+\frac{d\psi_{II}}{dx}|_{x=0^+}+\frac{d\psi_{III}}{dx}|_{x=l^-}&=0\\\left[\frac{ik}{\sqrt{k}}(1-R)\right]+\left[\frac{iq}{\sqrt{q}}(-a+be^{-i\alpha})\right]+\left[\frac{iq}{\sqrt{q}}(ae^{iql+I\alpha}-be^{-iql})\right]&=0\end{aligned} \tag{3.41}$$

Solving these two Eqs.(3.40) and (3.41), one can calculate the value of a, b and R. In Eq.(3.41), the first square bracket shows the current at $x=0^-$ denoted by $\frac{d\psi_I}{dx}|_{x=0^-}$. $x=0^-$ is a coordinate assigned in lead left to the junction J_1. Second square bracket shows the current at $x=0^+$. This coordinate is in the ring near junction when partial waves move clockwise. Third square bracket shows the current at $x=l^-$ which is again the coordinate in the ring near junction when partial waves move anti-clockwise. Magnetic field comes into the role after applying boundary conditions. In the effect of magnetic field Aharonov-Bohm flux Φ comes with the wave functions. Due to this flux a phase known as Aharonov-Bohm phase α is introduced in the wave functions (see Eq.(3.19)). Some terms acquire this phase factor and some of them do not that will be discussed in Section 3.4. Current density for propagating states from Kirchhoff's law will be zero at

junction J_1. From Eqs.(3.40) and (3.41)

$$J = \frac{e_0\hbar}{2m_0 i}\left[\psi_I^*\Delta\psi_I + \psi_{II}^*\Delta\psi_{II} + \psi_{III}^*\Delta\psi_{III} - \text{hc}\right] = 0 \tag{3.42}$$

Let's say first three terms are j_1 and Hermitian conjugate terms are j_2 in Eq.(3.42). Thus,

$$J = j_1 + j_2 = 0 \tag{3.43}$$

First, we write j_1 without the factor $\frac{e_0\hbar}{2m_0 i}$ that can be added later to the expression.

$$\begin{aligned} j_1 = &\left[(e^{ikx} + Re^{-ikx})^*\frac{d}{dx}(e^{ikx} + Re^{-ikx})\right]_{x=0^-} \\ &- \frac{1}{q}\left[(ae^{iqx} + be^{-iqx-i\alpha})^*\frac{d}{dx}(ae^{iqx} + be^{-iqx-i\alpha})\right]_{x=0^+} \\ &+ \frac{1}{q}\left[(ae^{iqx+i\alpha} + be^{-iqx})^*\frac{d}{dx}(ae^{iqx+i\alpha} + be^{-iqx})\right]_{x=l^-} \end{aligned}$$

hc (stands for Hermitian conjugate) or j_2 only for region II can written as

$$i|a|^2 - ia^*be^{-i\alpha} + ib^*ae^{i\alpha} - i|b|^2 \tag{3.44}$$

$$\text{and} \quad -i|a|^2 + iab^*e^{i\alpha} - iba^*e^{-i\alpha} + i|b|^2 \tag{3.45}$$

Difference between these two Eqs.(3.44) and (3.45) gives propagation current (Eq.(3.46))

$$\begin{aligned} J =& \frac{e_0\hbar}{2m_0 i}\left(-2i|a|^2 + 2i|b|^2\right) \\ J =& \frac{e_0\hbar}{m_0}\left(-|a|^2 + |b|^2\right) \end{aligned} \tag{3.46}$$

In the lead $|R|^2 = 1$ that implies current is zero in the lead. Lead plays a role as voltage probe. To Find the expression of current in region II we have to consider only second square bracketd term. Sign convention just depends on your choice from Kirchhoff's law total current ia always zero. When $\Phi = 0$, there is no current known as equilibrium current. This equilibrium current called persistent current. Current expression is for propagation current in Eq.(3.46). For case $E < e_0\,U$, evanescent current will be discussed in Chapter 7 of this thesis. This 1D quantum ring gives us three prong potential shown in figure 3.4. Applying boundary conditions at J_1

$$\begin{aligned} 1 + r &= t \\ i\,k\,(1 - r) - i\,k\,2\,t &= 0 \end{aligned} \tag{3.47}$$

Thus, the reflection and transmission values at junction J_I are $t = -\frac{2}{3}$ and, $r = -\frac{1}{3}$.

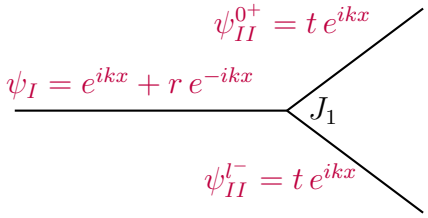

Figure 3.4: The junction J_1 in figure 3.3 where the lead connects to the ring, in isolation. It is three prong structure with reflection $r = -\frac{1}{3}$ and transmission $t = -\frac{2}{3}$.

3.4 Inclusion of magnetic field: Feynman path approach

As we have discussed in Section 3.1 that a quantum particle in a finite-thickness ring or disc can have many possible alternate classical trajectories to go from one point in the system to another. A classical particle chooses one particular trajectory from them which is determined by the least action principle. However, a quantum particle does not do that and in fact there are several alternate physical pictures that different schools have introduced. All these alternate pictures lead to the same final result. For example the Copenhagen school says that the quantum particle propagates as a wave as long as we leave it alone but as soon as we try to observe it, it tries to acquire particle like behaviour. The Feynman path approach is an alternate picture to that by which we say that the particle (not a wave) simultaneously go through all possible classical trajectories weighted down by the action along these trajectories that give a phase term. So different trajectories result in different phases and the amplitudes for different trajectories interfere to give the same final result as the Copenhagen school. Even for the 1D system of figure 3.3, an infinite number of trajectories are possible. Below we will use this Feynman path approach to justify the boundary conditions of Eqs.(3.40) and (3.41), which will also be a simple demonstration of how the Feynman path approach is applied. This has been briefly touched upon in [2] book on page 63, for the square well problem. Below we do it for the Aharonov-Bohm (AB) ring of figure 3.3.

In Feynman path approach, the system 1D quantum ring is decoupled into smaller parts or trajectories as would be necessary and explained below. These trajectories by an electron is broken at $x = 0^+$ and $x = l^-$ in figure 3.5. This method will help us to determine the wave functions in different regions. Region I and region II are shown similar to figure 3.3. Therefore the part depicted as region I is the three prong structure shown in figure 3.4. The part depicted as region II is the ring like structure enclosing the flux. This method provides a connection between canonical solutions (leading to Eqs.(3.40) and (3.41)) in quantum mechanics and physical motion resulting in currents through a sample. In the following we present a calculation of the wave function inside

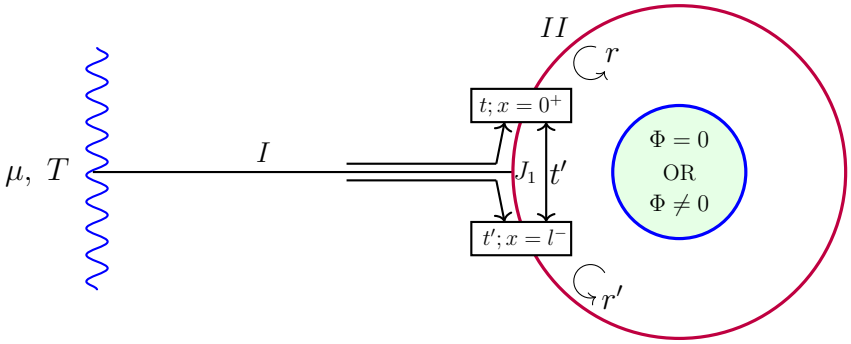

Figure 3.5: Decomposition of the system in figure 3.3 into a three prong structure (depicted as region I) of figure 3.4 and a ring (depicted as region II). t and r are the transmission and reflection amplitudes of figure 3.4 which means $t = \frac{2}{3}$ and $r = -\frac{1}{3}$. t' is related to t and r' is related to r in Eq.(3.60). Usually time reversal symmetry implies $t' = t$.

the ring at $x = 0^+$ and $x = l^-$, using the Feynman path approach. This will also justify the way in which the AB phase enter the boundary conditions expressed in Eqs.(3.40) and (3.41). The twist is that one has to sum the amplitudes for all possible classical trajectories (weighted by their classical action) starting at the near end of the lead ($x = 0^-$) and ending at the point of interest where we intend to find the wave function ($x = 0^+$ or $x = l^-$) inside the ring. To systematically include all possible trajectories, we find a way to classify the trajectories and that can be done by the number of reflections involved and described in detail below as zero reflection terms, first reflection terms etc.

Calculation of waveunction at $x = 0^+$:

a. Zeroth reflection term are written below and every term can be explained with trajectory in figure 3.6.

$$\psi_o^{tt}(0^+) = t\, e^{iql+i\alpha}\, t' + t\, e^{iql+i\alpha}\, t'\, e^{iql+i\alpha}\, t' + ... = \frac{t}{1 - t'\, e^{iql+i\alpha}} \tag{3.48}$$

In above equation superscript tt represents for "through top", subscript 0 represents "zero reflection term" and 0^+ in parenthesis denotes the coordinate where we intend to evaluate the wave function.

b. First reflection term: It can be explained corresponding to figure 3.7

$$\psi_1^{tt}(0^+) = t\, e^{iql+i\alpha}\, r'\, e^{iql-i\alpha} + t\, e^{iql+i\alpha}\, r'\, e^{iql-i\alpha}\, t'\, e^{iql-i\alpha} + ... = \frac{t\, r'\, e^{2iql}}{1 - t'\, e^{iql-i\alpha}} \tag{3.49}$$

c. Second reflection term: It can be explained corresponding to figure 3.8

$$\psi_2^{tt}(0^+) = t\, e^{iql+i\alpha}\, r'\, e^{iql-i\alpha}\, r + t\, e^{iql+i\alpha}\, r'\, e^{iql-i\alpha}\, r\, e^{iql+i\alpha}\, t' + ... = \frac{t\, r\, r'\, e^{2iql}}{1 - t'\, e^{iql+i\alpha}} \tag{3.50}$$

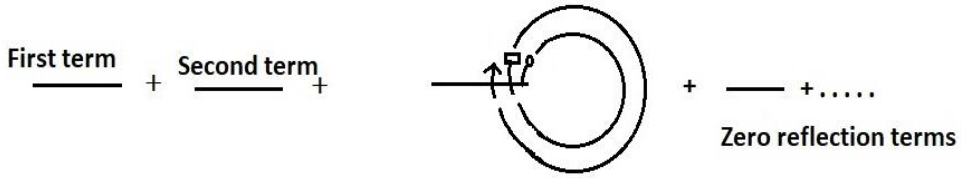

Figure 3.6: The "First term" and the "Second term" are not drawn but can be figured out from the third term which is drawn explicitly. The third term correspond to a Feynman trajectory where an electron comes from the reservoir and at the junction it is transmitted up to the position of the small circle. It then makes a full circle along the ring to reach the position of the small rectangle. And then it continues to make another full circle in the ring to get to the position where the arrow head points. As per the coordinate choice depicted in figure 3.5 this position is $x = 0^+$. The first term will be the situation if this third term is truncated at the small circle. The second term will be the situation when this third term is truncated at the small rectangle. The first term will give the first term in the series leading to Eq.(3.48). The second term will give the second term in the series in Eq.(3.48). The third term will give the third term in the series in Eq.(3.48). For example, getting to the small circle will involve a transmission amplitude of $t = \frac{2}{3}$ (first term in Eq.(3.48)). And then make a full circle propagation with appropriate action require us to multiply a factor $e^{iql+i\alpha}$ and another factor of t' (which may or may not be the same as t as will be discussed subsequently) to get to the small rectangle (second term in Eq.(3.48)). And finally to get to the point $x = 0^+$ at the end of the arrow require another factor of $e^{iql+i\alpha}t'$ (third term). None of the terms in Eq.(3.48) depend on r or r' and so all the terms are classified as zero reflection terms.

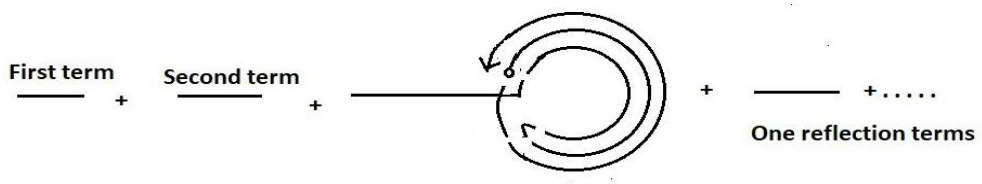

Figure 3.7: One should be able to understand this figure by reading the caption of figure 3.6 and extend the logic. It depicts the Feynman paths leading to the series in Eq.(3.49).

d. Third reflection term (self explanatory from earlier discussion)

$$\psi_3^{tt}(0^+) = t\, e^{iql+i\alpha}\, r'\, e^{iql-i\alpha}\, r\, e^{iql+i\alpha}\, r'\, e^{iql-i\alpha} + t\, e^{iql+i\alpha}\, r'\, e^{iql-i\alpha}\, r\, e^{iql+i\alpha}\, t'\, e^{iql-i\alpha} + ...$$

$$= \frac{t\, r'^2\, r\, e^{4iql}}{1 - t'\, e^{iql-i\alpha}} \tag{3.51}$$

Here, we have evaluated only four terms to reveal that after summation they form two

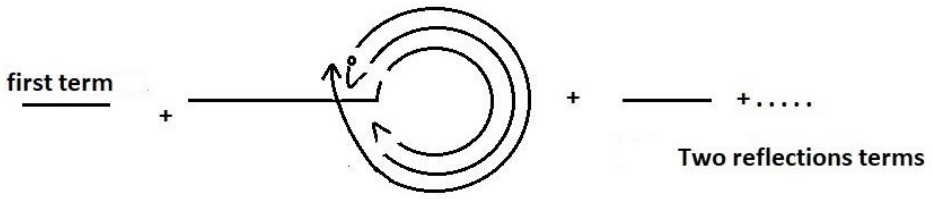

Figure 3.8: It depicts the Feynman paths leading to the series in Eq.(3.50)

geometric series. The even reflection terms and odd reflection terms form two different

series. So contribution to the wavefunction inside the ring at the point $x = 0^+$ coming from these diagrams in figures 3.6, 3.7, 3.8 etc., will be the sum of the RHS of Eqs.(3.48), (3.49), (3.50) and (3.51).

$$\begin{aligned}
\psi^{tt}(0^+) &= \left[\psi_0^{tt}(0^+) + \psi_2^{tt}(0^+) + ...\right] + \left[\psi_1^{tt}(0^+) + \psi_3^{tt}(0^+) + ...\right] \\
\psi^{tt}(0^+) &= \left[\frac{t}{1 - t'\ e^{iql+i\alpha}}(1 + r\ r'\ e^{2iql} + ...) + \frac{t\ r'\ e^{2iql}}{1 - t'\ e^{iql-i\alpha}}(1 + r'\ r\ e^{2iql} + ...)\right] \\
\psi^{tt}(0^+) &= \left[\frac{t}{1 - t'\ e^{iql+i\alpha}}\frac{1}{1 - r'\ r\ e^{2iql}} + \frac{t\ r'\ e^{2iql}}{1 - t'\ e^{iql-i\alpha}}\frac{1}{1 - r\ r'\ e^{2iql}}\right]
\end{aligned} \tag{3.52}$$

For the wavefunction at $x = 0^+$, we can get a different Feynman paths and the difference can be seen by comparings Eqs.(3.48) and (3.53).

g. Zeroth reflection term

$$\psi_0^{tb}(0^+) = t'\ e^{iql-i\alpha} + t'\ e^{iql-i\alpha}\ t'\ e^{iql-i\alpha} + ... = \frac{t'\ e^{iql-i\alpha}}{1 - t'\ e^{iql-i\alpha}} \tag{3.53}$$

Here tb shows for "through bottom".

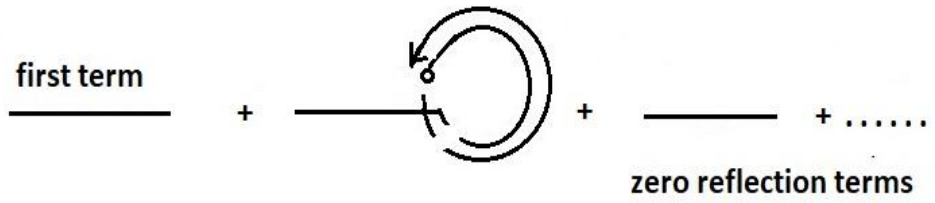

Figure 3.9: It depicts the Feynman paths leading to the series in Eq.(3.53)

h. First reflection term

$$\psi_1^{tb}(0^+) = t'\ e^{iql-i\alpha}\ r + t'\ e^{iql-i\alpha}\ r\ e^{iql+i\alpha}\ t' + ... = \frac{t'\ r\ e^{iql-i\alpha}}{1 - t'\ e^{iql+i\alpha}} \tag{3.54}$$

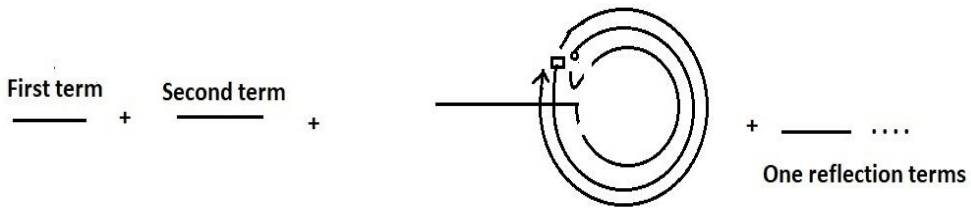

Figure 3.10: It depicts the Feynman paths leading to the series in Eq.(3.54).

i. Second reflection term

$$\psi_2^{tb}(0^+) = t'\ e^{iql-i\alpha}\ r\ e^{iql+i\alpha}\ r'\ e^{iql-i\alpha} + ...t'\ e^{iql-i\alpha} + ... = \frac{t'\ r\ r'\ e^{3iql-i\alpha}}{1 - t'\ e^{iqli\alpha}} \tag{3.55}$$

j. Third reflection term

$$\psi_3^{tb}(0^+) = t'\ e^{iql-i\alpha}\ r\ e^{iql+i\alpha}\ r'\ e^{iql-i\alpha}\ r + ...e^{iql+i\alpha}\ t' + ... = \frac{t'\ r^2\ r'\ e^{3iql-i\alpha}}{1-t'\ e^{iql+i\alpha}} \tag{3.56}$$

Again from Eqs.(3.53), (3.54), (3.55), and (3.56) give the contribution to the wavefunction inside the ring at the point $x = 0^+$ coming from these diagrams will again form two geometric series,

$$\begin{aligned}
\psi^{tb}(0^+) &= \left[\psi_0^{tb}(0^+) + \psi_2^{tb}(0^+) + ...\right] + \left[\psi_1^{tb}(0^+) + \psi_3^{tb}(0^+) + ...\right] \\
\psi^{tb}(0^+) &= \left[\frac{t'\ e^{iql-i\alpha}}{1-t'\ e^{iql-i\alpha}}(1 + r\ r'\ e^{2iql} + ...) + \frac{t'\ r\ e^{iql-i\alpha}}{1-t'\ e^{iql+i\alpha}}(1 + r'\ r\ e^{2iql} + ...)\right] \\
\psi^{tb}(0^+) &= \left[\frac{t'\ e^{iql-i\alpha}}{1-t'\ e^{iql-i\alpha}}\frac{1}{1-r'\ r\ e^{2iql}} + \frac{t'\ r\ e^{iql-i\alpha}}{1-t'\ e^{iql+i\alpha}}\frac{1}{1-r\ r'\ e^{2iql}}\right]
\end{aligned} \tag{3.57}$$

Net wavefunction at $x = 0^+$ in figure 3.5 from Eqs.(3.52) and (3.57)

$$\begin{aligned}
\psi(0^+) &= \left[\psi^{tt}(0^+)\right] + \left[\psi^{tb}(0^+)\right] \\
\psi(0^+) &= \left[\frac{t}{1-t'\ e^{iql+i\alpha}}\frac{1}{1-r\ r'\ e^{2iql}} + \frac{t\ r'\ e^{2iql}}{1-t'\ e^{iql-i\alpha}}\frac{1}{1-r\ r'\ e^{2iql}}\right] \\
&\quad + \left[\frac{t'\ e^{iql-i\alpha}}{1-t'\ e^{iql-i\alpha}}\frac{1}{1-r\ r'\ e^{2iql}} + \frac{t'\ r\ e^{iql-i\alpha}}{1-t'\ e^{iql+i\alpha}}\frac{1}{1-r\ r'\ e^{2iql}}\right] \\
\psi(0^+) &= \left[\frac{t}{1-r\ r'\ e^{2iql}}\left(\frac{1}{1-t'\ e^{iql+i\alpha}} + \frac{r'}{1-t'\ e^{iql+i\alpha}}\right)\right] \\
&\quad + \left[\frac{t'\ e^{iql-i\alpha}}{1-r\ r'\ e^{2iql}}\left(\frac{1}{1-t'\ e^{iql-i\alpha}} + \frac{r}{1-t'\ e^{iql+i\alpha}}\right)\right]
\end{aligned}$$

It is the form of $a + be^{-i\alpha}$, where

$$a = \frac{t}{1-r\ r'\ e^{2iql}}\left[\frac{1}{1-t'\ e^{iql+i\alpha}} + \frac{r'\ e^{2iql}}{1-t'\ e^{iql-i\alpha}}\right] \tag{3.58}$$

$$b = \frac{t'\ e^{iql}}{1-r\ r'\ e^{2iql}}\left[\frac{1}{1-t'\ e^{iql-i\alpha}} + \frac{r}{1-t'\ e^{iql+i\alpha}}\right] \tag{3.59}$$

Note that

$$r'e^{2iql} = r \tag{3.60}$$

this relation shows a relationship between r' and r. That means how r varies in presence of flux and if flux is zero $r'e^{2iql}$ will be equal to r. In absence of flux there is no current and in presence of flux, flux breaks the symmetry between a and b to give rise to current in the ring which magnetises the ring. This current is called purely equilibrium current

described earlier, also known as perpetual current. This current is produced due to interference effect and Aharonov-Bohm effect. This current has no need to driven any classical force.

Calculation of wavefunction at $x = l^-$: There is another set of diagrams for the wavefunction at $x = l^-$.

a. Zeroth reflection term

$$\psi_0^{tb}(l^-) = t' + t'e^{iql-i\alpha}t' + t'e^{iql-i\alpha}t'e^{iql-i\alpha}t' + ... = \frac{t'}{1 - t'e^{iql-i\alpha}} \tag{3.61}$$

b. First reflection term

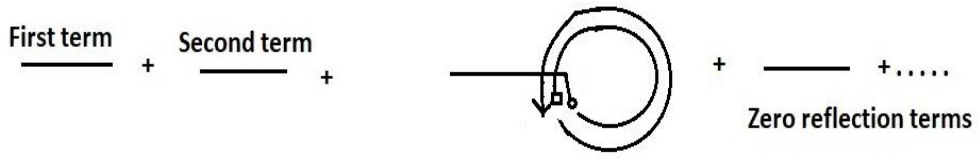

Figure 3.11: It depicts the Feynman paths leading to the series in Eq.(3.61).

$$\psi_1^{tb}(l^-) = t'\ e^{iql-i\alpha}\ r\ e^{iql+i\alpha} + t'\ e^{iql-i\alpha}\ r\ e^{iql+i\alpha}\ t'\ e^{iql+i\alpha} + ... = \frac{t'\ r\ e^{2iql}}{1 - t'\ e^{iql+i\alpha}} \tag{3.62}$$

c. Second reflection term

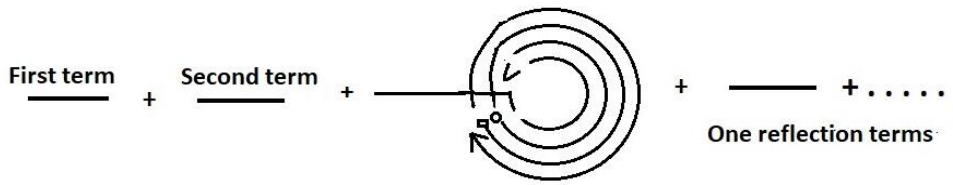

Figure 3.12: It depicts the Feynman paths leading to the series in Eq.(3.62).

$$\psi_2^{tb}(l^-) = t'\ e^{iql-i\alpha}\ r\ e^{iql+i\alpha}\ r' + t'\ e^{iql-i\alpha}\ r\ e^{iql+i\alpha}\ r'\ e^{iql-i\alpha}\ t' + ... = \frac{t'\ r\ r'\ e^{2iql}}{1 - t'\ e^{iql-i\alpha}} \tag{3.63}$$

d. Third reflection term

$$\psi_3^{tb}(l^-) = t'\ e^{iql-i\alpha}\ r\ e^{iql+i\alpha}\ r'\ e^{iql-i\alpha}\ r\ e^{iql+i\alpha} + t'\ e^{iql+i\alpha} + ... = \frac{t'\ r^2\ r'\ e^{4iql}}{1 - t'\ e^{iql+i\alpha}} \tag{3.64}$$

From Eqs.(3.61), (3.62), (3.63), and (3.64) give the contribution to the wavefunction inside the ring at the point $x = l^-$ coming from these diagrams will again form two

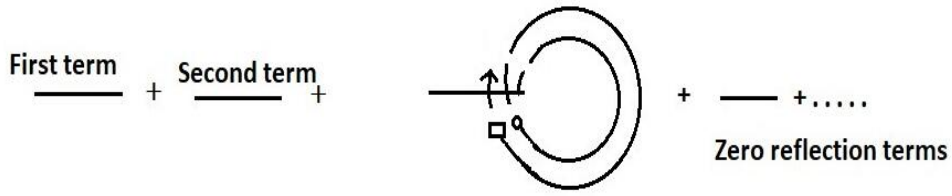

Figure 3.13: It depicts the Feynman paths leading to the series in Eq.(3.13).

geometric series to give,

$$\psi^{tb}(l^-) = \left[\psi_0^{tb}(l^-) + \psi_2^{tb}(l^-) + ...\right] + \left[\psi_1^{tb}(l^-) + \psi_3^{tb}(l^-) + ...\right]$$
$$\psi^{tb}(l^-) = \left[\frac{t'}{1 - t'\ e^{iql - i\alpha}}(1 + r\ r'\ e^{2iql} + ...) + \frac{t'\ r\ e^{2iql}}{1 - t'\ e^{iql+i\alpha}}(1 + r'\ r\ e^{2iql} + ...)\right]$$
$$\psi^{tb}(l^-) = \left[\frac{t'}{1 - t'\ e^{iql - i\alpha}}\frac{1}{1 - r'\ r\ e^{2iql}} + \frac{t'\ r\ e^{2iql}}{1 - t'\ e^{iql+i\alpha}}\frac{1}{1 - r\ r'\ e^{2iql}}\right] \tag{3.65}$$

a. Zeroth reflection term

$$\psi_0^{tt}(l^-) = t\ e^{iql+i\alpha} + t\ e^{iql+i\alpha} t'\ e^{iql+i\alpha} + ... = \frac{t\ e^{iql+i\alpha}}{1 - t'\ e^{iql+i\alpha}} \tag{3.66}$$

b. First reflection term

$$\psi_1^{tt}(l^-) = t\ e^{iql+i\alpha}\ r' + t\ e^{iql+i\alpha}\ r'\ e^{iql-i\alpha}\ t' + ... = \frac{t\ r'\ e^{iql+i\alpha}}{1 - t'\ e^{iql-i\alpha}} \tag{3.67}$$

c. Second reflection term

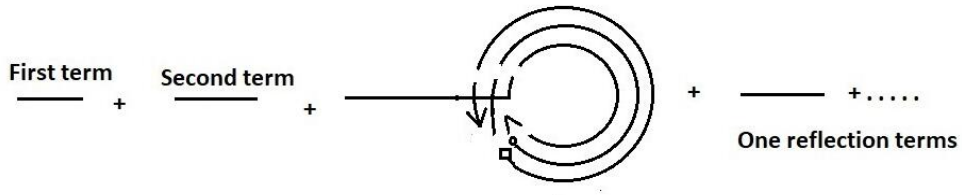

Figure 3.14: It depicts the Feynman paths leading to the series in Eq.(3.67).

$$\psi_2^{tt}(l^-) = t\ e^{iql+i\alpha}\ r'\ e^{iql-i\alpha}\ r\ e^{iql+i\alpha} + t\ e^{iql+i\alpha}\ r'\ e^{iql-i\alpha}\ r\ e^{iql+i\alpha}\ t'\ e^{iql+i\alpha} + ...$$
$$= \frac{t'\ r\ r'\ e^{3iql+i\alpha}}{1 - t'\ e^{iql+i\alpha}} \tag{3.68}$$

d. Third reflection term

$$\psi_3^{tt}(l^-) = t\, e^{iql+i\alpha}\, r'\, e^{iql-i\alpha}\, r\, e^{iql+i\alpha}\, r' + ...e^{iql-i\alpha}\, t' + ... = \frac{t\, r\, r'^2\, e^{3iql+i\alpha}}{1 - t'\, e^{iql-i\alpha}} \tag{3.69}$$

From Eqs.(3.66), (3.67), (3.68), and (3.69) give the contribution to the wavefunction inside the ring at the point $x = l^-$ coming from these diagrams will again form two geometric series to give,

$$\begin{aligned}
\psi^{tt}(l^-) &= \left[\psi_0^{tt}(l^-) + \psi_2^{tt}(l^-) + ...\right] + \left[\psi_1^{tt}(l^-) + \psi_3^{tt}(l^-) + ...\right] \\
\psi^{tt}(l^-) &= \left[\frac{t\, e^{iql+i\alpha}}{1 - t'\, e^{iql+i\alpha}}(1 + r\, r'\, e^{2iql} + ...) + \frac{t\, r'\, e^{iql+i\alpha}}{1 - t'\, e^{iql-i\alpha}}(1 + r'\, r\, e^{2iql} + ...)\right] \\
\psi^{tt}(l^-) &= \left[\frac{t\, e^{iql+i\alpha}}{1 - t'\, e^{iql+i\alpha}} \frac{1}{1 - r'\, r\, e^{2iql}} + \frac{t\, r'\, e^{iql+i\alpha}}{1 - t'\, e^{iql-i\alpha}} \frac{1}{1 - r\, r'\, e^{2iql}}\right]
\end{aligned} \tag{3.70}$$

Net wavefunction at $x = l^-$ in figure 3.5 from Eqs.(3.65) and (3.70)

$$\begin{aligned}
\psi(l^-) &= \left[\psi^{tb}(l^-)\right] + \left[\psi^{tt}(l^-)\right] \\
\psi(l^-) &= \left[\frac{t'}{1 - t'\, e^{iql-i\alpha}} \frac{1}{1 - r\, r'\, e^{2iql}} + \frac{t'\, r\, e^{2iql}}{1 - t'\, e^{iql+i\alpha}} \frac{1}{1 - r\, r'\, e^{2iql}}\right] \\
&\quad + \left[\frac{t\, e^{iql+i\alpha}}{1 - t'\, e^{iql+i\alpha}} \frac{1}{1 - r\, r'\, e^{2iql}} + \frac{t\, r'\, e^{iql+i\alpha}}{1 - t'\, e^{iql-i\alpha}} \frac{1}{1 - r\, r'\, e^{2iql}}\right] \\
\psi(l^-) &= \left[\frac{t\, e^{iql+i\alpha}}{1 - r\, r'\, e^{2iql}} \left(\frac{1}{1 - t'\, e^{iql+i\alpha}} + \frac{r'}{1 - t'\, e^{iql-i\alpha}}\right)\right] \\
&\quad + \left[\frac{t'}{1 - r\, r'\, e^{2iql}} \left(\frac{1}{1 - t'\, e^{iql-i\alpha}} + \frac{r\, e^{2iql}}{1 - t'\, e^{iql+i\alpha}}\right)\right]
\end{aligned}$$

It is the form of $ae^{iql+i\alpha} + be^{-iql}$ where,

$$a = \frac{t}{1 - r\, r'\, e^{2iql}} \left[\frac{1}{1 - t'\, e^{iql+i\alpha}} + \frac{r'}{1 - t'\, e^{iql-i\alpha}}\right] \tag{3.71}$$

$$b = \frac{t'\, e^{iql}}{1 - r\, r'\, e^{2iql}} \left[\frac{1}{1 - t'\, e^{iql-i\alpha}} + \frac{r\, e^{2iql}}{1 - t'\, e^{iql+i\alpha}}\right] \tag{3.72}$$

Note that

$$r' = r\, e^{2iql} \tag{3.73}$$

again with substituting this expressions for a and b become the same in absence of magnetic field. Also notice that it will give same current as that from Eqs.(3.71) and (3.72) at $x = 0^+$.

3.5 1.6 Scattering phase shift and DOS

Note that in figure 3.2 the coordinate in the right lead is taken as x' with the $x' = 0$ point depicted in the figure. $x = 0$ point is also depicted. One can write the wave function on the right as

$$\psi(x \geq l) = te^{ik(x-l)} = te^{-ikl}e^{ikx} = t'e^{ikx} \tag{3.74}$$

In this picture in absence of potential $t' = 1$, as the wave-function at $x = l$ should be e^{ikl}. So the entity $t = e^{ikl}$ in absence of scatterer. So in the absence of the potential, the phase of t i.e., θ_t will be

$$\theta_t = kl$$

Therefore, its derivative with respect to incident energy E will be

$$\frac{d\theta_t}{dE} = \frac{d\theta_t}{dk}\frac{dk}{dE} = \frac{d(kl)}{dk}\frac{1}{\frac{dE}{dk}} = l\frac{1}{\frac{d}{dk}\frac{\hbar^2k^2}{2m_0}} = \frac{2m_0l}{\hbar^2}\frac{1}{2k} = \frac{m_0l}{\hbar^2k} = \frac{2\pi l}{h}\frac{1}{\frac{\hbar k}{m_0}} = 2\pi l\frac{1}{hv}$$

The factor 2 comes because when we write the dispersion relation as $E = \frac{\hbar^2k^2}{2m_0}$ then both $\pm k$ states are taken into account. Therefore,

$$\frac{d\theta_t}{dE} = \pi\rho_0 \tag{3.75}$$

where $\rho_0 = \frac{1}{hv_0}$ per unit length is 1D DOS in absence of scatterer. Up to this the potential U is zero. We can either call t' to be the scattering amplitude or call t to be the scattering amplitude. In the first picture the scattering phase shift is the phase of t' and it is zero while in the second picture the scattering phase shift is the phase of t which is $\theta_t = kl$. Difference between t' and t is just a shift of origin.

In presence of a potential $U \neq 0$ again depending on where we fix the origin, we may work with t or with t'. In presence of scatterer one can show (see Chapter 4)

$$\frac{d\theta_t}{dE} \approx \pi\rho \tag{3.76}$$

As is evident from Eq.(3.74) that

$$\theta_{t'} = \theta_t - kl \tag{3.77}$$

This implies from Eqs.(3.75) and (3.76)

$$\frac{d\theta_{t'}}{dE} \approx \pi(\rho - \rho_0) \tag{3.78}$$

We will work with $te^{ik(x-l)}$ or $te^{ikx'}$ means x' is a new coordinate system that is 0 at $x = l$. It is just a change of variable but it makes keeping track of phase changes with

respect to the initial phase easier. In fact if the system has many such constituent parts joined by junctions, then it is suitable to assign a new origin for each region. However, the reflection and transmission at the different junctions in the Feynman path approach has to be appropriately corrected for the necessary phase factor required. For example in figure 3.4 t is transmission amplitude of the three prong potential and r is the reflection amplitude. A simple calculation shows $t = 2/3$ and $r = -1/3$. This is the special case for the system solved in detail in Chapter 5. However, when the reflection occurs at $x = l$ then the reflection amplitude should be written as r' and it is related to r as follows.

$$\langle re^{-ik0^-} | \, | e^{ik0^-} \rangle = \langle r' e^{-ikl^-} | \, | e^{ikl^-} \rangle \tag{3.79}$$

This explains the substitution used in Eq.(3.60). r' is the reflection amplitude at $x = l$ while r is the reflection amplitude at $x = 0$. By symmetry, the amplitude of r and r' will be the same and equal to $-\frac{1}{3}$ but their phases will differ. This can be further understood by comparing figures 3.5 and 3.6. For the same reason Eqs.(3.71) and (3.72) is explained since only anticlockwise moving $-k$ states are reflected at $x = 0$.

This chapter gives us an elementary introduction to open mesoscopic systems. A clear interpretation on mesoscopic systems is explored, including the Aharonov-Bohm effect, electron wavefunction in both absence and presence of magnetic field, current expressions, Landauer formalisms, and how to incorporate the Aharonov-Bohm flux in presence of magnetic field.

CHAPTER 4

LARMOR CLOCK AND HIERARCHY OF DENSITY OF STATES

In this chapter, we present a systematic derivation of Friedel Sum Rule (FSR) for mesoscopic systems [9, 10, 36] which is quite different from that used in condensed matter physics [66] in the sense that it consists of a hierarchy of formulas rather than a single formula. FSR like formulas are extensively used in condensed matter systems that are usually semi-classical. It eventually leads to a similar relation between density of states (DOS) and scattering phase shifts, but with important correction terms to the formula presented in condensed matter textbooks [66]. These formulas form the basic foundation for understanding mesoscopic systems [9, 67]. In Chapters 5, 6 and 7, we will show that the phase lapses discussed in [9, 15] further complicates the hierarchy of formulas, in fact in a beneficial manner. One can also give a proper interpretation of Landauer's phenomenology from Larmor clock theory which is consistent physically and theoretically.

In Section 4.1, we derive the Larmor precession time from Larmor clock theory. In Section 4.2, we classify objects of hierarchy of density of states (DOS) in detail. We will further elaborate these local objects of hierarchy in the next subsequent chapters with respect to the phase lapses [9, 27, 29].

4.1 Larmor precession time

In this section, we present a systematic derivation of the density of states (DOS) hierarchy based on the classical concept of Larmor precession. It is an elaboration of the proof presented by M. Buttiker [8]. Suppose there is an arbitrary potential $U(y)$ in figure 4.1. A quantum particle with unit charge is propagating in y-direction. The way we are going

to derive the objects of hierarchy, it can be considered as a scattering problem as figure 3.2 since potential $U(y)$ is zero at infinite or asymptotically i.e., $|y| \to \infty$ or $U(y) = 0$. The particle stationary beam has a spin polarised in the x-direction shown by dashed arrow in the figure 4.1. The incident stationary beam consists of an ensemble of particles. There is no net spin in y-direction and z-direction. This quantum ensemble (or wave packet) is different from mesoscopic grand canonical ensemble in the sense that even at zero temperature quantum ensemble can have fluctuations. The scattering matrix element, in the absence of the magnetic field $\vec{B}$, is given by $s_{\alpha\beta}(E, U(y))$ for spin up as well as spin down particles is a function of energy and functional of potential. Here, α and β are incoming and outgoing indices for asymptotic modes. Suppose there is a small non-uniform magnetic field $B(y)$ applied in the z-direction in the region where the potential $U(y)$ is non-zero, shown in figure 4.1. The presence of this small non-uniform magnetic field $B(y)$ induces spin dynamics. We are interested in the spin dynamics due to this small non-uniform magnetic field $B(y)$ which means $U(y)$ may well be an electrostatic potential but the magnetic field will add an infinitesimal potential on the spin that is attached to an electron charge. The electronic charge will feel the potential given by the dotted line in figure 4.1 while a spin attached to the charge will feel a potential that is given by the difference between the solid line and dotted line in figure 4.1 (in 1D $\vec{v} \times \vec{B} = 0$, beside $\vec{v}$ which is always in units of the velocity of light is extremely small and so is $\vec{B}$ which is an infinitesimal perturbation wherein higher order terms will be ignored). The magnetic field however creates a potential $\delta U(y)$ on the spin. Conventionally speaking, a rotating charge in a magnetic field creates a magnetic moment $\vec{\mu} = \frac{e_0}{2m_0}\vec{L}$. This is true classically as well as quantum mechanically as the $\hbar$ factor comes from the quantum mechanical calculation of $\hat{L}$. This $\hat{L}$ is orbital angular momentum operator while $\vec{L}$ is orbital angular momentum. We may use this analogy to say that associated with the spin of an electron there is a magnetic moment operator $\hat{\mu} = \frac{e_0}{2m_0}\hat{S}_z$. However, that is not rigorously true and it need two corrections that have completely different origins, and yet they almost cancel each other. The first correction is that $\hat{L}$ is quantised in units of $\hbar$ while $\hat{S}_z$ is in units of $\frac{\hbar}{2}$. Conventionally, we say when magnetic field is applied, magnetic moments experience a torque because of which they precess about the magnetic field but this is not at all necessary for the analysis to follow. This statement is generally made to draw an analogy between a precessing top and a precessing magnetic moment. If one wants to think of gravity as a force $\vec{F}$ then one tends to say that there is a torque given $\vec{\tau} = \vec{r} \times \vec{F}$ which makes the top precess but note that this is just an alternate way of thinking because after all gravity is not a force while electromagnetic interaction is a force. A spinning top on earth is equivalent to a spinning top in an accelerated reference frame and so the angle of precession has to comply with transformation properties of angles. Electric and magnetic fields too has to satisfy similar transformation properties but trying to draw such parallels

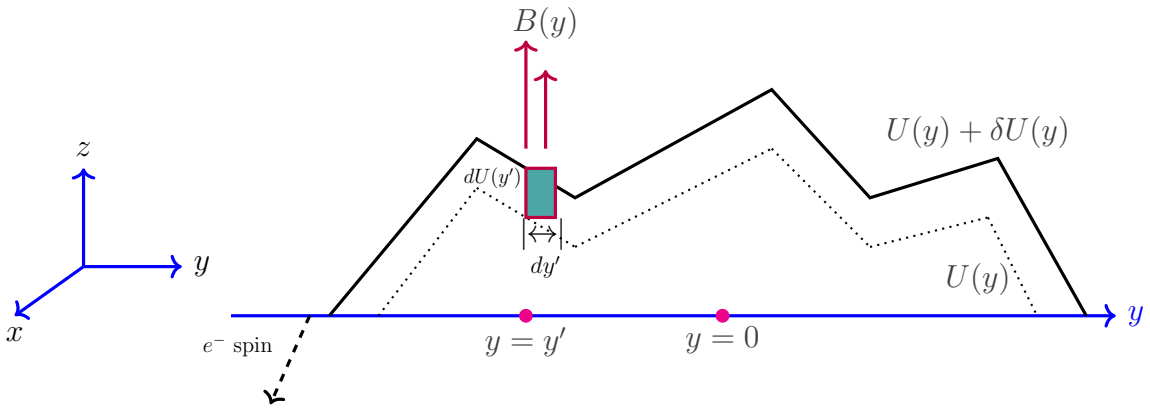

Figure 4.1: A schematic figure of an arbitrary scattering potential $U(y)$ with dotted line is shown. Thick solid line represents potential $U(y) + \delta U(y)$ where $\delta U(y)$ is a very small functional change in potential $U(y)$ due to a magnetic field in the z-direction. The dashed arrow represents incident particle beam spin polarised in x-direction. The magnetic field $B(y)$ is non-uniform (shown by arrows) in the y-direction. A differential change in potential $dU(y')$ at $y = y'$ is shown by the shaded square block between the dotted and solid lines. The area of this block $dU(y')dy'$ is therefore an integration measure. The axis directions and origin marked $y = 0$ are shown in the figure. As usual the region to the left of the potential is the left lead that can be labelled β and that to the right can be labelled α. So the incident particle or spin is coming from β and going towards α.

is not productive now. To analyse the problem quantum mechanically, we can discuss everything in an absolute stationary frame of reference as we will get stationary states as shown below. This is like quantum mechanically calculating the radius of a hydrogen atom where we do not discuss any boosted or accelerated reference frame.

Energy of a magnetic moment in a constant magnetic field $\vec{B}$ is $\delta U = -\vec{\mu}\cdot\vec{B}$. Typically, the terms "total spin operator" and "z-component of the spin operator" refer to the operators $\hat{S}$ and $\hat{S}_z$, respectively. In quantum physics, the total spin operator $\hat{S}$ represents the total angular momentum associated with a particle's spin. The z-component of the spin operator $\hat{S}_z$ explicitly projects the spin angular momentum along the z-axis. We know that $\hat{S}$ and $\hat{S}_z$ have simultaneous eigenfunctions. Hence $\hat{H}_s = -\hat{\mu}\cdot B = -\frac{g_\gamma e_0}{2m_0}\hat{S}_z \cdot B$, where H_s is the Hamiltonian of a quantum spin and g_γ is the gyromagnetic ratio, which is 2 for spin. Eigenfunction of the Hamiltonian of quantum spin will be spin half in positive z-direction denoted as $|+\rangle$ will have an eigenvalue $E_u = -\frac{g_\gamma e_0 B}{2m_0}\frac{\hbar}{2}$. Similarly, there will be an eigenfunction $|-\rangle$ with an eigenvalue $E_d = \frac{g_\gamma e_0 B}{2m_0}\frac{\hbar}{2}$. Therefore, the separation between the two eigenvalues can be written as $\hbar\omega = E_d - E_u = \frac{e_0 B}{m_0}\hbar$ or in other words $\omega = \frac{e_0 B}{m_0}$. Hence, in this eigenbasis, one can write $\hat{H}_s = \omega\hat{S}_z = \omega_L\hat{S}_z$. Where, ω_L is the classical Larmor frequency in analogy with a precessing angular momentum. We have seen that in going from classical angular momentum to angular momentum operator in quantum mechanics, we can just take that the eigenvalues of the angular momentum operator is quantised in units of $\hbar$. While for spin angular momentum there will be a $g_\gamma\frac{\hbar}{2} = \hbar$. Thus, the time evolution operator is $e^{-\frac{igH_s t}{\hbar}} = e^{-\frac{i\omega_L\hat{S}_z t}{\hbar}}$. Now, the eigenfunctions $|+\rangle$ and $|-\rangle$ can be used as a basis to write down an arbitrary spin state. So if we start with a spin

state written as a linear combination at $t = 0$

$$\psi(t=0) = \frac{1}{\sqrt{2}}|+\rangle + \frac{1}{\sqrt{2}}|-\rangle \tag{4.1}$$

and after time t

$$\psi(t \neq 0) = \frac{1}{\sqrt{2}} e^{-i\frac{\omega_L}{2}t}|+\rangle + \frac{1}{\sqrt{2}} e^{i\frac{\omega_L}{2}t}|-\rangle \tag{4.2}$$

The expectation value of $\langle \hat{S}_x \rangle$ can be computed as

$$\left\langle \hat{S}_x \right\rangle = \left(\frac{1}{\sqrt{2}} e^{\frac{i\omega_L t}{2}} \langle + | + \frac{1}{\sqrt{2}} e^{\frac{-i\omega_L t}{2}} \langle - | \right) \hat{S}_x \left(\frac{1}{\sqrt{2}} e^{\frac{-i\omega_L t}{2}} |+\rangle + \frac{1}{\sqrt{2}} e^{\frac{i\omega_L t}{2}} |-\rangle \right) \tag{4.3}$$

where, $\hat{S}_x = \frac{\hbar}{2}\hat{\sigma_x} = \frac{\hbar}{2}\begin{pmatrix} 0 & 1 \\ 1 & 0 \end{pmatrix}$ and after using the properties $\hat{\sigma_x}|+\rangle = |-\rangle$; $\hat{\sigma_x}|-\rangle = |+\rangle$, we get

$$\left\langle \hat{S}_x \right\rangle = \frac{\hbar}{2}\left\langle \hat{\sigma_x} \right\rangle = \frac{\hbar}{2}\cos(\omega_L t) \tag{4.4}$$

Similarly, the expectation value $\hat{S}_y$ can also computed, where, $\hat{S}_y = \frac{\hbar}{2}\hat{\sigma_y} = \frac{\hbar}{2}\begin{pmatrix} 0 & -i \\ i & 0 \end{pmatrix}$ and again after using the properties $\hat{\sigma_y}|+\rangle = i|-\rangle$; $\hat{\sigma_y}|-\rangle = -i|+\rangle$, we get

$$\left\langle \hat{S}_y \right\rangle = \frac{\hbar}{2}\left\langle \hat{\sigma_y} \right\rangle = \frac{\hbar}{2}\sin(\omega_L t) \tag{4.5}$$

Thus, we get stationary oscillations with frequency ω_L which we call Larmor frequency. Note that while for a rotating top the precession angle increases continuously, the quantum problem yields stationary state solutions. So a y dependent magnetic field is taken to subject the spin to a classical force in the y-direction given by $-\frac{\delta}{\delta y}\left(\mu \cdot B(y)\right) = -\frac{\delta}{\delta y}\delta U(y)$ and expect that in the y-direction the spin will change with time. Thus, the scattering matrix element can be expanded in the presence of small magnetic field

$$s^{\pm}_{\alpha\beta}(E, U(y) \mp \delta U(y)) = s_{\alpha\beta}(E, U(y)) \mp \int dy' \frac{\delta s_{\alpha\beta}(E, U(y'))}{\delta U(y')} \delta U(y') + ... \tag{4.6}$$

$\frac{s_{\alpha\beta}(E,U(y'))}{\delta U(y')}$ is a functional derivative. This is a general situation which in a special case for a differential change in potential at the fixed point $y = y'$ can be written as

$$s^{\pm}_{\alpha\beta}(E, U(y') \mp dU(y')) = s_{\alpha\beta}(E, U(y')) \mp \left[\frac{ds_{\alpha\beta}(E, U(y'))}{dU(y')} \right] dU(y')dy' + ... \tag{4.7}$$

The asymptotic states is a natural choice for the basis states of a scattering problem which in this case is a spinor. The basis spinor which we use to calculate the precession

angle of transmitted particles is given by

$$|\psi_2\rangle = \begin{bmatrix} \psi_2^+ \\ \psi_2^- \end{bmatrix} = \frac{1}{\sqrt{|s_{21}^+|^2 + |s_{21}^-|^2}} \begin{bmatrix} s_{21}^+ \\ s_{21}^- \end{bmatrix} \tag{4.8}$$

Incoming index is $\beta = 1$ and outgoing index is $\alpha = 2$. Likewise, $\beta = 1$ and $\alpha = 1$ can be used to do the same analysis for reflected particles while $\beta = 2$ will correspond to particles incident from the right. Here, $|\psi_2\rangle$ is transmitted wave vector, ψ_2^+ is the spin up component and ψ_2^- is the spin down component in transmitted channel 2. Here, $s_{\alpha\beta}^+$ and $s_{\alpha\beta}^-$ are the scattering matrix for spin up and spin down particles. For the scattering defined in figure 4.1, the expectation value of the y-component of spin in the transmitted channel is,

$$\langle \hat{S}_y \rangle_2 = \langle \psi_2 | \frac{\hbar}{2} \hat{\sigma}_y | \psi_2 \rangle \tag{4.9}$$

here, $\hat{\sigma_y}$ is y-component of Pauli matrices. The suffix 2 implies that we are taking transmitted channel.

$$\begin{aligned} \langle \hat{S}_y \rangle_2 =& \frac{\hbar}{2} \frac{1}{|s_{21}^+|^2 + |s_{21}^-|^2} \begin{bmatrix} s_{21}^{+*} \\ s_{21}^{-*} \end{bmatrix} \begin{bmatrix} 0 & -i \\ i & 0 \end{bmatrix} \begin{bmatrix} s_{21}^+ \\ s_{21}^- \end{bmatrix} \\ =& \frac{\hbar}{2} \frac{1}{|s_{21}^+|^2 + |s_{21}^-|^2} \Big(- i s_{21}^{+*} s_{21}^- + i s_{21}^{-*} s_{21}^+ \Big) = \frac{-i\hbar}{2} \frac{1}{|s_{21}^+|^2 + |s_{21}^-|^2} \Big(s_{21}^{+*} s_{21}^- - s_{21}^{-*} s_{21}^+ \Big) \end{aligned}$$

Using the expansion of $s_{21}^{\pm}$ from Eq.(4.6), we get

$$\begin{aligned} \langle \hat{S}_y \rangle_2 =& \frac{-i\hbar}{2(|s_{21}^+|^2 + |s_{21}^-|^2)} \left[\left(s_{21}^* - \int dy' \frac{\delta s_{21}^*}{\delta U(y')} \delta U(y') \right) \left(s_{21} + \int dy' \frac{\delta s_{21}}{\delta U(y')} \delta U(y') \right) \right] \\ &+ \frac{-i\hbar}{2(|s_{21}^+|^2 + |s_{21}^-|^2)} \left[\left(s_{21}^* + \int dy' \frac{\delta s_{21}^*}{\delta U(y')} \delta U(y') \right) \left(s_{21} - \int dy' \frac{\delta s_{21}}{\delta U(y')} \delta U(y') \right) \right] + ... \end{aligned}$$

Multiplying and retaining the terms up to first order in $\delta U(y')$, one gets

$$\begin{aligned} \langle \hat{S}_y \rangle_2 =& \frac{-i\hbar}{2T} \left[\int dy' s_{21}^* \frac{\delta s_{21}}{\delta U(y')} \delta U(y') - \text{hc} \right] \\ =& \frac{-i\hbar}{2T} \left[\int dy' \left(s_{21}^* \frac{\delta s_{21}}{\delta U(y')} - \text{hc} \right) \delta U(y') \right] \end{aligned}$$

here, $2T = |s_{21}^+|^2 + |s_{21}^-|^2$ and hc is for Hermitian conjugate. Consider that the magnetic field is constant in a small interval $[y, y + dy]$ and takes there the value B. $\delta U(y)$ is the perturbation in potential due to the presence of magnetic field, hence $\delta U(y)$ vanishes everywhere except in the interval $[y, y + dy]$, where it takes the value $dU = \frac{\hbar \omega_L}{2}$. The potential is reduced by $\frac{\hbar \omega_L}{2}$ for spin up particles and increases by $\frac{\hbar \omega_L}{2}$ for spin down particles that leads to the time evolution of a state we get in Eq.(4.2). Therefore, in this

interval, we can drop the integral and then the y-component of spin is given by,

$$\langle \hat{S}_y \rangle_2 = \frac{-i\hbar}{2T}\left[dy'\left(s_{21}^{*}\frac{\delta s_{21}}{\delta U(y')} - \text{hc}\right)\frac{-\hbar\omega_L}{2}\right] \tag{4.10}$$

Therefore, at point y' it is given by

$$\langle \hat{S}_y \rangle_2 = \frac{-i\hbar}{2T}\left[\left(s_{21}^{*}\frac{\delta s_{21}}{\delta U(y)} - \text{hc}\right)\frac{-\hbar\omega_L}{2}\right] \tag{4.11}$$

For unit spin, the y-component developed is given by,

$$\langle \hat{S}_y \rangle_2 \equiv \frac{\langle s_{21}^{y} \rangle}{\frac{\hbar}{2}} = \frac{i\hbar}{2T}\left[\left(s_{21}^{*}\frac{\delta s_{21}}{\delta U(y)} - \text{hc}\right)\omega_L\right] \tag{4.12}$$

The y-component of unit spin is equivalent to angle of precession of the particles. Dividing this quantity, $\langle \hat{S}_y \rangle_2$, by Larmor frequency ω_L, will give a time which is called Larmor precession time (LPT) that will be given by,

$$\tau_{21}^{y}(y', E) = \frac{i\hbar}{2T}\left[\left(s_{21}^{*}\frac{\delta s_{21}}{\delta U(y)} - \text{hc}\right)\right] = \frac{-h}{4\pi i T}\left[\left(s_{21}^{*}\frac{\delta s_{21}}{\delta U(y)} - \text{hc}\right)\right] \tag{4.13}$$

We are dividing a quantity calculated purely from quantum mechanics by the classical Larmor frequency ω_L. This is similar to Landau level eigenenergy divided by $\hbar$ giving cyclotron frequency $\omega_c = \frac{e_0 B}{m_0}$. In Chapters 5 and 6, a view has been presented that this is not an approximation but a consequence of the fact that the scattering matrix elements in quantum mechanics are analytic complex quantities that have to satisfy deeper principles of analyticity. The same calculations can be done for quasi-one dimension (Q-1D), that will be described in details in Chapter 5. To get the time spent by an particle going from β to α at the point $\mathbf{r}$ within the scattering region as given by

$$\tau_{\alpha\beta}(E, \mathbf{r}) = \frac{-h}{4\pi i |s_{\alpha\beta}(E)|^2} Tr\left(s_{\alpha\beta}(E)^{\dagger}\frac{\delta s_{\alpha\beta}(E)}{\delta U(\mathbf{r})} - s_{\alpha\beta}(E)\frac{s_{\alpha\beta}(E)^{\dagger}}{\delta U(\mathbf{r})}\right) \tag{4.14}$$

Tr is trace which represents summation over incident and outgoing transverse channel indices which are generally momentum indices while α and β are spatial indices corresponding to the spatial positions where the leads attach to the sample. Which means we should always follow different notations for indexing spatial channels (incoming and outgoing) and momentum channels (incoming or outgoing). We only require scattering matrix elements and its complex conjugation and no †. From now on position vector will be denoted as $\mathbf{r}$. From Larmor precession time, a hierarchy of density of states (DOS) is introduced in [8], discussed pedagogically in [9, 10], and below.

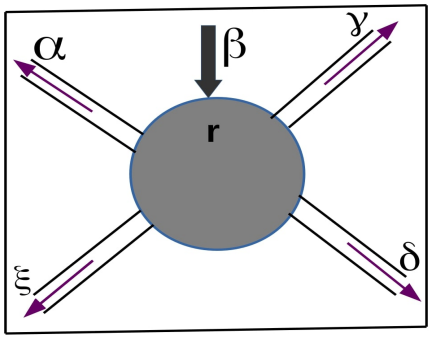

Figure 4.2: This is a schematic picture of a mesoscopic system. The mesoscopic sample is represented by shaded area, attached with several leads shown by α, β, γ and δ etc. indices. The reservoirs are kept at arbitrary value of chemical potentials which can be shown by μ_α, μ_β, μ_γ and μ_δ etc., respectively at zero temperature. The lead β is special lead, it is an scanning tunneling microscope (STM) tip. Lead β draws the current from the sample (or remote point $\mathbf{r}$) and delivers the current to the sample (or remote point $\mathbf{r}$). Rest of the leads are fixed. At zero temperature, the value of chemical potenial of each lead can set to be any.

4.2 Hierarchy of mesoscopic formulas

So far dU was of the dimension of $\vec{\mu}\cdot\vec{B}$, a time $\tau_{\alpha\beta}(E,\mathbf{r})$ which gives the time spent by an electron of incident energy E going from lead β to lead α through the point $\mathbf{r}$ of the potential shown by the dotted line in figure 4.1. The vanishingly small dU can be due to an electrostatic potential as well, and to be dimensionally correct $e_0\,dU$. By engaging the physical processes like Larmor clock and Larmor frequency will see the lowest object of the hierarchy i.e. Larmor Precession Time (LPT or τ_{lpt}). We now change the notation, according to figure 4.2, in order to discuss a hierarchy of relations between scattering phase shifts and DOS to write Larmor precession time of Eq.(4.13) [8, 9]

$$\tau_{lpt}(E,\alpha,\mathbf{r},\gamma) = -\frac{h}{4\pi i|s_{\alpha\gamma}(E)|^2}\left[s^*_{\alpha\gamma}\frac{\delta s_{\alpha\gamma}}{e_0\delta U(\mathbf{r})} - \frac{\delta s^*_{\alpha\gamma}}{e_0\delta U(\mathbf{r})}s_{\alpha\gamma}\right] = -\frac{h}{2\pi}\left[\frac{\delta\theta_{s_{\alpha\gamma}}}{e_0\delta U(\mathbf{r})}\right] \quad (4.15)$$

where $s_{\alpha\gamma} = |s_{\alpha\gamma}|e^{i\theta_{\alpha\gamma}}$, $s^*_{\alpha\gamma} = |s^*_{\alpha\gamma}|e^{-i\theta_{\alpha\gamma}}$ and $\delta s_{\alpha\gamma} = |s_{\alpha\gamma}|e^{i\theta_{\alpha\gamma}}\delta\theta_{\alpha\gamma}$, substitute all these values in Eq.(4.15). One can get LPT in terms of scattering phase shift $\theta_{s_{\alpha\gamma}}$. Similarly, rest of the objects of the hierarchy can be evaluated in terms of scattering phase shift $\theta_{s_{\alpha\gamma}}$. The ordering of the arguments on the LHS is important as $s_{\alpha\gamma}$ is a matrix element. The LHS, in Eq.(4.15), τ_{lpt} represents the time which is spent by an electron at the remote point $\mathbf{r}$, when electron goes from one lead index γ to the other lead index α which is like local version of quantum mechanism. Thus, all three indices γ, $\mathbf{r}$, and α are spatial indices and their ordering is important in all the subsequent formulas we discuss. In the arguments of τ_{lpt}, E is the incident energy of the electron which is equal to the Fermi energy of the respective reservoir. All electrons of an ensemble which incident from lead γ can not pass through the point $\mathbf{r}$, only a fraction of those electrons pass through the point $\mathbf{r}$ to α. Fraction of these number of electrons is given by $|s_{\alpha\gamma}|^2$ which is the

scattering probability of scattered electrons. The fraction $\frac{\delta s_{\alpha\gamma}}{e_0\delta U(\mathbf{r})}$ is a functional derivative of scattering matrix element $s_{\alpha\gamma}$ with respect to the local potential $U(\mathbf{r})$ at the point $\mathbf{r}$ inside the sample, and e_0 is the charge of an electron. Since time spent in a propagation is related to states accessed in the process, both being related to the imaginary part of the Green's function [66] one gets a local partial density of states (LPDOS) or ρ_{lpd} defined as $\frac{|s_{\alpha\gamma}(E)|^2}{h}\tau_{lpt}$.

$$\rho_{lpd}(E,\alpha,\mathbf{r},\gamma) = -\frac{1}{4\pi i}\left[s^*_{\alpha\gamma}\frac{\delta s_{\alpha\gamma}}{e_0\delta U(\mathbf{r})} - \frac{\delta s^*_{\alpha\gamma}}{e_0\delta U(\mathbf{r})}s_{\alpha\gamma}\right] = -\frac{1}{2\pi}\left[|s_{\alpha\gamma}|^2\frac{\delta\theta_{s_{\alpha\gamma}}}{e_0\delta U(\mathbf{r})}\right] \tag{4.16}$$

The electrons that are involved in going from γ to α are $|s_{\alpha\gamma}(E)|^2$ in number and these being indistinguishable the factor $|s_{\alpha\gamma}(E)|^2$ in going from Eq.(4.15) to Eq.(4.16) is just an averaging over individual electrons. In Eq.(4.16), first, we will see that without the lead indices we do not have any formula of the hierarchy. Second, ρ_{lpd} shows those number of states which are acquired by the electrons which are propagating from lead γ to α through the point $\mathbf{r}$. So, ρ_{lpd} gives us a count or number (real), now we are claiming this number can be negative [9, 10, 34]. At zero temperature, fermions occupy one state each and for non-interacting fermions doubling the input flux in γ will double the output flux in α as long as we are not in the limit of a completely filled band. We can integrate or sum over one or two or all of them (arguments), respective to that we will get higher objects of the hierarchy. These objects of the hierarchy can be physically interpreted as each sum or integration can interpreted for a particular object of the hierarchy. In Eq.(4.17), just by integrating $\rho_{lpd}(E,\alpha,\mathbf{r},\gamma)$ over $\mathbf{r}$ or over the spatial coordinates of the sample or over the region of the sample Ω then we will get partial density of states (ρ_{pd})

$$\begin{aligned}\rho_{pd}(E,\alpha,\gamma) &= -\frac{1}{4\pi i}\int_\Omega d^3\mathbf{r}\left[s^*_{\alpha\gamma}\frac{\delta s_{\alpha\gamma}}{e_0\delta U(\mathbf{r})} - \frac{\delta s^*_{\alpha\gamma}}{e_0\delta U(\mathbf{r})}s_{\alpha\gamma}\right] \\ &= -\frac{1}{2\pi}\int_\Omega d^3\mathbf{r}\left[|s_{\alpha\gamma}|^2\frac{\delta\theta_{s_{\alpha\gamma}}}{e_0\delta U(\mathbf{r})}\right]\end{aligned} \tag{4.17}$$

Here, Ω stands for the spatial region of the sample only, excluding the leads, which means the region enclosed by the wavy lines in figure 4.2. Moreover, summing over γ, which is incoming channel, means averaging over all outgoing channels like α, δ etc. gives injectivity in Eq.(4.18). Similarly, if we can sum over α, out going channel, means averaging over all incoming channels like γ, δ etc. gives emissivity in Eq.(4.19). To get injectivity ρ_i of a specific lead γ we sum ρ_{lpd} in Eq.(4.16) over all possible outgoing channels α.

$$\rho_i(E,\mathbf{r},\gamma) = -\frac{1}{4\pi i}\sum_\alpha\left[s^*_{\alpha\gamma}\frac{\delta s_{\alpha\gamma}}{e_0\delta U(\mathbf{r})} - \frac{\delta s^*_{\alpha\gamma}}{e_0\delta U(\mathbf{r})}s_{\alpha\gamma}\right] = -\frac{1}{2\pi}\sum_\alpha\left[|s_{\alpha\gamma}|^2\frac{\delta\theta_{s_{\alpha\gamma}}}{e_0\delta U(\mathbf{r})}\right] \tag{4.18}$$

Similarly, to get emissivity ρ_e

$$\rho_e(E,\alpha,\mathbf{r}) = -\frac{1}{4\pi i}\sum_{\gamma}\left[s^*_{\alpha\gamma}\frac{\delta s_{\alpha\gamma}}{e_0\delta U(\mathbf{r})} - \frac{\delta s^*_{\alpha\gamma}}{e_0\delta U(\mathbf{r})}s_{\alpha\gamma}\right] = -\frac{1}{2\pi}\sum_{\gamma}\left[|s_{\alpha\gamma}|^2\frac{\delta\theta_{s_{\alpha\gamma}}}{e_0\delta U(\mathbf{r})}\right] \quad (4.19)$$

Injectivity and emissivity are the important members of the hierarchy. These are like a correlation function between two spatial point γ and α to the remote point $\mathbf{r}$ where the lead indecies γ and α are actually a spatial indecies signifying the spatial point where the lead is attached. The definition of injectivity and emissivity hold in general even when a lead is partially bringing current and partially taking current away with some imbalance between the two. But here we are talking about the specific experimental setup that is explained in more detail in the caption of figure 4.2 and Chapter 6. We have shown [9] that injected current will see this density of states (DOS) in the hierarchy. What ρ_i in Eq.(4.18) means is that for those particular electrons that are coming from lead γ irrespective of to which lead it is going, the relevant part of DOS at the point $\mathbf{r}$ is $\rho_i(E,\mathbf{r},\gamma)$. Injectivity and emissivity can be integrated over $\mathbf{r}$ to give higher objects of the hierarchy called injectance and emittance. Injectance can thus be written from Eq.(4.18)

$$\begin{aligned}\rho(E,\gamma) &= -\frac{1}{4\pi i}\int_{\Omega} d^3\mathbf{r}\sum_{\alpha}\left[s^*_{\alpha\gamma}\frac{\delta s_{\alpha\gamma}}{e_0\delta U(\mathbf{r})} - \frac{\delta s^*_{\alpha\gamma}}{e_0\delta U(\mathbf{r})}s_{\alpha\gamma}\right]\\ &= -\frac{1}{2\pi}\int_{\Omega} d^3\mathbf{r}\sum_{\alpha}\left[|s_{\alpha\gamma}|^2\frac{\delta\theta_{s_{\alpha\gamma}}}{e_0\delta U(\mathbf{r})}\right]\end{aligned} \quad (4.20)$$

and emittance can also be written from Eq.(4.19)

$$\begin{aligned}\rho(E,\alpha) &= -\frac{1}{4\pi i}\int_{\Omega} d^3\mathbf{r}\sum_{\gamma}\left[s^*_{\alpha\gamma}\frac{\delta s_{\alpha\gamma}}{e_0\delta U(\mathbf{r})} - \frac{\delta s^*_{\alpha\gamma}}{e_0\delta U(\mathbf{r})}s_{\alpha\gamma}\right]\\ &= -\frac{1}{2\pi}\int_{\Omega} d^3\mathbf{r}\sum_{\gamma}\left[|s_{\alpha\gamma}|^2\frac{\delta\theta_{s_{\alpha\gamma}}}{e_0\delta U(\mathbf{r})}\right]\end{aligned} \quad (4.21)$$

Local density of states (LDOS) can be defined by summing the RHS of Eq.(4.16) over α and γ.

$$\rho(E,\mathbf{r}) = -\frac{1}{4\pi i}\sum_{\alpha\gamma}\left[s^*_{\alpha\gamma}\frac{\delta s_{\alpha\gamma}}{e_0\delta U(\mathbf{r})} - \frac{\delta s^*_{\alpha\gamma}}{e_0\delta U(\mathbf{r})}s_{\alpha\gamma}\right] = -\frac{1}{2\pi}\sum_{\alpha\gamma}\left[|s_{\alpha\gamma}|^2\frac{\delta\theta_{s_{\alpha\gamma}}}{e_0\delta U(\mathbf{r})}\right] \quad (4.22)$$

Integrating just above equation, $\rho(E,\mathbf{r})$, over $\mathbf{r}$ we obtain DOS

$$\rho_d(E) = -\frac{1}{4\pi i}\sum_{\alpha\gamma}\int_{\Omega} d^3\mathbf{r}\left[s^*_{\alpha\gamma}\frac{\delta s_{\alpha\gamma}}{e_0\delta U(\mathbf{r})} - \frac{\delta s^*_{\alpha\gamma}}{e_0\delta U(\mathbf{r})}s_{\alpha\gamma}\right] \quad (4.23)$$

$$\rho_d(E) = -\frac{1}{2\pi}\int_\Omega d^3\mathbf{r}\sum_\alpha |s_{\alpha\gamma}|^2 \frac{\delta\theta_{s_{\alpha\gamma}}}{e_0\delta U(\mathbf{r})} \tag{4.24}$$

It is to be noted that a particular channel α can act as an incoming channel as well as an outgoing channel and so double counting in the sums in Eqs.(4.22), (4.23) and (4.24) is allowed. Eq.(4.24) is the mesoscopic version of Friedel Sum Rule that relates scattering phase shift to DOS and does not depend on the lead indices or coordinate as they have been summed. Except Eq.(4.24) there are several lower objects that explicitly depend on the lead indices and let us discuss one of them, say $\rho_i(E, \mathbf{r}, \gamma)$, that is injectivity of lead γ to the remote point $\mathbf{r}$ and others can be similarly interpreted. It depends on the input lead index γ and physically means the following. The quantity applies to only those electrons that are incident along lead γ. Individual objects of this ensemble of electrons may or may not pass through a remote point $\mathbf{r}$ and in fact there is no equation of motion that tells us whether it will. Note that Schrödinger equation works only for an ensemble of electrons and gives only a probability for it. At zero temperature, below Fermi energy when we do not distinguish between counting electrons (that constitute a current) and counting states, $\rho_i(E, \mathbf{r}, \gamma)$ give the fraction of those electrons that come from γ and pass through $\mathbf{r}$. Quantum mechanics with its probabilistic interpretations is incapable of pointing at an arbitrary electron at point $\mathbf{r}$ and say if it came from lead γ and even if we try to do so it messes up the situation. Yet we can calculate this object of hierarchy which is a count or measure of such electrons and in case of some further lower objects one has to specify to which lead the electron finally goes. For example, ρ_{lpd} is a measure of electrons going from γ to α condition to the fact that they pass through the point $\mathbf{r}$. This may give the impression that some of these objects are over specified purely theoretical entities as there is no equation of motion for answering where does an electron coming from γ go after some time. But such $\mathbf{r}$ dependent density of states (DOS) can be theoretically derived using the idea of physical clocks like Larmor clock. We will see that such $\mathbf{r}$ dependent DOS can be demonstrated in experiments.

Injectance, Eq.(4.20), is the first member that can be defined and calculated in quantum mechanics as it requires us to specify only one incoming channel, all outgoing channels being summed and an integration made over all coordinates inside the sample. This can be calculated canonically or using Feynman paths, identically. Injectance is total injected current at zero temperature when only lead γ brings electrons into the system while all other leads carry electrons away from the system and $\mathbf{r}$ is also integrated out. This situation is shown in figure 4.2 as a theoretician will setup the scattering problem to be solved. Injected current is of the form $n\ e_0\ v_0$ or differential current is $\frac{dn}{dE}\ e_0\ v_0\ dE$. Electronic charge e_0 can be set to unity and if properly normalised wave functions are taken (see Eq.(3.31)) then we can also drop the v_0 factor making injected current to be $\frac{dn}{dE}$ at an energy E. Now that can be determined from internal wave function $\psi(\mathbf{r}, \gamma)$

when the scattering problem is also setup such that electrons are incident only along lead γ and all other leads carry electrons away from the system so that we do not have to bother where goes the electrons that pass through $\mathbf{r}$. That gives

$$\rho(E,\gamma) = \int_\Omega d^3\mathbf{r} \sum_{k_\gamma} |\psi(\mathbf{r},\gamma)|^2 \delta(E - E_{\gamma,k_\gamma}) \tag{4.25}$$

$$= -\frac{1}{2\pi} \int_\Omega d^3\mathbf{r} \sum_\alpha \left[|s_{\alpha\gamma}|^2 \frac{\delta\theta_{s_{\alpha\gamma}}}{e_0 \delta U(\mathbf{r})} \right] \tag{4.26}$$

Eq.(4.25) is the textbook definition of DOS, when only lead γ brings electrons into the system and the momentum states of these electrons in lead γ are determined by the wave vector k_γ. Eq.(4.26) follows from Eq.(4.20). Lower objects of the hierarchy cannot be defined in terms of internal wave function $\psi(\mathbf{r},\gamma)$ as one can never write down an internal wave function that depend on two lead indices and $\mathbf{r}$. But they can still be defined in terms of the scattering matrix elements or asymptotic wave functions far away from $\mathbf{r}$. By appealing to physical process like spin precession and Larmor frequency, we can address issues like a particle going from γ to α how much time it spends at the point $\mathbf{r}$ and how many (a count or a measure) partial states it occupied at the point $\mathbf{r}$. We thought wave function is the most fundamental entity in quantum mechanics that is determined once we know the internal potential $U(\mathbf{r})$ and hence the Hamiltonian. We always thought that a state is an entity in Hilbert space. Local density of states can only be defined through ensemble averaging wherein equal a priory probability implies that all states in Hilbert space are equally accessible by the electrons and time averages give phase space averages. Time averages in quantum mechanics give phase space averages in statistical mechanics. Averaging over all possible variations in $U(\mathbf{r})$ help taking the problem from Hilbert space to phase space. But say for a benzene molecule attached to leads if we change the internal potential $U(\mathbf{r})$, then it is no longer a benzene molecule. An electron coming from lead γ and going to lead α will not access all states of the benzene molecule but some partial states for which Eq.(4.17) give partial density of states that cannot be defined in terms of the internal wave function. The integrand in Eq.(4.26) can not be broken down into an α dependent quantity. If we remove the integration over $\mathbf{r}$ in Eq.(4.26) then the integrand does not give any lower object of hierarchy as fixing an $\mathbf{r}$ means infinite uncertainty in momentum and it is not enough to be limited to the momentum state at a particular energy E. Likewise, removing the sum over k_γ would mean looking at a particular momentum state and that would mean an infinite uncertainty in coordinate of the electron and so integrating the coordinate over the sample region does not give anything. Besides a delta function cannot be written unless there is a sum or an integration over its variable.

Note that the injectance as defined in Eq.(4.25) or (4.26) can also be measured in-

directly by an experimentalist. Just as Landauer resistance of a sample is defined with respect to the leads attached to the sample, the injectance in Eq.(4.25) is a property of the lead γ which is dependent on the sample to which it is attached. Any electron incident from γ at a particular energy E and wave vector k_γ has to go to some point $\mathbf{r}$ in the sample and eventually escape to some lead α including escape to lead γ and we have summed over all these possibilities in Eq.(4.26). Current delivering capacity of lead γ will be determined by the lateral confinement in the lead and the available modes. To measure this capacity of an scanning tunneling microscope (STM) tip (say) one has to just bring it close to a Landauer type reservoir or a perfect sink of electrons and measure how much tunneling current it delivers to the sink which will be independent of incident energy and the point of the sink to which it is attached. But once the STM tip tries to deliver a current to a particular point $\mathbf{r_p}$ of a mesoscopic sample, then this delivered current will strongly depend on the point $\mathbf{r_p}$ and incident energy E. Subtracting the current delivery capacity of the STM tip we can get the injectance. Similarly, one can measure the injectance of any Landauer lead γ (note that γ is a spatial index like $\mathbf{r_p}$) by attaching it to a Landauer sink and noting that there is a 12.9 kilo Ohms contact resistance. Then it can be attached to the point γ of the sample and the above procedure can be followed. This E dependent current is due to the available states in the system that the injected electrons can access and can never be found by box normalisation. In Landauer's phenomenology, the DOS in the lead per incident mode is $\frac{1}{hv_0}$, that is the same as an infinite 1D line obtained from box normalisation. We understand this coming from an incident wave packet made up of wavelets with appropriate normalisation constants. A wave packet is a localised pattern in physical space, propagating in time and does not care if the lead is attached to a sample or to a perfect sink. The particular normalisation constant in Eq.(3.31), takes care of current conservation via the available current carrying states. The wavelets, satisfy Schrödinger equation with or without the normalisation constant. In Chapters 6 and 7, we will show how some lower objects of the hierarchy can also be measured experimentally.

In this chapter, we have classified all local objects of the hierarchy in terms of scattering phase shift from the theory of the Larmor clock.

CHAPTER 5

FANO RESONANCE IN REALISTIC SYSTEMS

In 2DEG samples, a confinement potential leads to sub-band quantisation in narrow region as discussed in Chapter 2. These sub-bands show a physical phenomenon known as Fano resonance. A degeneracy between a bound state and a scattering state will always produce a Fano resonance [30, 31, 32], in figure 5.4, that will be accompanied by a discontinuous phase change of π at transmission zero. This phase change or drop is a rather novel phenomenon because our intuitive understanding of scattering says that time delays in electron propagation and phase accumulation of the wave function are related. So phase drop may naively suggest time gains rather than delays. But one has to carefully isolate what is a true physical phenomenon and what is artifact of approximations, and this will be done in subsequent chapters. In this chapter, we will be discussing about Fano resonance for realistic mesoscopic systems. To understand the Landauer-Büttiker formalism, the key to generalize this formalism is the Friedel Sum Rule (FSR). FSR relates scattering phase shift to density of states. Buttiker and his colleagues find a correction term to FSR and highlight the effects of lead in their study. FSR will collapse in quantum regimes, while FSR operates excellently when the system stays within the WKB limit. The reference [68] shows that FSR is exact at the Fano resonance (not in WKB regime) which is a pure quantum interference phenomenon and worse in the regimes away from the Fano resonance (in WKB regime). An impurity in quantum wire caused this result. A single attractive impurity can create many resonance states in a quantum wire, which can all be defined as Fano resonances. The majority of the resonances in the mesoscopic systems coupled to leads were found to be Fano resonances, and it was demonstrated that the unique nature of the scattering phase shift at Fano resonances accounts for the wide range of physical phenomena observed. It has

been shown in [54] that an impurity in quantum wire gives strong backscattering which is quantum mechanical in nature, and such backscattering does not disperse the wave packet. A correction term to FSR gives semi-classical formula which will also be covered in this chapter [9, 67]. We will also show that why semi-classical formulas are exact in a purely quantum-mechanical regime [9, 54, 55, 67]. Thus, a non-dispersive wavepacket can be created within quantum regime at Fano resonance [54]. We will point out that, from solutions reported in [54, 55], one can verify π phase slips of scattering phase shift that have somehow eluded attention before our works. Its implications will be discussed too. These scattering problems are generally hard to solve. And numerically, even simple cases require a good amount of computation time [56]. The only potential that can be solved exactly is that of a delta function potential [57] to give the scattering amplitudes. Fano resonance in low dimensional mesoscopic systems can occur for very natural reasons in a wide range of realistic parameter values [69]. Let us try to understand this further with the help of a schematic diagram in figure 5.1 that can be modeled and solved. In Chapters 6 and 7, we will generalize these results and make them independent of any model.

Recent developments in fabrication techniques allow us to fabricate a two-dimensional ($2D$) quantum wire with the confinement potential in the third direction so narrow that only one mode is populated and there are no degrees of freedom in the third direction. Hereafter, "quantum wire" refers to a $2D$ quantum wire with transverse modes quantised in the same way as a square well potential and plane wave propagating modes along the wire's length or in leads.

We discuss a realistic mesoscopic system in Section 5.1. In Section 5.2, we solve a typical scattering problem in quasi-1D, study Fano resonance and, show semi-classical formula become exact at Fano resonance. In Section 5.3, we show that Friedel Sum Rule can also become exact without making reflection, transmission and sine function zero. In Section 5.4, we define Burgers circuit. In Section 5.5, we provide a description of scattering phase shift and Argand diagram for square well potential. In Section 5.6, we discuss a multichannel case for delta function potential where again we show that semi-classical formula becomes exact.

5.1 A realistic mesoscopic setup

An illustrative picture of a realistic system is drawn in figure 5.1. The shaded region is the mesoscopic sample and it is connected to a source reservoir S and a drain reservoir D. The source and the drain have chemical potentials μ_1 and μ_2 as well as temperatures T_1 and T_2, respectively, as shown in the figure 5.1 [9]. However, these parameters, along with the Hamiltonian of the sample, are not enough to describe the properties of the

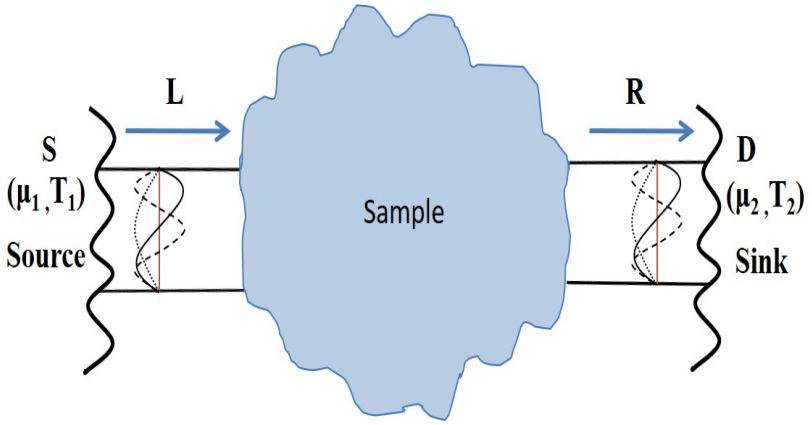

Figure 5.1: An schematic diagram of a general mesoscopic system. The LHS source (reservoir) has the parameters chemical potential μ_1 and T_1. Similarly, the RHS drain or sink (reservoir) has the parameters chemical potential μ_2 and T_2. L and R denotes left and right leads. In bothe leads we have shown propagation modes. The dotted line is for ground state, solid line is for first excited state, and dashed line is for second excited state in both leads. Current flows from source to drain. Shaded region is the sample.

system fully. We also need to consider the leads L and R that connect the sample to the reservoirs. The exchange of energy and particles between the system and the reservoirs take place through the leads, and the nature of the leads, along with the points where it connects to the sample are very important and are well accounted for in the Landauer-Buttiker formalism. If the leads are connected to different points of the sample then the properties of the system will change completely. If the confinement potential of the leads are different then the nature of the states in the leads will be different and again that will change the properties of the system. This is the reason why intrinsic length scales of the sample (shaded region) are not dominant and does not lead to material specific parameters like resistivity, etc. This confinement potential in the leads act in the transverse direction while in the longitudinal direction from S to D the states are plane wave propagating states. In the figure 5.1, the transverse confinement is taken to be hard wall which makes the transverse states like the states in a 1D infinite well (shown in the leads in figure 5.1). These will be mathematically shown subsequently.

We first discuss how the Fano resonances and the associated phase slips appear very naturally in quantum wires before moving on to the mathematical analysis. Consider a simplified version of the figure 5.1 as shown in figure 5.2. In figure 5.2, the shaded region of figure 5.1 has been simplified into a rectangular block extending from $x = -a$ to $x = a$ and from $y = -\frac{c}{2}$ to $y = \frac{c}{2}$. The leads extend from $y = -\frac{b}{2}$ to $y = \frac{b}{2}$. Section 5.1 will provide the mathematical solution of Schrödinger equation for this system. This system can be further simplified by making c equal to b in which case we will get the structure shown in figure 5.3. The physical reasons can be diagrammatically explained as follows. For example, consider the modes in the leads in figure 5.1. The dotted sinusoidal curve is the wave function for the ground state in an infinite potential well as the potential in

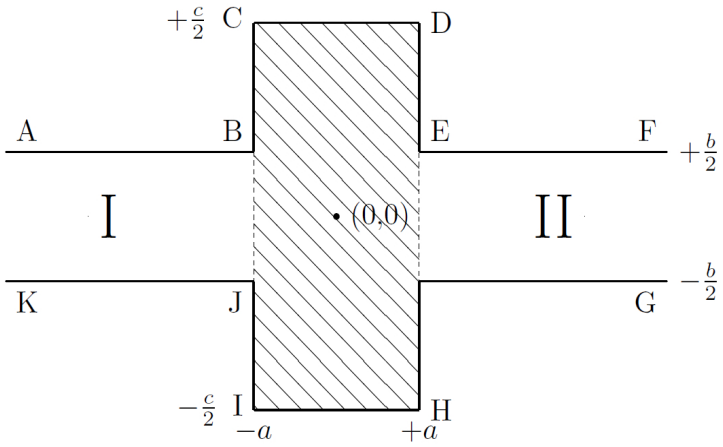

Figure 5.2: A simplified version of the system in figure 5.1. Region I and II is for leads. Leads height varies from -$\frac{b}{2}$ to $\frac{b}{2}$, sample or scatterer region varies from $-\frac{c}{2}$ to $\frac{c}{2}$, and width of scatterer varies from $-a$ to a. At the center of scatterer region, origin is marked $(0, 0)$.

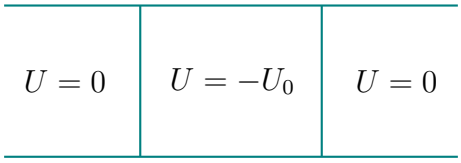

Figure 5.3: An intuitive picture of confinement potential in figure 5.1. This figure shows that confinement potential is zero in the region I and II of figure 5.1 whereas in scatterer region confinement potential is $-U_0$.

the direction transverse to the direction of current flow is taken as hard wall. The wave function in the propagating direction will be plane waves with usual parabolic dispersion curve as we will show in Section 5.2. The dotted parabolic curve in figure 5.4 is showing this dispersion (it is basically a plot of energy versus wave number). The solid sinusoidal curve in the leads of figure 5.1 is the first excited state (depicted as second state in figure 5.1) in an infinite potential well and for this we will get another parabolic dispersion curve shown by solid curve in figure 5.4. This parabola will be at a higher energy relative to the dotted parabola as the first excited state in the transverse direction has higher energy than the ground state (will be shown mathematically in Section 5.2). Similarly, corresponding to the dashed sinusoidal curve in figure 5.1 we will get the dashed parabola in figure 5.4. These parabolic dispersion curves correspond to scattering states only. If potential U in the sample region is negative (say $-U_0$) then corresponding to each parabola there will be bound states as well whose energies will be below the threshold energy of the parabolas. Thus, the dashed parabola will have some bound states shown by the dashed straight lines below the dashed parabola in figure 5.4. The solid parabola will also have some bound states shown by the solid straight lines below the solid parabola in figure 5.4. Now the solid bound states will not be true bound states as they are degenerate with a scattering state (shown by an arrow), of the dotted channel.

Suppose in figure 5.1 or figure 5.2 or 5.3, we want to consider just two transverse

channels. Which means in case of figure 5.1 we have the dotted curve and the solid curve depicting transverse modes. Suppose the propagating wave vector for these two channels are k_1 and k_2. As Eqs.(4.25) and (4.26) suggest that we have to define injectance separately for these two cases. Injectance of left lead for incidence along k_1 channel should be denoted as $\rho(E, \gamma = 1, k_1)$ but we call it $\rho(E, 1)$. Which means although according to Eq.(4.15) one has to make a distinction between spatial indices and momentum indices, here we simplify the notation. For this case semi-classical injectance will have two more terms compared to Eq.(5.70) and is given by, [55]

$$\rho(E,1) \approx \frac{1}{2\pi}\left[|r_{11}|^2\frac{d\theta_{r_{11}}}{dE} + |r_{21}|^2\frac{d\theta_{r_{21}}}{dE} + |t_{11}|^2\frac{d\theta_{t_{11}}}{dE} + |t_{21}|^2\frac{d\theta_{t_{21}}}{dE}\right] \tag{5.1}$$

One can break this up as

$$\rho(E,1) \approx \rho^L(E,1) + \rho^R(E,1) \tag{5.2}$$

where

$$\rho^L(E,1) = \frac{1}{2\pi}\left[|r_{11}|^2\frac{d\theta_{r_{11}}}{dE} + |r_{21}|^2\frac{d\theta_{r_{21}}}{dE}\right] \tag{5.3}$$

$$\rho^R(E,1) = \frac{1}{2\pi}\left[|t_{11}|^2\frac{d\theta_{t_{11}}}{dE} + |t_{21}|^2\frac{d\theta_{t_{21}}}{dE}\right] \tag{5.4}$$

That is, $\rho^L(E,1)$ consist of reflection channels and $\rho^R(E,1)$ consist of transmission channels. The correction term corresponding to Eq.(5.71) depends on parameters of the incident channel only and gives the following identity.

$$\rho(E,1) = \rho^L(E,1) + \rho^R(E,1) + \frac{1}{2\pi}\frac{m_0|r_{11}|}{\hbar k_1^2}\sin(\theta_{r_{11}}) \tag{5.5}$$

This is known in 1D, Eq.(5.5), the explicit calculation in this chapter reveals that this is also true for the multichannel situation and the correction term depend solely on the input channel parameters, provided we account for the evanescent modes to calculate them. In Section 5.3, we will demonstrate how these evanescent modes are included. Similarly, semi-classical injectance for incidence along left lead in k_2 channel is, [55]

$$\rho(E,2) \approx \frac{1}{2\pi}\left[|r_{22}|^2\frac{d\theta_{r_{22}}}{dE} + |r_{12}|^2\frac{d\theta_{r_{12}}}{dE} + |t_{22}|^2\frac{d\theta_{t_{22}}}{dE} + |t_{12}|^2\frac{d\theta_{t_{12}}}{dE}\right] \tag{5.6}$$

We can break this up as

$$\rho(E,2) \approx \rho^L(E,2) + \rho^R(E,2) \tag{5.7}$$

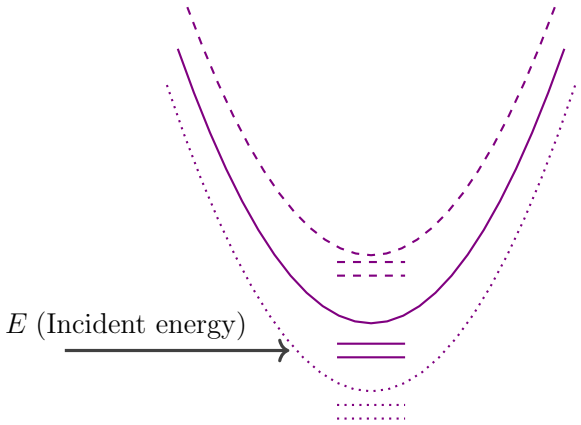

Figure 5.4: An intuitive picture of getting Fano resonances in mesoscopic systems. These are the modes or states which has shown in figure 5.1. Below parabolic curve (propagation modes), bound states are shown.

$$\text{where,} \quad \rho^L(E,2) = \frac{1}{2\pi}\left[|r_{22}|^2\frac{d\theta_{r_{22}}}{dE} + |r_{12}|^2\frac{d\theta_{r_{12}}}{dE}\right]$$
$$\rho^R(E,2) = \frac{1}{2\pi}\left[|t_{22}|^2\frac{d\theta_{t_{22}}}{dE} + |t_{12}|^2\frac{d\theta_{t_{12}}}{dE}\right]$$

and with the correction term we get

$$\rho(E,2) = \rho^L(E,2) + \rho^R(E,2) + \frac{1}{2\pi}\frac{m_0|r_{22}|}{\hbar k_2^2}\sin(\theta_{r_{22}}) \tag{5.8}$$

From the S-matrix, the RHS of Eqs.(5.1) and (5.6) can be found. Experimentalists can easily access this S-matrix approach. However, in mesoscopic systems that are in the quantum regime, the correction term can be very large. A significant modification is also required to the physical interpretation of the correction term which is covered in Section 5.3.

5.2 A typical scattering problem in quasi-1D

This section provides an analytical treatment of scattering in quasi-1D (Q1D) in terms of partial wave analysis for a general system of the type illustrated in figure 5.1. This will result in the general occurrence of Fano resonances, which will be accompanied by transmission zeroes and associated discontinuous π phase shifts. One can further understand in the next few chapters that this will lead to negative partial density of states and time travel. As previously mentioned [69], the analysis in this section can be used to explicitly solve the system in figure 5.2. Let us consider $U_g(x,y)$ to be the scattering potential in the shaded region of figure 5.2. The right reservoir serves as a sink and the left reservoir as a source of electrons (not shown in figure 5.2). As usual the x-direction is along the source to sink direction and the y-direction is perpendicular to

it. The confinement potential in the leads, i.e., in regions I and II, is taken to be hard wall in the y-direction (or transverse direction), given by

$$U(x,y) = U(y) = \begin{cases} \infty, & |y| \geq \frac{b}{2}, \quad |x| \geq a \\ 0, & |y| < \frac{b}{2}, \quad |x| \geq a \end{cases} \tag{5.9}$$

The potential in the shaded region is of the form

$$U(x,y) = \begin{cases} \infty, & \text{for } |y| \geq \frac{c}{2} \text{ and } |x| < a \\ U_g(x,y), & \text{for } |y| < \frac{c}{2} \text{ and } |x| < a \end{cases} \tag{5.10}$$

Thus, we have taken the system to be embedded in 2D and the reason for this is that the third direction is determined by the way the two dimensional electron gas (2DEG) is made and usually there is only one quantised energy mode for this degree of freedom, which can be set to zero by the choice of reference frame of energy.

We will first solve the Schrödinger equation in the leads, and then match them to the solutions in the sample region which is the shaded area in figure 5.2. The Schrödinger equation in the two dimensional lead is,

$$\frac{-\hbar^2}{2m_0}\frac{\partial^2}{\partial x^2}\psi(x,y) - \frac{\hbar^2}{2m_0}\frac{\partial^2}{\partial y^2}\psi(x,y) + U(y)\psi(x,y) = E\psi(x,y) \tag{5.11}$$

Since the potential depends only on y, from the separation of variables

$$\psi(x,y) = c_m(x)\,\chi_m(y) \tag{5.12}$$

From Eqs.(5.11) and (5.12), we get

$$\left[-\frac{\hbar^2}{2m_0}\frac{d^2}{dy^2} + U(y)\right]\chi_m(y) = \varepsilon_m\chi_m(y) \tag{5.13}$$

$$\text{and} \qquad -\frac{\hbar^2}{2m_0}\frac{d^2}{dx^2}c_m(x) = (E-\varepsilon_m)\,c_m(x) \tag{5.14}$$

$$\text{From Eq.(5.13)} \quad \chi_m(y) = \sqrt{\frac{2}{b}}\sin\left(\frac{m\pi}{b}(y+\frac{b}{2})\right); \qquad \varepsilon_m = \frac{\hbar^2 m^2\pi^2}{2m_0 b^2} \tag{5.15}$$

For $m = 1$ in Eq.(5.15), we get the dotted curve in the leads of figure 5.1. For $m = 2$ in Eq.(5.15), we get the solid curve in the leads of figure 5.1. For $m = 3$, we get the dashed curve in the leads of figure 5.1 and so on. From Eq.(5.14)

$$c_m(x) = e^{\pm ik_m x}; \qquad (E-\varepsilon_m) = \frac{\hbar^2 k_m^2}{2m_0} \tag{5.16}$$

For $m = 1$ in Eq.(5.16), we get the dotted parabolic curve in figure 5.4 which is a plot

of E versus k_1 . For $m = 2$ in Eq.(5.16), we get the solid parabolic curve in figure 5.4 which is a plot of E versus k_2. For $m = 3$ we get the dashed parabolic curve in figure 5.4. We have not yet obtained the bound states shown by the dotted straight lines or solid straight lines, or dashed straight lines in figure 5.4. For them we have to solve the Schrödinger equation in the shaded region of figure 5.2 which will be done from Eq.(5.27) onward.

From Eqs.(5.15) and (5.16)

$$E = E_{m,k_m} = \frac{\hbar^2 m^2 \pi^2}{2m_0 b^2} + \frac{\hbar^2 k_m^2}{2m_0} \tag{5.17}$$

Consistent with Eqs.(5.12), (5.15) and (5.16), we can write a general solution as a linear combination of $\frac{1}{\sqrt{k_m}}\,\chi_m(y)\,e^{\pm ik_m x}$, where $s_{nm}^{e/o}$ are coefficients to be determined. Therefore,

$$\begin{aligned}\psi(x,y) = {} & \frac{1}{2\sqrt{k_1}}\left[\delta_{11}e^{-ik_1x} - s_{11}^{e}e^{ik_1x}\right]\chi_1(y) + \frac{1}{2\sqrt{k_2}}\left[\delta_{21}e^{-ik_2x} - s_{21}^{e}e^{ik_2x}\right]\chi_2(y) + \ldots \\ & + \frac{1}{2\sqrt{k_1}}\left[\delta_{11}e^{-ik_1x} - s_{11}^{o}e^{ik_1x}\right]\chi_1(y) + \frac{1}{2\sqrt{k_2}}\left[\delta_{21}e^{-ik_2x} - s_{21}^{o}e^{ik_2x}\right]\chi_2(y) + \ldots\end{aligned} \tag{5.18}$$

Each term in Eq.(5.18) satisfy Eq.(5.11) and so their sum also satisfies Eq.(5.11) because it is a linear differential equation. For example, $\frac{1}{2\sqrt{k_1}}\,s_{11}^{e}\,e^{ik_1x}\,\chi_1(y)$ satisfies Eq.(5.11) with $E = \frac{\hbar^2 1^2\pi^2}{2m_0b^2} + \frac{\hbar^2 k_1^2}{2m_0}$ while $\frac{1}{2\sqrt{k_2}}\,s_{21}^{o}\,e^{ik_2x}\,\chi_2(y)$ satisfies Eq.(5.11) with $E = \frac{\hbar^2 2^2\pi^2}{2m_0b^2} + \frac{\hbar^2 k_2^2}{2m_0}$. One can find some more terms, or break up the terms above in to some strange terms and mathematically there is nothing wrong. However, Eq.(5.18) is supposed to correspond to some physical situation and we have to address that Eq.(5.18) is essentially a series

$$\begin{aligned}\psi(x,y) = {} & \sum_{m=1}^{\infty}\frac{1}{2\sqrt{k_m}}\left[\delta_{mm'}e^{-ik_mx} - s_{mm'}^{e}e^{ik_mx}\right]\chi_m(y) \\ & + \sum_{m=1}^{\infty}\frac{1}{2\sqrt{k_m}}\left[\delta_{mm'}e^{-ik_mx} - s_{mm'}^{o}e^{ik_mx}\right]\chi_m(y)\end{aligned} \tag{5.19}$$

$$\psi(x,y) = \frac{\psi^e(x,y) + \psi^o(x,y)}{2} \tag{5.20}$$

where $\psi^e(x,y)$ is an even function of x and $\psi^o(x,y)$ is an odd function of x. This can always be demanded by adjusting the unknown coefficients $s_{mm'}^{e}$ and $s_{mm'}^{o}$ because any arbitrary function can be decomposed into a sum of even and odd function, and any matrix into a sum of symmetric and anti-symmetric matrix (see Eq.(5.22)). Special situation here is that because the Schrödinger equation is a linear differential equation, both $\psi^e(x,y)$ and $\psi^o(x,y)$ independently satisfy Eq.(5.11). In Eq.(5.20), we can shuffle around the terms in the series and add them because the Hilbert space is complete by the

axioms. This implies that each term in the series is in Hilbert space and the entire series is also in Hilbert space and so different terms can be added. Note that these additions have the spirit of vector addition as the Hilbert space is a normed vector space.

$\psi(x,y)$ of Eq.(5.19) is valid for $|x| \geq a$ and hence also valid for $x < -a$. Therefore, to find the wave function in the left lead, we just have to use the coordinate value $-x$ in Eq.(5.19). For $x < -a$, $\psi(x,y)$ should correspond to a physical situation in the left lead of figure 5.2.

$$\begin{aligned}\psi(x,y) = &\sum_{m=1}^{\infty} \frac{1}{2\sqrt{k_m}} \left[\delta_{mm'} e^{ik_m x} - s^o_{mm'} e^{-ik_m x}\right] \chi_m(y) \\ &+ \sum_{m=1}^{\infty} \frac{1}{2\sqrt{k_m}} \left[\delta_{mm'} e^{ik_m x} - s^e_{mm'} e^{-ik_m x}\right] \chi_m(y) \qquad (5.21)\end{aligned}$$

$$\psi(x,y) = \frac{1}{\sqrt{k_{m'}}} e^{ik_{m'}x} \chi_{m'}(y) + \sum_{m=1}^{\infty} \frac{1}{\sqrt{k_m}} \frac{(-s^o_{mm'} - s^e_{mm'})}{2} e^{-ik_m x} \chi_m(y) \qquad (5.22)$$

Note that Eq.(5.22) is only valid for $x < -a$ and to obtain its value at some $x < -a$ we have to only use the value $x = |x|$ because the negative sign has been already accounted for in going from Eq.(5.19) to Eq.(5.21). Indeed when we match the boundary conditions in Eqs.(5.32) and (5.35), this is what we will do, as is evident from the discussions in the paragraph after Eq.(5.23) where we explicitly keep track of the sign of x, leading to Eq.(5.31). Let us compare with the usual way in which we write the wave function in 1D as $e^{ikx} + re^{-ikx}$. Like in 1D, we have in mind the following physical situation. That an ensemble of quantum particles are incident from the left. This incident ensemble in the left lead can be described by a wave packet whose components are $e^{ik_{m'}x}\,\chi_{m'}(y)$ and there is a reflected wave packet whose components are $\tilde{r}_{mm'}\, e^{-ik_m x}\,\chi_m(y)$. That $|\tilde{r}_{mm'}|^2$ can be read off from Eq.(5.22) and stated below in Eq.(5.23), can be interpreted as a fraction of the incident probability in the incoming m'th channel that is reflected to the mth channel. In Eq.(5.22), the incident wave packet has Fourier components $\frac{1}{\sqrt{k_{m'}}}\, e^{ik_{m'}x}\,\chi_{m'}(y)$ and several reflected wave packets in different channels indexed by m whose Fourier components are $\frac{1}{\sqrt{k_m}} \frac{(-s^o_{mm'} - s^e_{mm'})}{2}\, e^{-ik_m x}\,\chi_m(y)$.

$$\tilde{r}_{mm'} = -\frac{(s^o_{mm'} + s^e_{mm'})}{2} \qquad (5.23)$$

Therefore, $\tilde{r}_{mm'}$ is the reflection amplitude from the m'th incident channel to the mth channel in the left lead as Eq.(5.22) is defined only for $x < -a$.

Now let us come to the right lead, that is $x > a$. Once again we can start from Eq.(5.19) that is valid for $|x| \geq a$. To find the wave function at $x = +a$ we have to just substitute the coordinate value $x = +a$ in Eq.(5.19). But we can use symmetry to do

some simplification. We can try to find out the value of $\psi(x,y)$ at $x=a$ from its value at $x=-a$. Let us substitute $x\to -x$ in Eq.(5.19) and note that this is how we can relate the wave functions at positive and negative x. That means to find the wave function at $x=+a$ we first find its simplified value at $x=-a$, because the symmetry allows us to do some simplification. However, this simplification scheme can only be applied at one end (that is the left end) because the whole purpose is to get the boundary conditions at the two ends from one end. So there are two alternate approaches to this scattering problem. In this approach, we apply or calculate boundary conditions at only one end twice, once without applying symmetry and then by applying symmetry. In the other approach, we do not use any symmetry but apply or calculate boundary condition at both ends separately. Because the wave function at the two ends is always different and something has to be done differently at the two ends. Therefore, noting that the second series in Eq.(5.19) is odd, we get

$$\begin{aligned}\psi(x,y) &= \sum_{m=1}^{\infty}\frac{1}{2\sqrt{k_m}}\left[\delta_{mm'}e^{ik_mx}-s^e_{mm'}e^{-ik_mx}\right]\chi_m(y)\\ &\quad-\sum_{m=1}^{\infty}\frac{1}{2\sqrt{k_m}}\left[\delta_{mm'}e^{ik_mx}-s^o_{mm'}e^{-ik_mx}\right]\chi_m(y) \qquad (5.24)\\ \psi(x,y) &= \sum_{m=1}^{\infty}\frac{1}{\sqrt{k_m}}\frac{(-s^e_{mm'}+s^o_{mm'})}{2}e^{-ik_mx}\chi_m(y) \qquad (5.25)\end{aligned}$$

In this simplified value we re-substitute $x\to -x$ and in the expression that will be obtained, x can only admit positive values of $x>a$. So,

$$\begin{aligned}\psi(x,y) &= \sum_{m=1}^{\infty}\frac{1}{\sqrt{k_m}}\frac{(-s^e_{mm'}+s^o_{mm'})}{2}e^{ik_mx}\chi_m(y)\\ \tilde{t}_{mm'} &= \frac{(s^o_{mm'}-s^e_{mm'})}{2} \qquad (5.26)\end{aligned}$$

Again in comparison to a 1D scattering problem, $\tilde{t}_{mm'}$ is the transmission amplitude for an electron incident from left along m' channel and transmitted to the mth channel on the right.

So far we were solving the Schrödinger equation in the leads. Now let us come to the scattering region that is the shaded region in figure 5.2. The wave function in the scattering region with potential, $U(x,y)=U_g(x,y)$, can be written as

$$\eta^e(x,y)=\sum_{n=1}^{\infty}c_n\zeta^e_n(x,y) \qquad (5.27)$$

$$\eta^o(x,y)=\sum_{n=1}^{\infty}c_n\zeta^o_n(x,y) \qquad (5.28)$$

as internal wave function too can be written as

$$\eta(x,y) = \frac{\eta^e(x,y) + \eta^o(x,y)}{2} \tag{5.29}$$

From Eqs.(5.20) and (5.18) (valid for all $|x| \geq a$), we get

$$\psi^e(x,y) = \sum_{m=1}^{\infty} \frac{1}{\sqrt{k_m}} \left[\delta_{mm'} e^{-ik_m x} - s^e_{mm'} e^{ik_m x}\right] \chi_m(y) \tag{5.30}$$

It is also natural to introduce an index m' on the LHS to make it compatible with the RHS.

$$\psi^e_{m'}(x,y) = \sum_{m=1}^{\infty} \frac{1}{\sqrt{k_m}} \left[\delta_{mm'} e^{-ik_m x} - s^e_{mm'} e^{ik_m x}\right] \chi_m(y) \tag{5.31}$$

Thus, Eq.(5.31) is valid for $x = +a$ (see figure 5.2). Now we can equate ψ^e of Eq.(5.31) with η^e of Eq. (5.27) and similarly we can equate ψ^o with η^o, which will match ψ of Eq. (5.20) to η of Eq.(5.29) (crucially depends on axiomatic completeness of Hilbert space). But first let us apply current conserving boundary condition to get

$$\frac{d\psi^e_{m'}(x,y)}{dx}|_{x=a} = \frac{d\eta^e(x,y)}{dx}|_{x=a} \tag{5.32}$$

There are two quantum numbers involved that has to be respected. One is e that comes from spatial symmetry in x-direction and the other is m' coming from sub-band quantisation. So, we also introduce the index m' on the RHS of Eq.(5.32). Note that if the system did not have the symmetry of $x \to -x$ then we cannot match ψ^e to η^e alone but we will have to match ψ^e to the full linear combination given by η in Eq.(5.29).

$$\frac{d\psi^e_{m'}(x,y)}{dx}|_{x=a} = \frac{d\eta^e_{m'}(x,y)}{dx}|_{x=a} \tag{5.33}$$

Substituting from Eq.(5.27) and Eq.(5.31) into Eq.(5.32), and after further simplification we get (see Appendix A)

$$-i\sqrt{k_{m''}}\left(\delta_{m'm''} e^{-ik_{m''}a} + s^e_{m''m'} e^{ik_{m''}a}\right) = \sum_{m=1}^{\infty} c_m F^e_{m''m} \sqrt{k_{m''} k_m} \tag{5.34}$$

Now we apply another boundary condition to match wave functions at $x = a$.

$$\psi^e_{m'}(x,y)|_{x=a} = \eta^e_{m'}(x,y)|_{x=a} \tag{5.35}$$

Substituting from Eqs.(5.27), (5.31), (5.15) into Eq.(5.35), and after simlpification we get

(see Appendix A)

$$\sum_{m=1}^{\infty} \left(F^e_{m''m} - i\delta_{m''m}\right) e^{ik_m a} s^e_{mm'} = \left(F^e_{m''m'} + i\delta_{m''m'}\right) e^{-ik_{m'}a} \tag{5.36}$$

This is the equation that we have to solve to find $s^e_{mm'}$. Similarly, we will get an equation for $s^o_{mm'}$. Multiplying identical terms on both sides of Eq.(5.36), we get

$$\begin{aligned} &\sum_{nm}\sum_{m''} \left[(F^e - iI)^{-1}\right]_{nm''} \left[F^e - iI\right]_{m''m} e^{ik_m a} s^e_{mm'} \\ &= \sum_{n}\sum_{m''} \left[(F^e - iI)^{-1}\right]_{nm''} \left[F^e + iI\right]_{m''m'} e^{-ik_{m'}a} \end{aligned} \tag{5.37}$$

In quantum mechanics, a series can be seen as a limit of a finite sum and so we can talk of Eq.(5.36) as a matrix equation. In this particular case, the series has a natural truncation because very high k_m values correspond to very high energy states that are not possible in condensed matter systems. The work function of a material provides a natural cut off. Since on LHS, after the sum over m'', we are multiplying matrix elements from two matrices that are inverse to each other, two matrix elements must multiply to give a 0 or 1.

$$\sum_{n} e^{ik_n a}\, s^e_{nm'} = \sum_{n} \left[(F^e - iI)^{-1}(F^e + iI)\right]_{nm'} e^{-ik_{m'}a} \tag{5.38}$$

Since, this is true for any arbitrary $k_n a$, we can remove the sum from both sides.

$$s^e_{nm'} = e^{-ik_n a} \left[(F^e - iI)^{-1}(F^e + iI)\right]_{nm'} e^{-ik_{m'}a} \tag{5.39}$$

Now binomial expansion like procedure can be followed because the identity matrix commutes with any matrix and we get (see appendix A)

$$(F^e - iI)^{-1}(F^e + iI) = 1 + 2i(F^e - iI)^{-1} \tag{5.40}$$

From Eq.(5.39), where we drop the superscript e for convenience, which we will bring back after some simplification.

$$s_{nm'} = e^{-ik_n a} \left[1 + 2i(F - iI)^{-1}\right]_{nm'} e^{-ik_{m'}a} \tag{5.41}$$

To explain the straight lines in figure 5.4, representing bound states and resonant states, let us reconsider Eq.(5.17)

$$E = \frac{\hbar^2 m^2 \pi^2}{2m_0 b^2} + \frac{\hbar^2 k_m^2}{2m_0}$$

If we take $m = 1$ and plot E versus k_1 then we get the dotted parabola in figure 5.4

where the minimum of the parabola is $\epsilon_1 = \frac{\hbar^2 1^2 \pi^2}{2m_0 b^2}$ and referred to as the propagating threshold for the $m = 1$ channel. If we take $m = 2$ and plot E versus k_2 then we get the solid parabola in figure 5.4 where the minimum of the parabola is $\epsilon_2 = \frac{\hbar^2 2^2 \pi^2}{2m_0 b^2}$ and referred to as the propagating threshold for the $m = 2$ channel. There can be thus an infinite number of these parabolas and figure 5.4 depicts only three of them.

In mesoscopic physics an experimentalist can fix the incident energy E and the range in which it can vary. So suppose

$$\frac{\hbar^2 \pi^2}{2m_0 b^2} < E < \frac{\hbar^2 4\pi^2}{2m_0 b^2} \tag{5.42}$$

That is

$$\epsilon_1 < E < \epsilon_2 \tag{5.43}$$

If we substitute an E value in this range in Eq.(5.17) then we can see that k_1 is real and k_2, k_3, ... are all imaginary. What it physically means with respect to figure 5.4 is the following. It means the incident energy E is varying between the minimum of the dotted parabola and the minimum of the solid parabola. In this regime, only k_1 is a propagating mode and the rest are evanescent modes. For example, if k_2 is imaginary then we can substitute $k_2 \to i\kappa_2$ and substitute in Eq.(5.22) to see this. However, in this energy range there can be some discrete real values of k_2 for which one can find solutions to Eq.(5.36) or (5.41). These will give the bound states like the dashed lines in figure 5.4. Bound states can be determined from the singularities of the matrix equation, that is from Eq.(5.36) or (5.41) we can say that solutions to the following equation will give the bound states.

$$\det\left[F^e_{cc} - iI\right] = 0 \tag{5.44}$$

As stated above, Eq.(5.36) can be seen as a matrix equation, where the RHS terms are known, and the coefficients of $s^e_{mm'}$ on LHS are also known. We can drop the superscript e for convenience, that will be introduced later. Here 'cc' means evanescent channel (or closed channel, see Eq.(5.44) for which both k_m and $k_{m'}$ in Eq.(5.36) are imaginary. For these values of k_m and $k_{m'}$, we can still find solutions to Eq.(5.36) with $s^e_{mm'} = 0$ for $m = m'$ only for some discrete values of k_m. Note that for $m = 2$ these solutions will be for $E < \epsilon_2 = \frac{\hbar^2 4\pi^2}{2m_0 b^2}$. An electron in such a state gets trapped in an eigenstate with no reflection or transmission. To explain F_{cc} further we can partition the matrix F into its open and closed channel parts as follows.

$$F = \begin{bmatrix} F_{oo} & F_{oc} \\ F_{co} & F_{cc} \end{bmatrix} \tag{5.45}$$

The subscripts 'o' refers to open and 'c' refers to closed channels. Suppose for m' and m

taking values from the set $\{1, 2\}$, F_{oo} will be a 2×2 matrix while F_{cc} will be an infinite dimensional matrix that can be truncated at some point based on physical arguments. The completeness of the Hilbert space ensures that the truncation is physical. F_{oo} is a matrix whose elements are of the form $F_{mm'}$ where m and m' are indices for open channels. Similarly, F_{cc} is a matrix whose elements are of the form $F_{mm'}$ where m and m' are indices for closed channels. Thus, F_{oc} is a matrix whose elements are of the form $F_{mm'}$ where m is an index for an open channel while m' is an index for a closed channel. Similarly, F_{co} is a matrix whose elements are of the form $F_{mm'}$ where m is an index for a closed channel while m' is an index for an open channel. Thus, we may write on dropping the superscript e which will be reintroduced latter

$$[F - iI]^{-1} = \begin{bmatrix} A & B \\ C & D \end{bmatrix} \tag{5.46}$$

We found (see Appendix A)

$$A = \left(F_{oo} - iI - F_{oc}(F_{cc} - iI)^{-1}F_{co}\right)^{-1} \tag{5.47}$$

From Eq.(5.46) we see that (see Appendix A)

$$A = \left[(F - iI)^{-1}\right]_{oo} \tag{5.48}$$

In Eq.(5.41), if n and m' are open channels, then substituting A from Eq.(5.48) in Eq.(5.41)

$$s_{nm'} = e^{-ik_n a}\,[1 + 2iA]_{nm'}\,e^{-ik_{m'}a} \tag{5.49}$$

Substituting from Eq.(5.47) into Eq.(5.49)

$$s_{nm'} = e^{-ik_n a}\left[1 + 2i\left(F_{oo} - iI - F_{oc}(F_{cc} - iI)^{-1}F_{co}\right)^{-1}\right]_{nm'} e^{-ik_{m'}a} \tag{5.50}$$

$$\text{or} \qquad s_{nm'} = e^{-ik_n a}\left[1 + 2i\,(G - iI)^{-1}\right]_{nm'} e^{-ik_{m'}a} \tag{5.51}$$

$$\text{where,} \qquad G = \left[F_{oo} - F_{oc}(F_{cc} - iI)^{-1}F_{co}\right] \tag{5.52}$$

From Eq.(5.51) and comparing with Eq.(5.40)

$$s_{nm'} = e^{-ik_n a}\left[(G - iI)^{-1}(G + iI)\right]_{nm'} e^{-ik_{m'}a} \tag{5.53}$$

Suppose there is only one propagating channel in both the leads. Then we put $n = m' = 1$

in Eq.(5.53) and also from Eq.(5.52) we see that G is a number.

$$G = F_{11} - \sum_{m'=2,m=2} F_{1m}[(F_{cc} - i1)^{-1}]_{mm'} F_{m'1} \tag{5.54}$$

From Eq.(5.53)

$$s_{11} = e^{-ik_1 a}\left[\frac{G+iI}{G-iI}\right]e^{-ik_1 a} \tag{5.55}$$

From Eqs.(5.53) and (5.54)

$$s_{11} = e^{-2ik_1 a}\left[1 + 2i\left(F_{11} - \sum_{m',m=2} F_{1m}[(F_{cc} - i1)^{-1}]_{mm'} F_{m'1} - i1\right)^{-1}\right] \tag{5.56}$$

We reintroduce the superscript e to write

$$G^e = \cot(\theta^e) \text{ (say)} \tag{5.57}$$

From Eq.(5.55)

$$\begin{aligned} s_{11}^e &= e^{-2ik_1 a}\frac{\cot(\theta^e) + i1}{\cot(\theta^e) - i1} = e^{-2ik_1 a}\frac{e^{i\theta^e}}{e^{-i\theta^e}} = e^{-2ik_1 a}e^{2i\theta^e} \\ &= e^{2i\,\mathrm{arccot}(G^e) - 2ik_1 a} = e^{2i(\theta^e - k_1 a)} = e^{2i\delta^e} \end{aligned}$$

where $\delta^e = \theta^e - k_1 a$

Similarly, we can get $s_{11}^o = e^{2i\delta^o}$ and $\delta^o = \theta^o - k_1 a$

According to the convention of Eq.(3.77) in Chapter 3 of [9], $\delta \equiv \theta_{t'}$, whereas we work with θ_t. Therefore,

$$s_{11}^e = e^{2i\theta^e} \tag{5.58}$$

$$s_{11}^o = e^{2i\theta^o} \tag{5.59}$$

Now from Eq.(5.26), we find that transmission amplitude ($\tilde{t}_{11}$) is given by

$$\tilde{t}_{11} = \frac{-s_{11}^e + s_{11}^o}{2} = \frac{-e^{2i\theta^e} + e^{2i\theta^o}}{2} \tag{5.60}$$

We define new variables as

$$\phi = \theta^e - \theta^o \text{ and } \theta_r = \theta^e + \theta^o \tag{5.61}$$

$$\tilde{t}_{11} = -i\sin(\phi)e^{i\theta_r} \tag{5.62}$$

Similarly from Eq.(5.23) we find the reflection amplitude to be

$$\tilde{r}_{11} = -\frac{s^e_{11} + s^o_{11}}{2} = -\frac{(e^{2i\theta^e} + e^{2i\theta^o})}{2} \tag{5.63}$$

$$\text{and,} \quad \tilde{r}_{11} = -\cos(\phi)e^{i\theta_r} \tag{5.64}$$

Thereby, we get transmission amplitude and reflection amplitude as

$$\tilde{t}_{11} = -i\sin(\phi)\, e^{i\theta_r} \text{ and } \quad \tilde{r}_{11} = -\cos(\phi)\, e^{i\theta_r} \tag{5.65}$$

One can see [9, 53] for further details, but the discontinuous scattering phase shifts at the resonances or bound states was overlooked there. We can see them as follows. Since the system has reflection symmetry in x, bound states will be either an even state or an odd state. At an even bound state G^e will blow up as is clear from Eqs.(5.54) and (5.44). That is because the second term in G^e, as given by Eq.(5.54) has the inverse of a matrix and when the bound state condition given by Eq.(5.44) is satisfied, this second term will diverge. Therefore, at a bound state $\theta^e = \text{arccot}[G^e]$ (see Eq.(5.57)) will go to zero. So at an even bound state $|\tilde{t}_{11}| = \sin(\phi) = \sin(\theta^e) = 0$ (see Eqs.(5.61) and (5.62)).

The correction term of Eq.(5.5) in case of this system is $\frac{m_0|\tilde{r}_{11}|}{\hbar k_1^2}\sin(\theta_r) = \frac{m_0|\tilde{r}_{11}|}{\hbar k_1^2}\sin(\theta^e)$ (see Eq.(5.61)), and therefore that too is zero from Eq. (5.57). Thus, we have shown that the correction term in Eq.(5.5) is zero because $\sin(\theta_r) = 0$. At this point $\mid r \mid = \mid -\cos(\phi) \mid$ (see Eq.(5.64)) $= \mid -\cos(\theta^e) \mid = \cos(0)$ (we have already shown $\sin(\theta^e) = 0$) and so $\mid r \mid \neq 0$. As stated earlier, if the correction term can be ignored or set to zero then the semi-classical formulas can be very useful to experimentalists.

5.3 Semi-classicality and Friedel Sum Rule

Eq.(4.24) is the mesoscopic version of Friedel Sum Rule (FSR). In this equation too we get the derivative of the scattering phase shift with respect to the local potential $U(\mathbf{r})$ along with an integration over $\mathbf{r}$ and so this is not of much use to an experimentalist. One may consider the following substitution

$$\int_{global} d^3\mathbf{r}\, \frac{\delta}{e_0\delta U(\mathbf{r})} = -\frac{d}{dE} \tag{5.66}$$

therefore,

$$\int_{\Omega} d^3\mathbf{r} \frac{\delta}{e_0\delta U(\mathbf{r})} \approx -\frac{d}{dE} \tag{5.67}$$

$$\text{thus,} \quad \rho_d(E) \approx \frac{1}{2\pi}\sum_{\alpha\gamma}\left[|s_{\alpha\gamma}|^2 \frac{d\theta_{s_{\alpha\gamma}}}{dE}\right] \tag{5.68}$$

The Eq.(5.68) is true because the global integration on LHS of Eq.(5.66) implies that the potential can be increased (or decreased) by a constant amount globally which is identical to not shifting the potential but decreasing (or increasing) the incident energy. An experimentalist can easily achieve this by changing the Fermi energy but what appears in Eq.(4.24) is not a global integration but a sample integration. For a large bulk system one need not make a difference between the two but for a mesoscopic system we may only write the approximate equality in Eq.(5.68). Further simplifications of RHS in Eq.(5.68) gives

$$\pi\rho_d(E) \approx \frac{d}{dE}\theta_f(E) \tag{5.69}$$

The Friedel phase is denoted by $\theta_f(E) = \frac{1}{2i}\log(\det[s])$, the scattering matrix is denoted by s, and the density of states is represented by $\rho_d(E) = \frac{dn(E)}{dE}$. This equation is referred to as the Friedel Sum Rule (FSR). But even though all of the leads add up to give DOS, each lead's injectance is random.

In 1D α and γ can each take two values leading to the fact that $s_{11} = r$, the reflection amplitude when incidence is from the left. Similarly, $s_{21} = t$, the transmission amplitude when incidence is from the left, $s_{12} = t$, the transmission amplitude when incidence is from the right, and $s_{22} = r^*$, the reflection amplitude when incidence is from the right. There are many other conventions of representing this that does not compromise the physical reality. We can substitute these values in Eq.(4.26) and then use the substitution from Eq.(5.67) to get

$$\rho(E,1) \approx \frac{1}{2\pi}\left[|r|^2\frac{d\theta_r}{dE} + |t|^2\frac{d\theta_t}{dE}\right] \tag{5.70}$$

Note that when talking of injectance of lead 1, we have to only consider incidence from the left. In 1D it was shown [70] that the correction term can be determined in 1D to give

$$\rho(E,1) = \frac{1}{2\pi}\left[|r|^2\,\frac{d\theta_r}{dE} + |t|^2\,\frac{d\theta_t}{dE} + \frac{m_0|r|}{\hbar k^2}\,\sin(\theta_r)\right] \tag{5.71}$$

which indicates that the final term is the quantum interference effects correction term to the semi-classical formula. $\sin(\theta_r)$ goes to zero, and the textbook FSR is recovered if we take into account a semi-classical regime in which the electron behaves like a classical particle. Taking ensemble averaging that removes any dependence on $\sin(\theta_r)$ and effectively causes the system to behave semi-classically is one way to realize the semi-classical regime. Speaking of a purely quantum system, we can observe a semi-classical behaviour as $|r| \to 0$ without resorting to statistical mechanics concepts such as ensemble averaging. A quantum particle above the barrier may be fully reflected back in what is referred to as the WKB regime if the scale at which the potential varies is substantially larger than the quantum particle's wavelength. We will discuss a scenario where $|r| \to 0$, but the correction term goes to zero because $\sin(\theta_r) = 0$. This can only be obtained in a purely

quantum regime if the evanescent modes are properly taken into account; in a quantum regime, the semi-classical formula becomes exact. When we need to compute the derivatives and make minor adjustments to the incident energy, as we can see in Eq.(5.70), semi-classical formulas are always simple to work with. So, an experimentalist or theorist can benefit greatly if a semi-classical formula becomes exact in a quantum regime. Even though we have shown that Eq.(5.70) can become exact in a quantum regime, we will continue to refer to it as the semi-classical formula, see [67].

5.4 Burgers circuit

A Burgers circuit is about phase changes and lapses being determined by phase singularities, and an Argand diagram is a plot of the real versus imaginary parts of an analytic complex function. I is a topological quantum number that is always conserved in an interaction given a complex function t and a phase singularity in its complex plane. Since I am a sign, I can also be +1, -1, or 0. According to M.V. Berry (1998) [71], for a generalized "Burgers circuit" (BC),

$$\oint_C d\phi = 2\pi I \tag{5.72}$$

Here, $\phi = \arctan\left[\frac{\mathrm{Im}(t)}{\mathrm{Re}(t)}\right]$. C stands for contour. I is 0 if the phase singularity is not enclosed by the contour C. The value of I is -1 when the contour C enclosing a phase singularity is in a clockwise direction, and $+1$ when it is in a counterclockwise direction. A scattering matrix element is a complex function that can be represented by an Argand diagram and used to apply the Burgers circuit principle. When we refer to the scattering matrix element in the remaining sections of this chapter, we mean the scattering matrix element of a quantum mechanical particle, such as an electron. When the incident energy of the scattering particle increases, the Argand diagram for a scattering matrix element typically goes counter-clockwise. At the phase singularity, Re(t) = 0 and Im(t) = 0, implying the phase singularity is at the origin.

We will show that the scattering phase shift behaviour of various experimentally and theoretically studied systems can be understood from the Argand diagrams analytically. Each such system has its own peculiarities and therefore required to be understood with rigorous mathematical principles like Burgers circuit and Argand diagram. Argand diagram for the scattering matrix element of these systems can be classified in universality classes as, a) Argand diagram is closed, b) Argand diagram is open, c) Argand diagram encloses the phase singularity, d) Argand diagram does not enclose the phase singularity, e) Argand diagram is simply connected and f) Argand diagram is multiply connected due to the presence of sub-loops. Specific properties of the scatterer only matter to the ex-

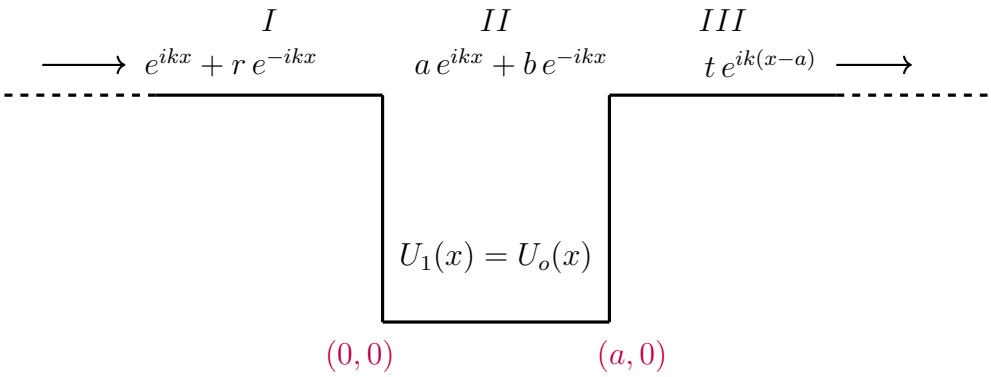

Figure 5.5: Schematic representation for scattering of electrons by a square well potential in one dimension. The direction of incident and transmitted electrons are represented by arrows. The solid line represents a quantum wire with square well potential. The dashed lines represent the fact that the quantum wire is connected to electron reservoirs via leads.

tent that the Argand diagram changes from one of these to another. Among them some changes are topologically possible and others are not. Understanding how an Argand diagram changes from one to the other explains most of the puzzles.

5.5 Square well potential in one dimension

Let us first consider scattering by a square well function potential in one dimension (1D) schematically shown in figure 5.5. This potential shows same result as Dirac delta potential in U. Satpathi and P. Singha Deo, IJMPB 26 1250028 (2012) [55]. Although a simple potential, it exhibits pronounced Breit-Wigner (BW) resonances. We will use Eq.(5.72) to understand the scattering phase shift for this system and hence for BW resonances. The scattering potential for this system can be written as,

$$U_1(x) = U_0(x) \tag{5.73}$$

The wave function in different regions marked I, II and III are (see figure 5.5),

$$\psi(x) = \begin{cases} e^{ikx} + re^{-ikx}, & \text{for } x < 0, \\ a\,e^{ikx} + b\,e^{-ikx}, & \text{for } 0 \leq x \leq a, \\ te^{ik(x-a)}, & \text{for } x > a. \end{cases}$$

Here, r and t are the reflection and transmission amplitudes, $k = \sqrt{\frac{2m_0e_0}{\hbar^2}E}$ is the wave vector and E is incident Fermi energy. $t = \mid t \mid e^{i\theta_t}$, where, $\theta_t = \arctan\frac{\mathrm{Im(t)}}{\mathrm{Re(t)}}$ is transmission phase shift and $|t| = \sqrt{\mathrm{Im(t)}^2 + \mathrm{Re(t)}^2}$ is transmission modulus. The Argand diagram for t is shown in figure 5.6, where energy is varied to remain within the first Riemann

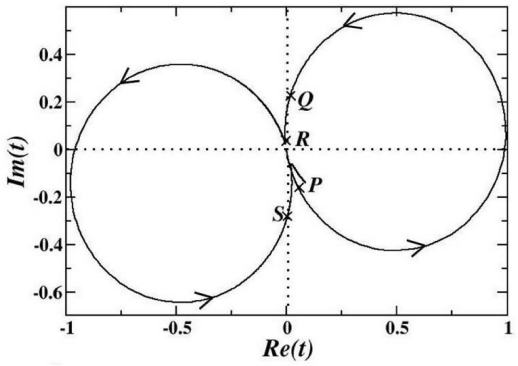

Figure 5.6: Argand diagram for transmission amplitude for the square well potential using parameters $e_0U_1a = e_0U_1a = 40$, $a = 1$, $e_0 = 1, 2m_0e_0 = 1$ and $\hbar = 1$. The Dirac delta potential also shows the same result, as mentioned in U. Satpathi and P. Singha Deo, IJMPB 26 1250028 (2012) [9, 55].

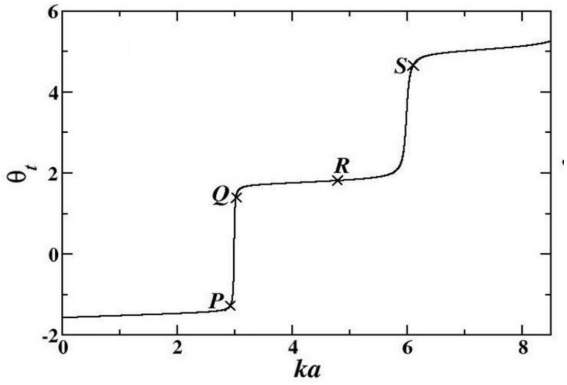

Figure 5.7: Plot of transmission phase shift θ_t versus ka, for the square well potential using parameters $e_0U_1a = e_0U_1a = 40$, $a = 1$, $e_0 = 1, 2m_0e_0 = 1$ and $\hbar = 1$. This result also smiliar to U. Satpathi and P. Singha Deo, IJMPB 26 1250028 (2012) [9, 55].

surface. There is a phase singularity at the origin where $t = 0$. The Argand diagram encloses the singularity but is not closed in the first Riemann surface. Figures 5.7 and 5.8 show the transmission phase shift θ_t and the transmission coefficient $|t|^2$, respectively, as a function of ka, using the same parameters as in figure 5.6.

In figure 5.6, the contour starts from the origin where $E = 0$, goes first through point P and then through Q, R and S. The trajectory facing the singular point at the origin is concave throughout the phase increases continuously. This is evident in figure 5.7 where the points P, Q, R and S are also shown at their respective values of ka. As the trajectory comes closer to the point of phase singularity, phase changes are very small and energy cost is very high. In figure 5.6, the energy at the points marked P, Q, R and S are $8.614a$, $9.12a$, $23.61a$ and $37.58a$. Thus, the energy change in going from P to Q (a large arc in the trajectory in figure 5.6) is very small, whereas the energy change in going from Q to R (a small arc in the trajectory in figure 5.6 is very high). The point R is very close to the singular point. Thus, it costs a lot of energy as the Argand diagram trajectory tries to approach the point of phase singularity.

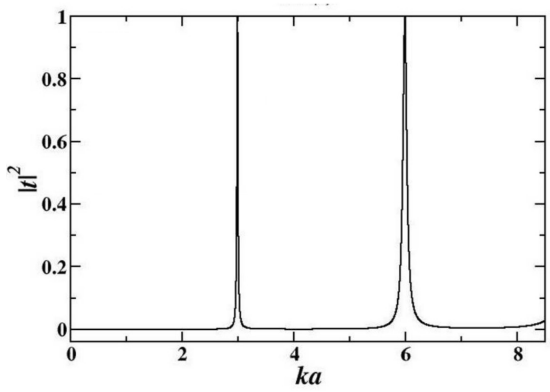

Figure 5.8: Plot of transmission coefficient $|t|^2$ versus ka, for the square well potential using parameters $e_0U_1a = e_0U_1a = 40$, $a = 1$, $e_0 = 1, 2m_0e_0 = 1$ and $\hbar = 1$. This graph is similar to U. Satpathi and P. Singha Deo, IJMPB 26 1250028 (2012) [9, 55].

The fact that partial density of states (PDOS) can be determined exactly from semi-classical formula at the Fano resonances can be very useful. Because an experimentalist can just vary the Fermi energy of the incident particle in a typical mesoscopic scattering scenario and measure the scattering phase shift as was demonstrated by [29]. From the energy derivative of the phase shift the PDOS can be determined without any knowledge of the exact potential profile and impurity configuration inside the system. Thus, several objects in the hierarchy of DOS that determine thermodynamic and transport properties of the sample can be known. This will be specially useful because mesoscopic systems are not in the ergodic regime allowing us to average over impurity configurations.

5.6 Delta function potential in quasi-1D

We cannot solve the multichannel case (apart from truncating the series of evanescent modes and applying numerical techniques) for any potential except for the case described in this section. However, our main results can be proved generally using mathematical theorems and principles for any potential and this will be presented in the next two chapters.

Here, we will study the two propagating channel (with arbitrary number of evanescent channel) case for a particular potential, i.e., $U_g(x, y) = \gamma\delta(x)\delta(y - y_i)$, because it can be exactly solved and certain facts can be exhibited explicitly. In figure 5.9, the shaded region of figure 5.1 reduces to give a two-dimensional quantum wire with a delta function potential at position $(0, y_i)$ marked X. The dashed lines in figure 5.9 represent the fact that the quantum wire is connected to electron reservoirs.

We will first calculate this injectance from internal wave function $\psi(x, y, 1)$ which allows one to make numerical verification of the semi-classical formulas in Eqs.(5.1) and (5.6), along with their correction terms in Eqs.(5.5) and (5.8). We know that when

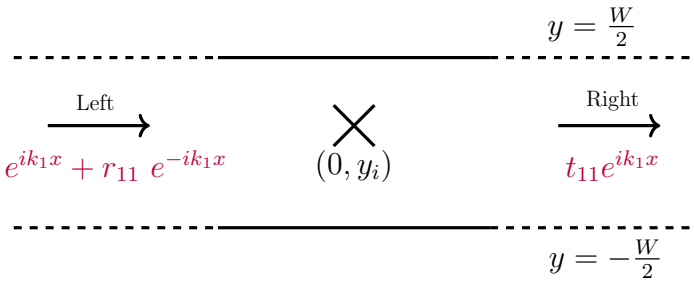

Figure 5.9: A Dirac delta function potential is shown in a quantum wire. In this figure, the shaded region of figure 5.1 reduces to give a two-dimensional quantum wire with a delta function potential. The cross sign shows the delta function potential at $(0, y_i)$. The width in y-direction is shown from $y = -\frac{W}{2}$ to $y = \frac{W}{2}$. Incident and transmitted wave packets are shown with solid arrows. The dashed lines represent the fact that the quantum wire is connected to electron reservoirs.

incidence is along n=1 channel

$$\rho(1, E) = \int_{-\infty}^{\infty} dx \int_{-\frac{W}{2}}^{\frac{W}{2}} dy \sum_{k_1} \mid \psi(x, y, 1) \mid^2 \delta(E - E_{1,k_1}) \tag{5.74}$$

Here, E_{1,k_1} is the energy of the incident electron along channel $n = 1$ with wave vector $k_{n=1}$ or k_1. Summing over n one can get the standard expression for DOS according to spectral theorem. Note that although k_1 can vary continuously, one can write sum over k_1 precisely because of the spectral theorem. One can write for the system represented in figure 5.9 [57] when incidence is along n=1 channel

$$\psi(x, y, 1) = \sum_m f_m(x, 1)\chi_m(y) \tag{5.75}$$

Here, $\chi_m(y)s$ are solutions in Eq.(5.15) in the leads in the transverse direction which is an infinite square well potential in y-direction. $\chi_m(y)s$ form a complete set and Eq.(5.75) is derived from the fact that at a given point x, the wave function in the scattering region can be expanded in terms of $\chi_m(y)s$. We will present our results for the case of two propagating channels but the analysis and results are same for any number of channels. f_ms are generally of the form given below,

$$f_1(x, 1) = \begin{cases} e^{ik_1x} + r_{11}e^{-ik_1x} & \text{for } x < 0 \\ t_{11}e^{ik_1x} & \text{for } x > 0 \end{cases} \tag{5.76}$$

$$f_2(x, 1) = \begin{cases} r_{21}e^{-ik_2x} & \text{for } x < 0 \\ t_{21}e^{ik_2x} & \text{for } x > 0 \end{cases} \tag{5.77}$$

$$\text{and for } m > 2, \qquad f_m(x, 1) = \begin{cases} r_{m1}e^{\kappa_m x} & \text{for } x < 0 \\ t'_{m1}e^{-\kappa_m x} & for\ \ x > 0 \end{cases} \tag{5.78}$$

$$\text{and for } m > 2, \qquad f_m(x,1) = \begin{cases} r_{m1}e^{\kappa_m x} & \text{for } x < 0 \\ t'_{m1}e^{-\kappa_m x} & \text{for } x > 0 \end{cases} \tag{5.79}$$

For $m > 2$, $(\varepsilon_m - E) = \frac{\hbar^2\kappa_m^2}{2m_0}$, κ_m being positive define evanescent modes as now $E < \varepsilon_m$. r_{mn}, t_{mn}, r'_{mn} and t'_{mn} are unknowns to be determined. The scattering problem described above can be solved using mode matching technique. The reflection amplitudes are given by [57],

$$r_{mn}(E) = -\frac{i\frac{\Gamma_{mn}}{2\sqrt{k_m k_n}}}{1 + \sum_e \frac{\Gamma_{ee}}{2k_e} + i\sum_m \frac{\Gamma_{mm}}{2k_m}} \tag{5.80}$$

Γ_{mn} is the coupling strength between mth and nth modes, given by

$$\Gamma_{mn} = \gamma \sin\left(\frac{m\pi}{W}(y_i + \frac{W}{2})\right) \sin\left(\frac{n\pi}{W}(y_i + \frac{W}{2})\right) \tag{5.81}$$

The transmission amplitudes are given by

$$t_{mn} = r_{mn}(E) \text{ for } m \neq n \tag{5.82}$$

$$\text{and } t_{mm}(E) = 1 + r_{mm}(E) \tag{5.83}$$

Along the same line one can show that

$$r'_{m1} = t'_{m1}(E) = -\frac{\frac{\Gamma_{m1}}{2\kappa_m}}{1 + \sum_e \frac{\Gamma_{ee}}{2k_e} + i(\frac{\Gamma_{11}}{2k_1} + \frac{\Gamma_{22}}{2k_2})} \tag{5.84}$$

$\sum_e$ denote sum over evanescent modes and run from m =3 to ∞, while $\sum_m$ denote the same for propagating modes (i.e., $m = 1$ and $m = 2$). If the delta function potential is negative ($\gamma < 0$), then there can be bound states as argued before. As explained in figure 5.4 it will always be a quasi-bound state. The quasi-bound state for channel $m = s \geq 2$ is given by [57],

$$1 + \sum_{e=s}^{\infty} \frac{\Gamma_{ee}}{2k_e} = 0 \tag{5.85}$$

Only bound state for $m = 1$ channel is a true bound state and it is given by the solution to the following equation, $1 + \sum_{e=1}^{\infty} \frac{\Gamma_{ee}}{2k_e} = 0$. The bound state for $m = 2$ is given by

$$1 + \sum_{e=2}^{\infty} \frac{\Gamma_{ee}}{2k_e} = 0 \tag{5.86}$$

At this energy, we get a bound state for $m = 2$, but at that very energy $m = 1$ channel (or k_1 channel) is a propagating channel as can be seen in Eq.(5.42). Hence, the bound state given by this Eq.(5.86) is a quasi-bound state or a resonance. The delta function

in Eq.(5.74) summed over k_1 essentially yield a factor $\frac{1}{hv_1}$, where $v_1 = \frac{\hbar k_1}{m}$. Substituting for $\psi(x, y, 1)$ from Eq.(5.75) and using the orthogonality of $\chi_m(y)s$, we get,

$$\rho(E,1) = \frac{1}{hv_1}\left[\int_{-\infty}^{\infty} dx \sum_m \mid f_m(x,1) \mid^2\right] \tag{5.87}$$

$$= \frac{1}{hv_1}\left[\int_{-\infty}^{\infty} dx \mid f_1(x,1) \mid^2 + \int_{-\infty}^{\infty} dx \mid f_2(x,1) \mid^2 + \right.$$
$$\left.\int_{-\infty}^{\infty} dx \mid f_3(x,1) \mid^2 + \int_{-\infty}^{\infty} dx \mid f_4(x,1) \mid^2 + ...\right] \tag{5.88}$$

Substituting the values of $f_m(x,1)s$ from Eqs.(5.76)-(5.79), we get

$$\rho(E,1) = \frac{1}{hv_1}\left[\int_{-\infty}^{0} dx\,[1+ \mid r_{11} \mid^2 + 2 \mid r_{11} \mid \cos(2k_1x + \phi_1)]\right.$$
$$\left. + \int_0^{\infty} dx \mid t_{11} \mid^2 + \int_{-\infty}^{0} dx \mid r_{21} \mid^2 + \int_0^{\infty} dx \mid t_{21} \mid^2 + H\right] \tag{5.89}$$

Here, $r_{11} =\mid r_{11} \mid e^{-i\phi_1}$. Note that for $m > 2$,

$$H = \int_{-\infty}^{\infty} dx \sum_{m>2} \mid f_m(x,1) \mid^2 = \sum_{m>2} \mid t'_{m1} \mid^2 \left[\int_{-\infty}^{0} e^{2\kappa_m x} dx + \int_0^{\infty} e^{-2\kappa_m x} dx\right]$$
$$= \sum_{m>2} \frac{\mid t'_{m1} \mid^2}{\kappa_m} \tag{5.90}$$

Thus,

$$\rho(E,1) = \frac{1+ \mid r_{11} \mid^2 + \mid r_{21} \mid^2}{hv_1}\int_{-\infty}^{0} dx + \frac{\mid t_{11} \mid^2 + \mid t_{21} \mid^2}{hv_1}\int_0^{\infty} dx$$
$$+ \frac{2 \mid r_{11} \mid}{hv_1}\int_{-\infty}^{0} dx\, \cos(2k_1x + \phi_1) + \frac{1}{hv_1}\left(\frac{\mid t'_{31} \mid^2}{\kappa_3} + \frac{\mid t'_{41} \mid^2}{\kappa_4} + ...\right) \tag{5.91}$$

Adding and subtracting the following terms,

$$\frac{\mid t_{11} \mid^2}{hv_1}\int_{-\infty}^{0} dx, \quad \frac{\mid t_{21} \mid^2}{hv_1}\int_{-\infty}^{0} dx$$

and using the fact that,

$$\frac{\mid t_{11} \mid^2}{hv_1}\int_{-\infty}^{0} dx = \frac{\mid t_{11} \mid^2}{hv_1}\int_0^{\infty} dx$$

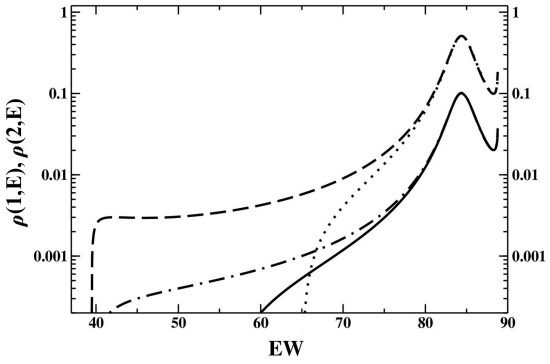

Figure 5.10: The plot is of injectance versus incident energy EW. We have used $e_0\gamma W = -15$, and $y_i = 0.45W$. The figure shows that semi-classical formula becomes exact at resonance where there is a peak in injectance. Injectance of first transverse mode is less than that of the second. This result is in U. Satpathi and P. Singha Deo, IJMPB 26 1250028 (2012) [9, 55].

and $\mid r_{11} \mid^2 + \mid r_{21} \mid^2 + \mid t_{11} \mid^2 + \mid t_{21} \mid^2 = 1$, we get,

$$\rho(E,1) = \frac{1}{hv_1}\int_{-\infty}^{\infty} dx + \frac{\mid r_{11} \mid}{hv_1}\int_{-\infty}^{\infty} dx\, \cos(2k_1x + \phi_1) + \frac{1}{hv_1}\left(\frac{\mid t'_{31} \mid^2}{\kappa_3} + \frac{\mid t'_{41} \mid^2}{\kappa_4} + ...\right) \tag{5.92}$$

$\frac{1}{hv_1}\int_{-\infty}^{\infty} dx = P_0(E)$ is the injectance in the absence of scatterer. Again if the scattering phase shift is defined with respect to the phase shift in absence of scatterer then this term can be dropped as shown in Eqs.(3.75) and (3.78) in [9]. Now,

$$\int_{-\infty}^{\infty} dx\, \cos(2k_1x + \phi_1) = \delta(2k_1)\, \cos(\phi_1)$$

As $k_1 = 0$ is not a propagating state contributing to transport, this term in Eq.(5.92) becomes zero, and we are left with,

$$\rho(E,1) = \frac{1}{hv_1}\left(\frac{\mid t'_{31} \mid^2}{\kappa_3} + \frac{\mid t'_{41} \mid^2}{\kappa_4} + ...\right) \tag{5.93}$$

Similarly, for incidence along channel 2, one can obtain the injectance.

$$\rho(E,2) = \frac{1}{hv_2}\left(\frac{\mid t'_{32} \mid^2}{\kappa_3} + \frac{\mid t'_{42} \mid^2}{\kappa_4} + ...\right) \tag{5.94}$$

In figure 5.10, we make a comparison between the semi-classical injectance $\rho(E,1)$ (solid curve) from Eq.(5.1) and the same from the exact formula in Eq.(5.93) (dash-dot curve). The resonance condition in Eq.(5.86) is satisfied at $EW = 84.29$ at which the

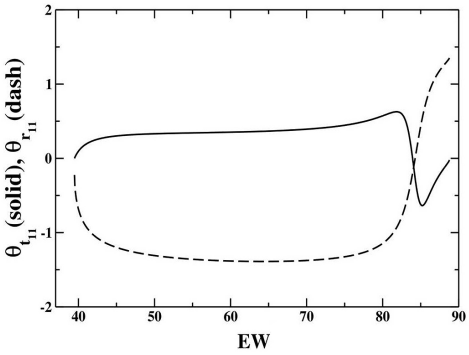

Figure 5.11: Here, we plot reflection phase shift $\theta_{r_{11}}$ (dashed curve) and transmission phase shift $\theta_{t_{11}}$ (solid curve) versus incident energy for the same parameter values as in figure 5.10. The figure shows that the scattering phase shifts become simultaneously zero at the resonance while being out of phase for the rest of the energy regime. And so the initial phase of the wave function which is usually undetermined do not play a role. That initial phase can be absorbed in $\theta_{r_{11}}$ to give the same conclusion. This result is also in U. Satpathi and P. Singha Deo, IJMPB 26 1250028 (2012) [9, 55].

injectance peaks. Surprisingly, at the resonance the semi-classical formula becomes exact. The same happens for $\rho(E, 2)$ for which the semi-classical formula in Eq.(5.6) gives the dotted curve and the exact formula in Eq.(5.94) gives the dashed curve. That this is not a special situation for the delta function potential but a general feature of Fano resonances will be shown in the next chapter. We have also stated earlier that the exactness of a semi-classical formula can find applications which will be further elaborated in the next two chapters.

It is to be noted that that the semi-classical formula becomes exact (not a good approximation but exact) in a quantum regime which will be proved in the next two chapters and physical reasons will be given. But here we demonstrate in figure 5.11, plotted for the same parameters as in figure 5.10, the fact that at the resonance $EW = 84.29$ the phase fluctuations maximise. However, at the resonance the correction term goes to zero as $\theta_{r_{11}}$ goes to zero resulting in $\sin(\theta_{r_{11}})$ becoming zero in Eq.(5.5). The same happens for $\theta_{r_{22}}$. Hence, this situation is different from what was thought earlier that only in the semi-classical regime when $|r_{11}|^2$ becomes negligible, the correction term can be ignored. In a semi-classical regime, a particle is expected to behave like a classical particle which is entirely transmitted. This chapter is discussed in [9, 55].

CHAPTER 6

EXPERIMENTAL MANIFESTATIONS OF NEGATIVE LOCAL PARTIAL DENSITY OF STATES

Time in quantum mechanics appear as a parameter and there is no self-adjoint time operator consistently defined yet. This is not a serious problem, as experimentalists only measure time intervals. This suits mesoscopic physics, wherein we have a system that acts as a quantum scatterer coupled to reservoirs via perfectly conducting leads. The reservoirs are completely thermalized and classical, and inside the reservoirs, time will be just the classically recorded time. The reservoirs also ensure that states do not naturally form linear superpositions in the leads, and this results in a textbook style scattering phenomenon that can be studied by constructing an incident wave packet or plane partial waves. The electron propagation from one lead to another takes place via scattering through the sample, and this dynamics is purely guided by quantum mechanics. Thus, a propagation or traversal time does not violate any principle. However, theoretical problems remain and that is what we intend to address in this chapter. Quantum mechanics gives this measured time interval very correctly in the semi-classical limit [72]. The low energy quantum limit is so far not understood in 1D, 2D and 3D since calculated time interval is not always consistent with the Copenhagen interpretation of quantum mechanics. It is known that quantum mechanics starts from a very different set of axioms and does not have to respect theory of relativity within the single particle coherence length. At the low energies of the mesoscopic systems, the Schrödinger equation determines the dynamics within this single particle coherence length, and it is completely independent of the speed of light. Beyond this coherence length, all phenomena have to respect a special

theory of relativity, and information speed is limited by the speed of light. We go beyond 1D, 2D and 3D and look into quasi 1D (Q1D) in Chapter 5.

In [34], we have argued that the experimental data has to also be represented in the form of Argand diagrams (ADs) so that we can see the loops and sub-loops, rather than plotting scattering phase shifts and cross-sections separately. We can see in figure 5.6 and 5.7 that a small change in scattering cross-section is associated with a large change (in quality and quantity) in phase shifts and vice versa. Data can be represented in multiple ways but the ADs allow us to interpret in terms of topology and analysis which goes beyond quantum mechanics. We believe there are many other subtle aspects in ADs that are very informative and one has to study them in the future. To provide a proper justification, we need more densely obtained experimental data plotted in the form of ADs. Below, we talk about some other experiments that can be done with present-day technologies that can tell us more about the hierarchy of density of states (DOS), mesoscopic response, and time travel. This kind of experiment has already been done but one has to redo them focusing on specific aspects to be highlighted below.

In Section 6.1, we describe an experimental setup of three-terminal in which lead β serves as a weak coupling to the sample or voltage probe. Furthermore, we extend our discussion on the same experimental setup, considering a theoretical 1D three-prong potential. In Section 6.2, we predict the experimental results for three probe setup and show in plots.

6.1 Three probe setup: a theoretical experiment

We consider a special case of the system which is shown in figure 4.2. We have only two fixed leads and an scanning tunneling microscope (STM) tip making it a three probe setup [8, 10, 11]. The STM tip is given a lead index β, and the fixed leads are indexed γ and α, as shown in figure 6.1. The STM tip is such that we can vary its proximity to the sample and thus can have four possible cases. The first case is that it does not make an actual contact and also does not draw or deliver any current but can locally change the electrostatic potential by $\delta U(\mathbf{r})$ at a point $\mathbf{r}$. The second case is that it does not make a contact but can draw or deliver a current via weak coupling to the states of the system. What it means is that the STM tip is weakly coupled to the states of the sample and exchange of current do not alter the states of the sample to an approximation. The third case is that it makes an actual contact and becomes like any other lead. The fourth is that it makes a contact and yet does not draw or deliver a current because its chemical potential is so adjusted. The fourth case is the typical situation of the Landauer-Büttiker three probe conductance setup which is now well established as a mesoscopic phenomenon greatly studied theoretically as well as experimentally [8, 10, 11]. We will first analyse

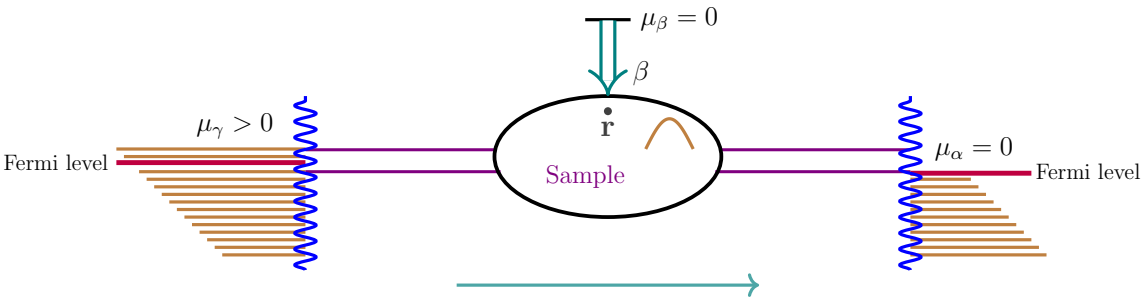

Figure 6.1: This setup is simplest form of figure 4.2. In this figure, there are only two lead indicies α and γ expect STM tip or lead β. This is a cartoon of a realistic experimental setup that help us measure some of the lower members in the hierarchy of DOS. Let's say chemical potential of lead α and γ are μ_α and μ_γ, respectively. Lead β is being earthed, chemical potential of lead β, μ_β, will be zero. Lead β allows tunneling when it is brought to the local coordinate $\mathbf{r}$. The chemical potential of lead γ is higher than lead α and β. As one can see in this figure that chemical potential of lead α and β is zero. So, current will go from lead γ to lead α, shown with arrow. Electrons are also allowed to go to lead β as well. The wavy sign is shown for Fano resonance.

the second case with respect to negative density of states (DOS) object and show that it is a paradigm to indirectly test time travel experimentally [9, 10, 11]. And then we will show how these predictions naturally come up in well studied case four as well and were not noticed before as the specific design was not considered.

We will first show how some of the lower objects of DOS can manifest in this experimental setup of figure 6.1 that can be measured. Here, the sample is the shaded region between the two leads that are indexed γ and α, while the STM tip is indexed β. We have seen in Chapter 5 that such a realistic system can generally exhibit Fano resonances. At zero temperature below the Fermi energy the transmission probability T of quantum mechanics is $\frac{h}{e_0}$ of electronic current (see Eq.(3.30)) at that particular energy E and that is how the following formulas are to be interpreted. Let us consider the situation when the tip of β is not making a physical contact with the sample but close enough to deliver (or draw) a current to (or from) the sample due to weak coupling (case II). Experimentally, we can create special situations when only one lead injects current and all other leads carry current away or only one lead emits current while all other leads inject current. Otherwise, current could be come from any lead and take away by any lead, and it is not possible to trace which current goes where, but the following quantities that depend on objects of the hierarchy of density of states can experimentally manifest [8].

$$T^e_{\beta\alpha} = 4\,\pi^2\,\nu_\beta\,|t|^2\rho_i(E,\mathbf{r},\alpha) \tag{6.1a}$$
$$T^i_{\alpha\beta} = 4\,\pi^2\,\nu_\beta\,|t|^2\rho_e(E,\alpha,\mathbf{r}) \tag{6.1b}$$
$$T^e_{\beta\gamma} = 4\,\pi^2\,\nu_\beta\,|t|^2\rho_i(E,\mathbf{r},\gamma) \tag{6.1c}$$
$$T^e_{\gamma\beta} = 4\,\pi^2\,\nu_\beta\,|t|^2\rho_e(E,\gamma,\mathbf{r}) \tag{6.1d}$$

Let us interpret one of them; the rest can be similarly interpreted. In Eq.(6.1a), trans-

mission probability $T^e_{\beta\alpha}$ is probability of lead β when lead α is injecting current at the remote point $\mathbf{r}$, and lead β is emitting current away from the sample. This quantity, $T^e_{\beta\alpha}$, is proportional to the injectivity of lead α to a remote point $\mathbf{r}$, i.e., $\rho_i(E, \mathbf{r}, \alpha)$. The ν_β is the density of states in lead β that couples with the quantum states of the sample that coupling is represented by coupling strength parameter t. Eqs.(6.1a) and (6.1c) correspond to current taken away by lead β and Eqs.(6.1b) and (6.1d) correspond to current brought into the sample by lead β. In all these equations, we used $|t|^2$, which can be evaluated in principle. By taking a final state in the sample and an initial state in lead β and then calculating an integration by time-independent Fermi's golden rule. But we are not interested in doing exact calculations, so we just used the parameter $|t|^2$.

Let us now setup the biases in figure 6.1 correspond to the situation such that classically, electrons can be incident along only one lead γ and scattered to α or β. Lead β is weakly coupled to the sample or shaded region in figure 6.1 in order to correspond to second case of lead β. Let say chemical potential of left reservoir connected to lead γ be μ_γ, and chemical potential of right reservoir connected to lead α be μ_α, and other end of lead β is being earthed. Incident energy of electrons is such that $0 < \mu_\alpha < E < \mu_\gamma$, only lead γ can inject current inside the sample. Such a setup can be obtained in the laboratory and we want to address the coherent current flowing from γ to α. It was shown [8] that in such a situation

$$|s'_{\alpha\gamma}|^2 - |s_{\alpha\gamma}|^2 = -4\,\pi^2\,\nu_\beta\,|t|^2\;\rho_{lpd}(E, \alpha, \mathbf{r}, \gamma) \tag{6.2}$$

Here, $s'_{\alpha\gamma}$ is the scattering matrix element for scattering from γ to α when the STM tip is drawing a current given by the term on RHS. $s'_{\alpha\gamma} = s_{\alpha\gamma}$ is the scattering amplitude that results from $t \to 0$ removing the STM tip. Intuitively speaking, ρ_{lpd} is positive definite and RHS is negative accounting for loss of coherent electrons to the earthed lead β. The measured current between γ and α is $|s_{\alpha\gamma}|^2$ multiplied by a factor $\frac{h}{e_0}$ give the measured mesoscopic current from lead γ to lead α. These scattering probabilities $|s'_{\alpha\gamma}|^2$ and $|s_{\alpha\gamma}|^2$ are very well defined in quantum mechanics and when multiplied by a factor $\frac{h}{e_0}$ they give the measured mesoscopic current from γ to α. One of the facts that has emerged from the study of Fano resonances in this thesis is that $\rho_{lpd}(E, \alpha, \mathbf{r}, \gamma)$ can be positive as well as negative, implying that $|s'_{\alpha\gamma}|^2 - |s_{\alpha\gamma}|^2$ can be also positive as well as negative according to Eq.(6.2). When $\rho_{lpd}(E, \alpha, \mathbf{r}, \gamma)$ is positive, then the sample will lose coherent current to the earthed STM tip, and when it is negative, it will draw coherent current from the earthed STM tip, which is counter-intuitive. As $|s'_{\alpha\gamma}|^2$ and $|s_{\alpha\gamma}|^2$ are both measurable and so if the equality in Eq.(6.2) can be justified, then in relative proportions $\rho_{lpd}(E, \alpha, \mathbf{r}, \gamma)$ is also measurable which is good enough to confirm its sign. One may always try to justify that from a brute force practical experiment, but we will show below that it can be justified by what we call a theoretical experiment.

We examine a system depicted in figure 6.2 as a theoretical experiment. Exact quantum mechanical computations can be performed for this system, which shows pronounced Fano resonances. As pointed out in Chapter 5, there are 6 universality classes based on Argand diagram (AD). We have said how the topology of the complex plane of $\mathrm{Im}(s_{\alpha\gamma})$ versus $\mathrm{Re}(s_{\alpha\gamma})$ give us these universality classes of Argand diagrams. Some of those classes may not have examples, but a couple of them can be easily realised and happen because of the nature of the resonances involved. For example, Breit-Wigner resonance give AD that is not closed in one Riemann surface but goes round the singularity. We know the system in figure 6.2 will produce an AD that has closed sub-loops within a single Riemann surface that does not enclose the phase singularity as a consequence of Fano resonance. Since it is a matter of finding a particular class of AD, one can study a 1D system as a representative of a class. In this sense, the system in figure 6.1 at Fano resonances with the modification that the upper lead is weakly coupled to earth via a strong potential can be represented by the 1D system in figure 6.2. Besides, if it is a question of whether local partial density of states is present at all in a quantum system and more importantly whether its negativity is allowed in quantum mechanics, then demonstrations in 1D quantum mechanics should suffice.

One has to further observe the fact that quantum mechanics is a theory for objects to be found in nature but everything that can be calculated from quantum mechanics may not be found in nature. Quantum mechanics does not prohibit the possibility of calculating an object like $\rho_{lpd} = -\frac{1}{2\pi}\,|s'_{\alpha\gamma}|^2\,\frac{\delta\theta_{s_{\alpha\gamma}}}{\delta U(\mathbf{r})}$, but cannot asceratin its occurence in nature. Such a coordinate dependent local partial density of states (LPDOS) cannot be defined from the wave function at the point $\mathbf{r}$ and so cannot be reconciled with the probabilistic interpretation of quantum mechanics. In quantum mechanics, an electron coming from γ can go to the STM tip or to the lead α or can get reflected back rather randomly, and there is no equation of motion for such an electron. Schrödinger equation is an equation for an ensemble of electrons and gives a probabilistic answer of $T_{\alpha\gamma} = |s_{\alpha\gamma}|^2$ completely ignoring how the individual electrons are behaving. So within the axiomatic framework of quantum mechanics, one cannot provide a quantitative or qualitative value for the number of γ to α bound electrons that pass through the point $\mathbf{r}$ of the sample and this has been discussed in detail in Chapter 4 while discussing Eqs.(4.25) and (4.26). In short, the LHS of Eq.(6.2) is physical according to quantum mechanics but the RHS is not. Suppose the system in figure 6.2 is configured in two different ways corresponding to different values of U_1. One is for primed terms and another is unprimed terms, where $|s_{31}|^2 = |t_{31}|^2$, $|s_{21}|^2 = |t_{21}|^2$, $|s_{11}|^2 = |r_{11}|^2$, etc.

$$|s'_{31}|^2 + |s'_{21}|^2 + |s'_{11}|^2 = 1 \tag{6.3}$$

$$|s_{31}|^2 + |s_{21}|^2 + |s_{11}|^2 = 1 \tag{6.4}$$

This is a consequence of unitarity or current conservation. With difference of primed Eq.(6.3) and unprimed Eq.(6.4) current conservation, one gets

$$|s'_{31}|^2 - |s_{31}|^2 = |s_{21}|^2 - |s'_{21}|^2 + |s_{11}|^2 - |s'_{11}|^2 \tag{6.5}$$

which means the LHS of Eq.(6.2) is well defined in quantum mechanics.

Larmor clock on the other hand uses analyticity of scattering matrix elements, and gives ρ_{lpd} as a physical quantity that says number of electrons going from γ to α access these partial states that are located at the point $\mathbf{r}$. Thus, Eq.(6.2) given by Buttiker says that in a quantum system, there is a local coordinate dependent DOS called local partial density of states (LPDOS) that can manifest in experiments although the standard theory of quantum mechanics says that is not possible. Existence of LPDOS failed to pass the test for two reasons.

- The original derivation of LPDOS in Chapter 4 uses the analyticity property of scattering matrix element but also has to use a number of ingredients from quantum mechanics as well as classical mechanics, for example spin precession and Larmor frequency.
- Also there was no way to reconcile the numerical values of LPDOS with Wigner delay time (WDT) in general or in regimes when both of them become negative.

The issue of negativity was explained in [33, 34], chapter 6 of the textbook [9], as a signature of time travel that manifests in complete consistency between Wigner delay time (WDT) and local partial density of states (LPDOS) if one makes use of special resonances called Fano resonances, which are easy to find in mesoscopic systems, as shown in Chapter 5. Time travel experiments may still be difficult to conduct practically. While the kinds of experiments schematically seen in figures 6.1 and 6.2 have been already done in mesoscopic systems. The Schrödinger equation gives quantum states on an infinite 1D line with density of states (DOS) being $\frac{1}{hv_0}$ which is independent of whether of these states are occupied by bosons or fermions and independent of temperature. Similarly, we say that the STM tip has a DOS given by ν_β and the point $\mathbf{r}$ in the sample with which the STM tip interacts. Thus, there are two DOS featured in Eqs.(6.1a)-(6.1d). One is ν_β and another one is an $\mathbf{r}$ dependent DOS. Each DOS quantity contains a factor of $\frac{1}{2\pi}$ that cancels the factor of $4\pi^2$. This $\frac{1}{2\pi}$ factor appears in Eq.(6.2). A simple interpretations for these factors can be given as follows. Note that LHS in these Eq.(6.2) give a current generated by a countable number of electrons while the states from a continuum to which we can only assign a density called DOS in units of $2\pi\,\rho(E,\gamma)$, and the RHS in terms of $\theta_{s_{\alpha\gamma}}(E)$ corresponding to a continuous relation. This is why we get a factor 2π on the RHS of Eq.(5.72). Second, we remove a further factor $|t|^2\,\nu_\beta$ from the same Eq.(6.2) since these factors are only required when utilising a commercially available STM tip, in

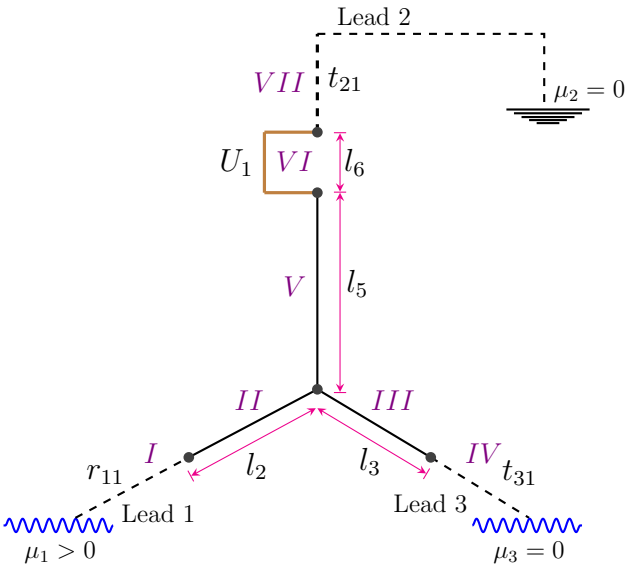

Figure 6.2: The sample is the three prong potential of figure 5.6 in [9] shown by the solid lines and the entire system consist of the sample connected to three reservoirs via three leads. Different regions of the system is marked by Roman numbers, I, IV and VII being the leads, shown by dashed lines. There is potetial U_1 in region VI of 1D three-prong potential, elsewhere potential U is zero. Lead 2 is made exactly like that in figure 5.6 [9] by earthing it and the chemical potential of lead 3 is also set to zero. In that case for a small positive chemical potential will create a situation wherein only lead 1 inject a current while the two other leads carry some current away from the sample. Lead 2 connects to the sample through a tunneling barrier shown as region VI. Lengths of different regions is shown as l_2, l_3 etc. This system is a 1D version of the system in figure 6.1 where lead γ is renamed as lead 1, etc, and as a result $t_{31} = s_{31}$, $t_{21} = s_{21}$, and $r_{11} = s_{11}$, see [33].

which case the STM tip is characterised by this factor. For the system in figure 6.2, a first principle calculation indicates that

$$|s'_{\alpha\gamma}|^2 - |s_{\alpha\gamma}|^2 = -2\pi\rho_{lpd}(E, \alpha, \mathbf{r}, \gamma) \tag{6.6}$$

Now correspond to figure 6.2

$$|t'_{31}|^2 - |t_{31}|^2 = -2\pi\rho_{lpd}(E, 3, \mathbf{r}, 1) \tag{6.7}$$

6.2 Results and discussions

We plot AD for the scattering matrix element t_{31} for the theoretical mesoscopic setup depicted in figure 6.2 by varying the tunneling potential U_1, which links the three prong potential with earthed lead 2. The AD diagram make smooth sub-loops within one Riemann surface and each sub-loop is due to a Fano resonance. Any physical quantity that depend on t_{31} will go through a cycle over one particular sub-loop. For one closed

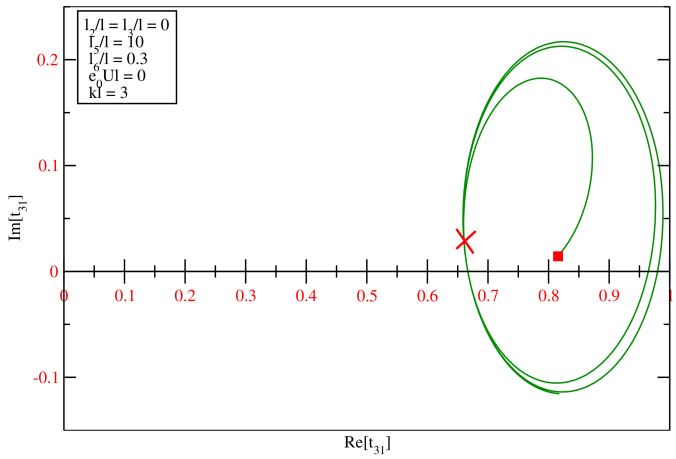

Figure 6.3: In this figure, we plot the Argand diagram for t_{31} of the system shown in figure 6.2 for the coupling potential U_1 varying in a range that give three sub-loops, all within one Riemann surface. The starting point is marked by a small square block corresponds to $e_0U_1l = -10000$. The end point is unmarked and corresponds to a value $e_0U_1l = -10$. All the sub-loops smoothly come back to a point marked by a cross. Other parameters are mentioned inside the figure.

sub-loop generated by monotonously varying a parameter, say U_1

$$\oint_c \Delta\theta_{t_{31}} = 0$$

here $\theta_{t_{31}} = \arctan \frac{\mathrm{Im}[t_{31}]}{\mathrm{Re}[t_{31}]}$

$$\text{or} \quad \oint_c \frac{\delta\theta_{t_{31}}}{\delta U_1(\mathbf{r})} \Delta U_1(\mathbf{r}) = 0 \tag{6.8}$$

$U_1(\mathbf{r})$ being a localised potential at the point $\mathbf{r}$.

$$\text{or} \quad \oint_c \frac{1}{2\pi} |t_{31}|^2 \frac{\delta\theta_{t_{31}}}{\delta U_1(\mathbf{r})} \Delta U_1(\mathbf{r}) = 0 \tag{6.9}$$

$$\text{or} \quad -\oint_c \rho_{lpd}(E, 3, \mathbf{r}, 1) \delta U_1(\mathbf{r}) = 0 \tag{6.10}$$

Similarly, over the same sub-loop for another value of $U_1(\mathbf{r})$

$$\oint_c \frac{\delta |t'_{31}|^2}{\delta U_1(\mathbf{r})} \Delta U_1(\mathbf{r}) = 0$$

$$\oint_c \Delta |t_{31}|^2 = 0 \tag{6.11}$$

Essentially, $\oint_c \delta |\mathrm{Re}[t_{31}] + \mathrm{Im}[t_{31}]|^2 = 0$. Therefore, from Eq.(6.9) and (6.11), we get the

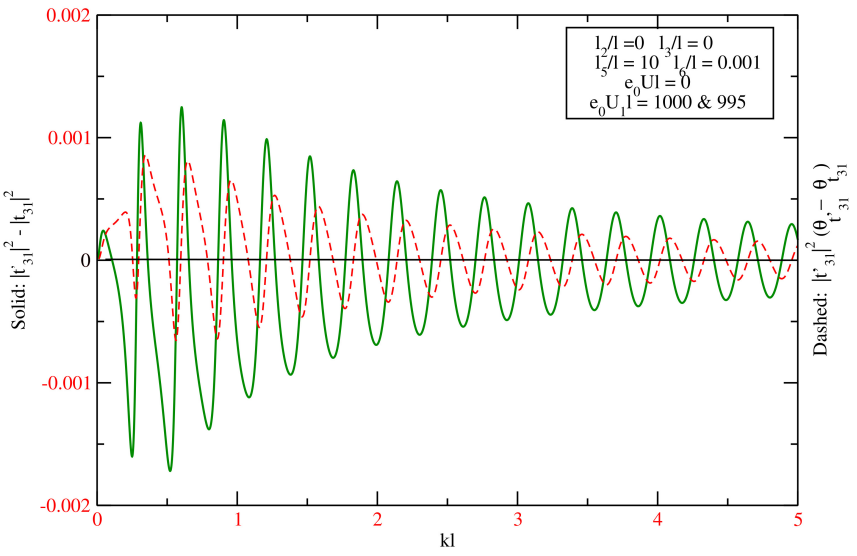

Figure 6.4: In this figure, we are plotting the LHS and RHS of Eq.(6.14) vs kl to show that both physical quantities can oscillate between positive and negative values. The primed and unprimed values are for small differences in U_1 at a k value that we vary continuously. The sign change and magnitude of both the curves originate from the smooth cyclic Argand diagram of figure 6.3.

equality

$$\oint_c \Delta|t_{31}|^2 = \oint_c \frac{1}{2\pi}|t_{31}|^2 \frac{\delta\theta_{t_{31}}}{\delta U_1(\mathbf{r})}\Delta U_1(\mathbf{r}) = 0 \tag{6.12}$$

purely as a consequence of the topology of a complex plane. The topology also tells that for loops that are not completely closed in one Riemann surface like that in the case of Briet-Wigner resonance in figure 6.5 (in this case system will considered like [11]), there will be correction term that has been discussed in Chapter 5 of this thesis. Now one can compare integrands in Eq.(6.12) we need extra

$$\Delta|t'_{31}|^2 \approx |t_{31}|^2 \frac{\delta\theta_{t_{31}}}{\delta U_1(\mathbf{r})}\Delta U_1(\mathbf{r}) = 0 \tag{6.13}$$

viewing a derivative as an effect of an infinitesimal change in U_1, we get

$$|t'_{31}|^2 - |t_{31}|^2 \approx |t'_{31}|^2(\theta_{t'_{31}} - \theta_{t_{31}}) \tag{6.14}$$

where primed quantities and unprimed quantities are calculated for an infinitesimal difference of U_1. If we want to compare integrands then we can only write an approximate equality because unlike in the case of Eq.(5.67) where we were comparing the same object over two sub-loops that are counterparts of each other, here we are comparing two

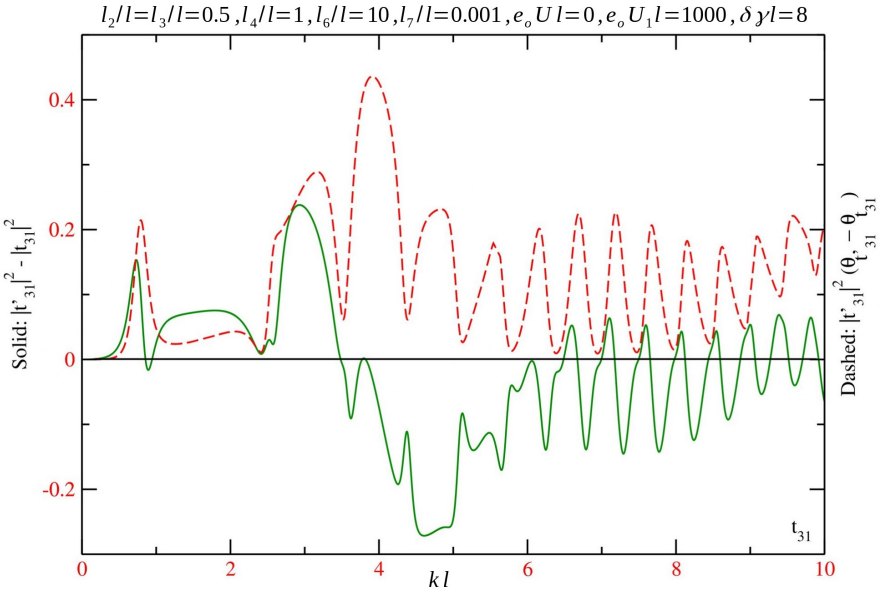

Figure 6.5: In this figure, we are plotting the LHS and RHS of Eq.(6.14) vs $k\,l$ to show that both sides of Eq.(6.2) do not oscillate between positive and negative values. The primed and unprimed values are for small differences in U_1 at a k value that we vary continuously. This curve has plotted in absence of Fano resonance.

different objects over one sub-loop. There will always be in the least a phase difference between the two quantities. From Eqs.(6.10) and (6.11) one gets

$$\oint_c \Delta|t_{31}|^2 = -\oint_c \rho_{lpd}(E,3,\mathbf{r},1)\Delta U_1(\mathbf{r}) = 0 \tag{6.15}$$

Therefore, it is obvious that $\Delta|t_{31}|^2$ will go through a positive-negative cycle over a closed sub-loop as a consequence of the topology of the relevant complex plane. Given the fact that LHS is physical, the cycles of ρ_{lpd} is also physical as they are just different expressions of the same sub-loop made by the Argand diagram (AD) of t_{31}. Fano resonances can be used to give a clear indication of that although the principle works for other resonances.

In figure 6.4, we plot LHS and RHS of Eq.(6.14) where the primed values and unprimed values are again for small differences in U_1 as the incident wave vector k is varied and that is the horizontal axis. It becomes clear that LHS and RHS of Eq.(6.14) oscillate with positive and negative values. Initially, the two curves are a little different but as k increases, effects of dispersion is minimized, and magnitudes of the two curves are similar with a phase difference between them. The oscillations of both the curves are due to the smooth cyclic nature of the AD in figure 6.3. In other words, the underlying principle behind the oscillation of both curves is the same.

We are all along considering the temperature to be zero, wherein the number of states is equal to the number of electrons, and in that case, it is easy to switch between statistical mechanics at zero temperature and pure quantum behaviour. Now in statistical

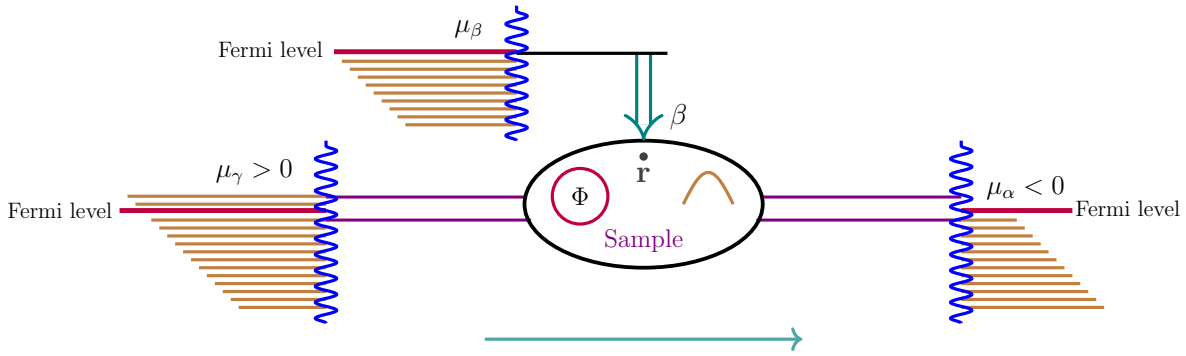

Figure 6.6: The role of lead β (an STM tip) is to inject or remove electrons from the system as well as causing some decoherence. The STM tip makes an actual contact with the sample at point $\mathbf{r}$ and μ_β is so adjusted that there is no net current flowing through the STM tip but it can still cause decoherence. At 0^oK, a current flows from lead γ to lead α in the energy interval $(\mu_\gamma - \mu_\alpha)$. One can put an Aharonov-Bohm flux Φ through the sample which is very useful to separate coherent and incoherent effects. In this setup, electrons are only allowed to lead α not to lead β from lead γ. The wavy sign is shown for Fano resonance.

mechanics, we can change many parameters and study an observable current. In the subsequent discussion, we will describe a setup that require us to tune and adjust the chemical potential μ_β of lead β. We focus on the situation shown in figure 6.6 where we have also taken an applied Aharonov-Bohm flux as that helps separate coherent and incoherent processes. Here, the reservoirs are explicitly shown as electron reservoirs with definite chemical potentials μ_γ, μ_α and μ_β. In a situation, wherein the probe β makes an actual contact with the sample we get a three probe setup and also the probe β is made like a voltage probe in the sense that its chemical potential is so adjusted that it does not draw any net current from or into the system. This setup is ideal for studying the celebrated Landauer-Büttiker three probe conductance given by [8]

$$\mathtt{G} = -\mathtt{G}_{\alpha\gamma} - \frac{\mathtt{G}_{\alpha\beta}\mathtt{G}_{\beta\gamma}}{\mathtt{G}_{\beta\alpha} + \mathtt{G}_{\beta\gamma}} \tag{6.16}$$

$$\text{Here,} \qquad \mathtt{G}_{\alpha\beta} = \frac{2e_0^2}{h}|s_{\alpha\beta}|^2 \quad \text{for} \quad \alpha \neq \beta \quad \text{etc.} \tag{6.17}$$

is the β to α conductannce. Eq.(6.16) can be rewritten in terms of the objects of the hierarchy of density of states (DOS) given as [8]

$$\mathtt{G} = \frac{2e_0^2}{h}\left(|s_{\alpha\gamma}|^2 - 4\pi^2|t|^2\rho_{lpd}(E,\alpha,\mathbf{r},\gamma) + 4\pi^2|t|^2\frac{\rho_e(\alpha,\mathbf{r})\rho_i(\mathbf{r},\gamma)}{\rho_{ld}(\mathbf{r})}\right) \tag{6.18}$$

So the three terminal formula of Eq.(6.16) is now restated in the form of Eq.(6.18). We will try to understand Eq.(6.18) when ρ_{lpd} is positive as that will naturally tell us what will happen if it is designed to be negative. Note that in the above formula if the lead β is completely removed then $|t|^2 = 0$ and we will be left with only the first of the three terms. This is the standard two probe Landauer conductance formula. The second term

comes with a negative sign and accounts for the loss of coherent electrons due to the lead β as can be concluded by comparing with the RHS of Eq.(6.2). This comparison tells us that when lead β make an actual contact then ν_β has no role and so in the three probe Landauer conductance formula, only the density of states (DOS) of the incoming lead matters. These lost coherent electrons would have escaped to the earthed lead in case of figure 6.2 but now they are not escaping, as β is not drawing any net current. Only those partial electrons, that are going from γ to α, coherently are targeted in both the cases and hence this term depend on Aharonov-Bohm flux in the same way as $|s_{\alpha\gamma}|^2$, reducing the overall flux dependence of $\mathtt{G}$ in Eq.(6.18). Note that Eq.(6.18) also suggests that while quantum mechanics is non-local, decoherence happens locally. Meaning an STM tip attached to point $\mathbf{r}$ gives the last two terms on the RHS of Eq.(6.18) that does not depend on any other point $\mathbf{r}'$.

The lost electrons are momentarily incoherent particles at the point $\mathbf{r}$ and eventually redistribute to γ and α. The question arises what will be the ratio of this redistribution and this will again be determined by the objects of the hierarchy of density of states. Redistribution contribution to $\mathtt{G}$ is the third term in Eq.(6.18) separately written below.

$$4\pi^2|t|^2\frac{\rho_e(\alpha,\mathbf{r})\rho_i(\mathbf{r},\gamma)}{\rho_{ld}(\mathbf{r})} \tag{6.19}$$

Note that this term, in Eq.(6.19), consists of the product of two separate probabilities associated with two independent processes. Each of the two separate processes are however coherent, that is one coherent process gives a $\rho_e(\alpha,\mathbf{r})$ and the other gives $\rho_i(\mathbf{r},\gamma)$. One is an emissivity from $\mathbf{r}$ to α and the other an injectivity from γ to $\mathbf{r}$. Essentially, a coherent current loss from γ to α via $\mathbf{r}$ is compensated by a gain due to two coherent terms, one from γ to $\mathbf{r}$ and the other from $\mathbf{r}$ to α, due to decoherence at the point $\mathbf{r}$. Hence the gain term and the loss term will be of opposite signs. To understand the denominator in Eq.(6.19) let us consider the following. Total number of incoherent electrons at the point $\mathbf{r}$ must be

$$4\pi^2|t|^2\frac{\rho_e(\alpha,\mathbf{r})\rho_i(\mathbf{r},\gamma)}{\rho_{ld}(\mathbf{r})}+4\pi^2|t|^2\frac{\rho_e(\gamma,\mathbf{r})\rho_i(\mathbf{r},\gamma)}{\rho_{ld}(\mathbf{r})} \tag{6.20}$$

Total number of incoherent electrons at the point $\mathbf{r}$

$$4\pi^2|t|^2\frac{\left(\rho_e(\alpha,\mathbf{r})+\rho_e(\gamma,\mathbf{r})\right)\rho_i(\mathbf{r},\gamma)}{\rho_{ld}(\mathbf{r})} \tag{6.21}$$

The first term in Eq.(6.20) is just the term in Eq.(6.19) and gives the fraction of incoherent electrons at $\mathbf{r}$ that goes to α and the second term is that which goes to γ. Which means Eq.(6.21) give the total incoherent electrons at the point $\mathbf{r}$ originating due to the loss of γ to α coherent electrons contributing to the 2nd term on the RHS of Eq.(6.18). Therefore,

in a situation when lead β is not drawing or delivering current, the quantity in Eq.(6.21) will be equal and opposite to the second term on the RHS of Eq.(6.18). This however is not a mathematical equality but an equality due to the balancing act of μ_β. The second term in Eq.(6.18) is independent of μ_β and the balancing act of μ_β make Eq.(6.21) equal to it. Given the fact that $\rho_e(\alpha, \mathbf{r}) + \rho_e(\gamma, \mathbf{r}) = \rho_{ld}(\mathbf{r})$, Eq.(6.21) is simply proportional to $\rho_i(\mathbf{r}, \gamma)$. Essentially the emissivity of the point $\mathbf{r}$ to all possible outgoing channels is the local density of states at the point $\mathbf{r}$. This $\rho_i(\mathbf{r}, \gamma)$ is the quantity that has to be balanced against the chemical potential of the lead β at all flux so that lead β does not draw or deliver any net current. This is a situation wherein we are at 0^oK and in the regime of incident energy E being such that $\mu_\gamma > E > \mu_\alpha$. In this regime, there is no injectivity from lead α and so only the injectivity of lead γ matters.

So if local partial density of states (ρ_{lpd}) is made negative then the RHS in Eq.(6.2) becomes positive implying the system draws in coherent electrons to the point $\mathbf{r}$ instead of loosing them. This can be also interpreted as loosing coherent electrons in reverse time. Thus, in that case, the lead β can enhance coherence. The same signature can also be seen from Eq.(6.18) which too can be experimentally verified. Also if the second term on the RHS in Eq.(6.18) becomes positive then $\rho_i(\mathbf{r}, \gamma)$ becomes negative which can be verified by the way one has to balance μ_β. A negative number of states accommodating negatively charged electrons can behave as a positive charge cloud. If it can attract one electron, it can also attract another electron and thus mediate an electron-electron attraction. We have thereby alternately justified Eqs.(6.2) and (6.18) purely from analyticity and topology of complex plane. Quantum mechanics is an axiomatic framework or a model that is artificially tuned to explain a variety of physical phenomenon. We can say from Goedel's incompleteness theorem that there can be some more facts and phenomena that can be physically seen in quantum systems but never pop up in the axiomatic framework. Therefore, it is not a surprize that ρ_{lpd} cannot be explained by quantum mechanics but is very much present in a quantum system. The reason why asymptotic solutions of the Schrödinger equation can be used to calculate ρ_{lpd}, is because after all the Hilbert space is isomorphic to the complex plane and has to respect the topology of the complex plane. Within the model, we can talk about precession of a spin or a small time-dependent potential on top of the static potential $U(\mathbf{r})$ [72], the outcome of something that we can calculate from the model has to respect the topology of the complex plane. We have also established that the equality in Eq.(6.2) and (6.18) will be approximate equalities. This work is published in [10, 11].

CHAPTER 7

TIME REVERSED STATES IN BARRIER TUNNELING

One of the most mysterious aspects of quantum physics is the existence of evanescent modes, which is situation in which a particle with energy less than the barrier height can tunnel through the barrier without a classical equivalent. While electromagnetic wave packets have mathematical analogies, but physical interpretations pose a searious challenge. One cannot create a wave packet with such evanescent states and therefore it is difficult to define propagation of the particle under the barrier. Tunneling time [73] is one of the elements of states under the barrier that have been studied as a result of this. Since a group velocity cannot be defined in the absence of a wave packet, solving the issue produced multiple conundrums [60]. It is challenging to interpret experiments when a suitable theory or formalism is absent [72]. Physical clocks such as the Larmor clock and Wigner delay time can be used to solve the problem, although doing so always resorts to semi-classical ideas like spin precession and stationary phase approximations [8, 9, 16]. The Feynman path approach has also been applied [72] and different approaches give different results. The Hartman effect-like phenomena [58, 59] show that a tunneling particle can come out of the barrier before entering it which raises questions about whether propagation occurs under the barrier at all. Here, we outline a scenario in which a theoretical experiment could be conducted to verify current resulting from evanescent modes and, thus, determine propagation under the barrier. It will also serve as a testing ground for physical clocks, such as the Larmor clock. Of course, one way to validate Larmor clock is to appeal to Burgers circuit and analyticity, which we have done. Even if one is unable to demonstrate the existence of current under the barrier solely by the application of quantum mechanics, there is no harm in providing an alternative validation by demonstrating that the measurable quantity may be created from the analyticity

of scattering matrix elements. We will utilise the setup outlined in the Section 7.1. We restrict ourselves to the most simple system of 1D rings due to the intricacy of physical interpretations. As previously stated in Chapter 3, the sample in the form of a 1D quantum ring does not represent a loss of generality. Experimentally, 1D rings may be produced with materials whose effective mass approximation works and lateral confinement [2]. Furthermore, it is possible to create finite thickness rings made up of numerous independent 1D channels. Multiple channels can exist in a finite thickness lead or ring, but the density of states (DOS) per channel is just the 1D density of states that can be obtained in an experiment using sub-band quantisation [32].

In Section 7.1, we provide an experimental setup of 1D quantum ring, to verify the existence of tunneling current under the barrier. In Section 7.2, we also discuss theoretical treatment of mesoscopic system with two alternate approaches. One is Larmor clock theory, and another is quantum mechanical theory. This section also formulates evanescent current expression and density of states from quantum mechanical theory which are consistent with Larmor clock theory. These consistencies is shown and discussed in Section 7.3.

7.1 The setup

We will first provide a simple description of the mesoscopic setup, and then discuss how this setup helps us address the problems discussed in the previous paragraph. The mesoscopic sample is taken to be a ring pierced by a magnetic flux Φ through the center of the ring such that there is no magnetic field on the electrons confined to the ring. The ring is usually made up of gold, copper, or semiconductors that can accommodate an electron gas. We are interested in the equilibrium response of this sample, which in this case is response to a magnetic field. There is a reservoir shown as a 3D block, which is a source of electrons at chemical potential μ and temperature T, making it a grand canonical system. The reservoir injects electrons to the sample or to the ring through a lead, as shown as region A. The ring can thus exchange electrons with the reservoir through the lead. This exchange does not result in a net current in the lead because electrons that go into the ring also come out of it and escape to the classical reservoir which is very typical of a voltage probe. The system, therefore, constitutes an equilibrium system where the reservoir also acts as a source of decoherence according to the Landauer-Büttiker formalism [44, 45, 46, 47, 48, 49]. The electrons in the lead and inside the ring are purely described by quantum mechanics. If the ring is isolated, then it will have some eigenfunctions and eigenenergies that were obtained from the Schrödinger equation and shown in figure 2.3 of [9]. But once connected to the reservoir, the states in the ring will be affected. They will no longer be eigenstates of the Hamiltonian and the

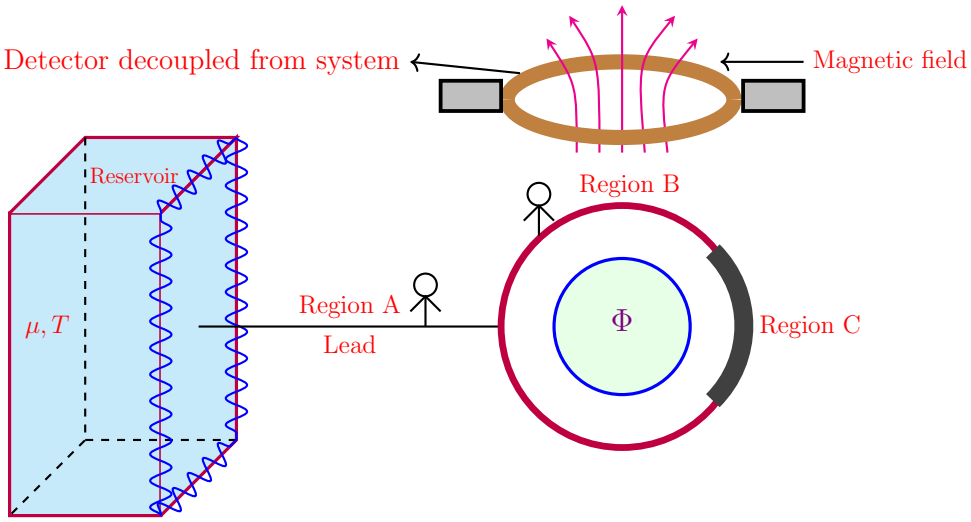

Figure 7.1: A typical mesoscopic grand canonical system is shown in equilibrium and described in detail in Section 7.2. The 3D block is electron reservoir with chemical potential μ and temperature T. The system is 1D quantum ring (pink colour) which is connected to 3D block or electron reservoir via lead. Lead is quanum wire. Aharonnov-Bohm (AB) flux Φ is applied at the center of the ring which is confined inside of the ring. It induces persistent current in the ring. The wide region C of the ring is shown with potential. This region C can be extended to all over the region of the ring or can be confiend in some part of the ring. The probability current in region B is well known in quantum mechanics textbooks but tunneling current ($E < e_0\, U$) for region C is unknown. In ring, we use quantum mechanical theory in order to derive current and density of states for tunneling region. One can measure this tunneling current using magneto devices placing much above from ring so that measurement devices cannot entangle with quantum ring. Theoretically, we use Larmor clock theory in region A or lead which uses analyticity of scattering matrix element (which is reflection in this case) and gives exactly the same result what we get from quantum mechanical theory.

eigenenergies will acquire some broadening due to life time related effects as the states can now leak into the reservoir. One can use a setup to control the broadening and recover the results obtained from the spectrum shown in figure 2.3. of [9]. The states in the lead is unaffected by the ring because it is an ideal 1D system with a typical DOS is given by $\frac{1}{hv_0}$. A part of the ring (region C) in figure 7.1 has a potential U that is shown as a thickened line. U can be so adjusted that an electron can tunnel through this region C. This region C can be extended to the entire ring wherein the entire ring can be made into a tunneling region. We know the Aharonov-Bohm flux can drive a persistent current in the ring and this current can thus be a tunneling current in part of the ring or in the entire ring. This allows us to extend the theoretical consistency of quantum currents to the tunneling regime. We have shown in Eq.(7.15) that one has to follow a different approach under the barrier using analytic continuity that does not lead to a straightforward probabilistic interpretation of quantum mechanical currents. When the barrier is located only in a part of the ring, then the persistent current in the ring can flow in a quantum state that is partly in the propagating regime (for example, in the region B in figure 7.1) and partly in the evanescent regime (for example, in the region C in figure 7.1). Consistency between them has to conserve the current at the point of

propagating to evanescent crossover at the junction between regions B and C, there being no puzzle about the current in region B. For resolving the puzzle of current in region C we have put forward an expression in Eq.(7.15) that follow from a different approach under the barrier using analytic continuity that does not lead to a straightforward probabilistic interpretation of quantum mechanical currents. Also such an analytic continuation does not preserve the structure of Hilbert space.

Apart from the consistency check, the primary advantage of theoretically studying such mesoscopic tunneling currents is that there are alternate theoretical formalisms in mesoscopic regime to verify the existence of currents inside the system under the barrier from propagating asymptotic states far from the barrier. That means there are theoretical cross checks for propagation under the barrier without studying the states under the barrier. Thus, observations and calculations on current under the barrier can help us support or eliminate ideas. In short, there are asymptotic states for the current carrying states in the ring and one can determine the current in the ring from these asymptotic states [74, 75], that is again similar to the Larmor clock. One can make the entire ring to be in the evanescent regime and the currents due to evanescent states has to be consistent with the asymptotic theory. A cartoon observer is shown in region A or lead of figure 7.1 and another cartoon observer is shown inside the ring. Observer A need not have any idea about the potential inside the ring. This observer does not know if the tunneling region extend over the entire ring or only a part of the ring. This observer only needs to know the infinitesimal change of $dU = \epsilon$, without any knowledge of U. He can measure the scattering phase shift (a theoretical measurement using analysis) in the wave function in the lead and from there infer the current inside the ring from the analyticity of the scattering matrix elements. Observer A can vary the incident energy and check the analyticity of scattering matrix elements from Eqs.(7.3) and (7.4). The observer B in the ring can extend or shrink the tunneling region and also determine the tunneling current from the analytic continuation of the internal wave function which is an unsettled issue in quantum mechanics. If the two measurements agree then the measurement by observer in the ring has to be theoretically correct.

In terms of practical measurements, there are problems associated with measuring tunneling currents in quantum mechanics and whatever we know about quantum measurements through an entanglement of sample states with the states of the detector do not apply for evanescent modes. One can also not measure tunneling currents classically as that will require the detector to be placed under the barrier and classical detectors can not work under the barrier. These problems can be avoided in the above described mesoscopic setup. Because such currents can also cause magnetisation that can be observed in a practical experiment for further validation. This magnetisation can be measured without disturbing the state in the system and thus not invoking the unresolved issues

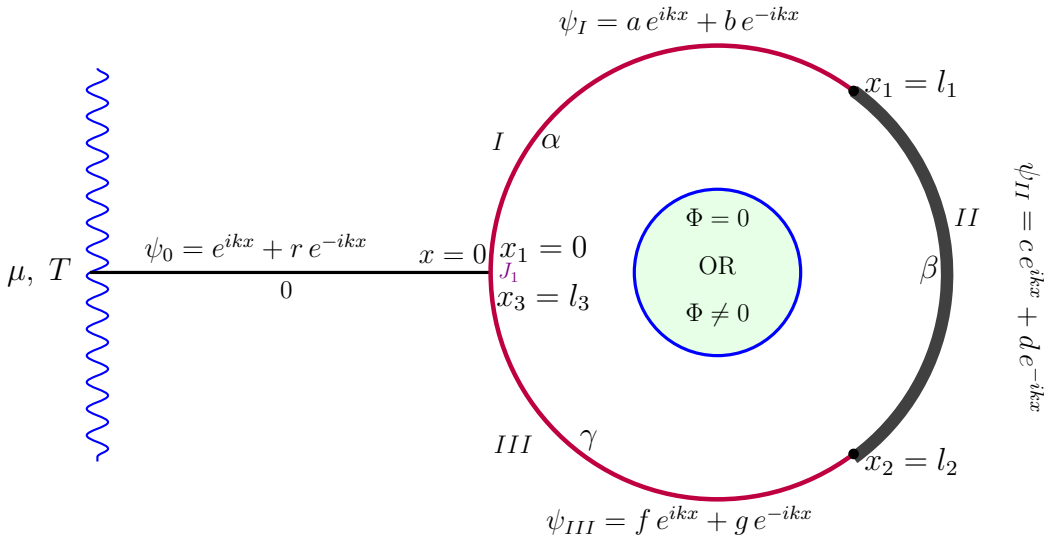

Figure 7.2: The same ring as in figure 7.1 is depicted here where the lead is shown by region 0, and one can clearly see three regions of length l_1, l_2 and l_3 marked inside the ring and called regions I, II and III respectively. The total length of the ring is $L = l_1 + l_2 + l_3$. The region II has a potential U and so this region is depicted by thick lines. Elsewhere the potential is zero. The ring is pierced by an Aharonov-Bohm (AB) flux Φ but the wave functions in the different regions is depicted for zero flux. For non-zero flux we will typically include the Aharonov-Bohm effect through the boundary conditions with the help of the parameters α, β and γ to be explained later. In this figure, α, β and γ are the AB phase for traversing region I, II and III, respectively. These phases appear in boundary conditions although the observable quantities like current can only depend on $\alpha + \beta + \gamma = \frac{2\pi\Phi}{\Phi_0} = \Phi'$ (say). The choice of coordinates with their origin is depicted in the figure. μ and T are the chemical potential and temperature of the reservoir, respectively.

of quantum measurement. In mesoscopic systems, electrons are quantum mechanical but fields are classical. We can measure the magnetisation due to the currents classically using hall magnetometers or squids remotely. This is why figure 7.1 shows a detector to measure magnetisation, placed above the ring. Thus, currents due to evanescent modes inside a ring can be measured non-invasively without encountering the above mentioned problems of quantum measurement. So it makes a lot of sense to study persistent currents due to evanescent modes inside the ring in the setup of figure 7.1.

7.2 Theoretical treatment

In figure 7.2, we redraw the system in figure 7.1 in order to depict the parameters used and the wave functions in the different regions for which the details can be seen in the figure caption. Here, the reservoir is shown as an irregular thick line on the left. Region A of figure 7.1 is called region 0 and the three regions in the ring are labelled I, II and III. The Schrödinger equation in 1D is

$$\frac{-\hbar^2}{2m_0}\frac{d^2\psi(x)}{dx^2} + U(x)\psi(x) = E\psi(x) \tag{7.1}$$

The solutions of Schrödinger equation in region 0 (or lead), region I, region II and region III of figure 7.2 give the wave functions in absence of magnetic field as

$$\psi_0 = \frac{1}{\sqrt{k}}(e^{ikx} + Re^{-ikx}) \tag{7.2}$$

$$\psi_I = \frac{1}{\sqrt{k}}(ae^{ikx_1} + be^{-ikx_1}) \tag{7.3}$$

$$\psi_{II} = \frac{1}{\sqrt{q}}(ce^{iqx_2} + de^{-iqx_2}) \tag{7.4}$$

$$\psi_{III} = \frac{1}{\sqrt{k}}(fe^{ikx_3} + ge^{-ikx_3}) \tag{7.5}$$

Here,

$$q = \left[\frac{2m_0}{\hbar^2}(E-U)\right]^{1/2} \quad \text{and} \quad k = \left[\frac{2m_0}{\hbar^2}E\right]^{1/2} \tag{7.6}$$

This kind of normalisation constants $\frac{1}{\sqrt{k}}$ and $\frac{1}{\sqrt{q}}$ are very special to mesoscopic systems. Differential current density for region I, without potential, will be (see Eq.(3.46))

$$dJ(k,\Phi) = \frac{e_0}{h}\left[|a|^2 - |b|^2\right] dE \tag{7.7}$$

If $E > e_0 U$, then the current in the system or in the region I, in the region II and in the region III will be given by $\frac{e_0\hbar}{m_0}(|a|^2-|b|^2)$, $\frac{e_0\hbar}{m_0}(|c|^2-|d|^2)$ and $\frac{e_0\hbar}{m_0}(|f|^2-|g|^2)$, respectively, and this follows from the standard definition of quantum mechanical current even in the presence of flux Φ. Continuity of current implies that they are all equal. In absence of flux a, c and f are the amplitude of clockwise moving electrons and b, d and g are the same amplitude of anticlockwise electrons and they can only differ by a relative phase because none of them is preferred over the other. So $(|a|^2 - |b|^2)$ is the difference between the number of electrons moving clockwise and those moving anticlockwise in region I and that constitutes a current. Flux breaks this symmetry so that $(|a|^2 - |b|^2)$ is the difference between the number of electrons moving clockwise and those moving anticlockwise in region I and that constitutes a current. This means that when Φ is zero then there is no current in the system as is expected for an equilibrium situation. However for $\Phi \neq 0$ the current is finite. It is an equilibrium current called persistent current, purely quantum mechanical current.

Here, we would like to note that an interesting situation occurs when $E < e_0 U$ in Eqs.(7.4) and (7.6). Then, the persistent current is carried by evanescent modes. In this situation, $q \to is$ and the expression for the current can be derived using the same scheme as before. Which means we substitute $q \longrightarrow is$ and from Eqs.(7.4) and (7.6), ψ_{II} and k become

$$\psi_{II} = \frac{1}{\sqrt{i\kappa}}(fe^{i(i\kappa)x_4} + ge^{-i(i\kappa)x_4}) \tag{7.8}$$

$$q = i\left[\frac{2m_0}{\hbar^2}(U-E)\right]^{1/2} = i\kappa \tag{7.9}$$

When $E < e_0\,U$, the probability current density in region II from Eq.(7.8) can be written as

$$J = \frac{e_0\hbar}{2m_0 i}\left[\psi_I^*\Delta\psi_I + \psi_{II}^*\Delta\psi_{II} - \text{hc}\right] \tag{7.10}$$

one can break this expression in two parts j_1 and j_2 of Eq.(7.10). Total current will be zero at $x_1 = 0$. j_1 is written as

$$\begin{aligned} j_1 =& \frac{1}{k}\left[(e^{ikx} + Re^{-ikx})^*\frac{d}{dx}(e^{ikx} + Re^{-ikx})\right]_{x=0^-} \\ &- \frac{1}{(is)}\left[(ae^{i(is)x} + be^{-i(is)x-i\alpha})^*\frac{d}{dx}(ae^{i(is)x} + be^{-i(is)x-i\alpha})\right]_{x_1=0^+} \\ &+ \frac{1}{(is)}\left[(ae^{i(is)x+i\alpha} + be^{-i(is)x})^*\frac{d}{dx}(ae^{i(is)x+i\alpha} + be^{-i(is)x})\right]_{x_3=l_3^-} \end{aligned}$$

The factor $\frac{e_0\hbar}{2m_0 i}$ can be added to expression later. For region II

$$-|a|^2 + a^*be^{-i\alpha} - b^*ae^{i\alpha} + |b|^2 \tag{7.11}$$

hc or j_2 can be written only for region II in figure 7.2 as

$$-|a|^2 + ab^*e^{i\alpha} - ba^*e^{-i\alpha} + |b|^2 \tag{7.12}$$

After subtracting the Eq.(7.11) from Eq.(7.12), the current expression for evanescent states will be with the factor $\frac{e_0\hbar}{2m_0 i}$ and, we get

$$J = \frac{e_0\hbar}{m_0 i}\left[ba^*e^{-i\alpha} - b^*ae^{i\alpha}\right] \tag{7.13}$$

$$\text{or} \quad J(k,\Phi) = \frac{e_0\hbar}{m_0 i}\left[dc^*e^{-i\Phi'} - cd^*e^{i\Phi'}\right] \tag{7.14}$$

Therefore differential current density in an interval dE will be

$$\begin{aligned} dJ(k,\Phi) &= \frac{e_0\hbar}{m_0 i}\left[dc^*e^{-i\Phi'} - cd^*e^{i\Phi'}\right]\frac{dn}{dE}dE \\ dJ(k,\Phi) &= \frac{e_0}{\hbar i}\left[dc^*e^{-i\Phi'} - cd^*e^{i\Phi'}\right]dE \end{aligned} \tag{7.15}$$

Where, $\Phi' = \frac{2\pi\Phi}{\Phi_o}$. Eq.(7.15) is far more complicated to be interpreted physically. Simple decoupling in terms of clockwise moving electron probability and anticlockwise moving

electron probability is not possible. Time reversed amplitudes c^* and d^* appear in the expression. Tunneling under the barrier has long been studied as an avenue for superluminality but conclusive results do not exist as discussed at the beginning of this section. Current expression with current conservation conclusively show that time reversed states have a role to play in the propagation. The factor $\frac{dn}{dE}$ can be removed completely in case one uses the normalisation constant given by Eq.(3.31) and normalisation constant is a freedom. We have so far used normalisation constant of $\frac{1}{\sqrt{k}}$ and an additional factor which is a square of $(\frac{2\pi m_0}{h^2})^{\frac{1}{2}}$ can be multiplied. Instead if we solved the scattering problem with a normalisation constant of unit incident flux then $\frac{dn}{dE} = \frac{1}{hv_0}$.

This current is therefore flowing in the ring and magnetising the ring. This magnetisation can be measured by the detector on top and hence can be also experimentally verified. Without resorting to a practical experiment, this current expression for evanescent modes can be subjected to several tests. Firstly, it satisfies current continuity at the junction of regions I and II or II and III (see figure 7.2). Secondly, an experimentalist can non-invasively measure and verify the numerical values of the current. As a third verification consider theoretically reducing the regions I and III to zero lengths, in which case the current and magnetisation will be entirely due to evanescent modes. Regions I and III being reduced to zero any magnetisation observed has to be purely due to current carried by evanescent modes. Such a magnetisation of an entire ring carrying current due to tunneling will prove propagation under the barrier. Without waiting for an experimentalist to measure and verify this there can be an independent theoretical verification which works only in the mesoscopic regime as has been elaborated. An observer in the lead can remotely calculate this current without even knowing if the regions I and III are reduced to zero length or they have a finite length. For that we have a novel expression for current derived in [74, 75] and stated below.

$$dJ(E,\Phi) = \frac{c}{\pi}\frac{\partial\theta_R}{\partial\Phi}dE = \frac{2e_0}{h}\frac{\partial\theta_R}{\partial\Phi'}dE \tag{7.16}$$

Where $dJ(E,\Phi)$ known to be differential current density within an energy interval dE keeping fixed value of Φ. Φ' is given by $\frac{2\pi\Phi}{\Phi_o}$. The quantity θ_R is the reflection (or scattering) phase shift, given by $\arctan[\frac{\mathrm{Im}(R)}{\mathrm{Re}(R)}]$, from the asymptotic wave function in lead far away from the 1D quantum ring. Measurable current is given by

$$I = \int_0^{k_f} dJ(k,\Phi) \tag{7.17}$$

and k_f is called as Fermi wave vector. Since our concern is what happens to tunneling electrons that seem to come out of the barrier before entering it, it makes sense to ask if there is density of states (DOS) under the barrier as well. Again standard approach is that this can be determined from internal wave functions as well as asymptotic wave

function. However, the internal wave function in tunneling regime is not consistent with the axioms of quantum mechanics because they cannot form a wave packet, they are not elements of Hilbert space, they are at most analytic continuation of wave functions above the barrier. On the other hand, the asymptotic wave function does not care if there is a state inside the ring or not and so if it gives the same value as that determined from analytic continuation of wave function inside the ring, it can only mean two things. First, tunneling electrons do propagate under the barrier and second, the asymptotic formalism settles a theoretical problem in the sense that analytical continuation implies physical continuation. So this is a theoretical experiment in the sense that what cannot be concluded from axioms of quantum mechanics can be concluded from the idea of a physical clock like Larmor clock. Of course, currents are a better candidate as they can also be measured in a practical experiment and they do support this point of view as will be plotted and shown below. Never the less, it does not harm to get further confirmation from density of states (DOS) because after all DOS is a far more valuable quantity than just the currents. It is linked to all thermodynamic properties and not just currents. Besides, current conservation ensures certain features that can be settled purely at a level of counting with numbers without caring for a theory. DOS cannot be directly measured like one can measure current from magnetisation, but is a much more complex concept connected to normalisation, renormalisation, regularisation etc, and if there is a scope to check purely theoretical consistency with the Larmor clock, that can be exploited by checking the following Eq.(7.20). For different systems in the propagating regime, we have already discussed that in Chapters 5 and 6. But now we have the DOS also leading to a current in the tunneling regime and current can be practically measured and so in our opinion worth studying in future very specifically. Usual wisdom is that currents are carried by quantum states and will qualitatively and quantitatively reflect the DOS. That is we expect using Eq.(7.8)

$$\text{DOS} = \int_0^{l_2} (ce^{-\kappa x_3} + de^{\kappa x_3})(c^* e^{-\kappa x_3} + d^* e^{\kappa x_3}) dx$$

l_2 is the length of region II.

$$\text{DOS} = \left[\frac{|c|^2}{2\kappa} \left[1 - e^{-2\kappa l_2}\right] + c\, d^*\, l_2 + d\, c^*\, l_2 + \frac{|d|^2}{2\kappa} \left[e^{2\kappa l_2} - 1\right] \right] \tag{7.18}$$

Eq.(7.18) is the expression of DOS for evanescent modes in absence of magnetic field. It can be written, in Eq.(7.19), in presence of magnetic field as well

$$\text{DOS} = \left[\frac{|c|^2}{2\kappa} \left[1 - e^{-2\kappa l_2}\right] + c\, d^*\, l_2\, e^{i\beta} + d\, c^*\, l_2\, e^{-i\beta} + \frac{|d|^2}{2\kappa} \left[e^{2\kappa l_2} - 1\right] \right] \tag{7.19}$$

DOS in terms of q, substitute $\kappa = -iq$ in Eq.(7.19), one gets

$$\frac{d\theta_R}{e_0 dU} = \pi\ \rho_d^u = \frac{m_0}{2\hbar^2\kappa}\left[\frac{|c|^2}{2\kappa}(1-e^{-2\kappa l_2}) + \frac{|d|^2}{2\kappa}(e^{2\kappa l_2}-1) + (c\ d^*\ l_2\ e^{i\Phi'} + d\ c^*\ l_2\ e^{-i\Phi'})\right] \tag{7.20}$$

Here, ρ_d^u is the DOS in region II under the barrier and hence the superscript u. The LHS giving the expression that can be obtained from asymptotic wave function, while the RHS is that obtained by integrating the local density of states (LDOS) from the analytic continuation of internal wave function. Let us first discuss the LHS of Eq.(7.20). Only for a constant potential of finite length, the integration in Eq.(4.24) can give a simple form as the LHS of Eq.(7.20). That the LHS of Eq.(7.20) will give $\pi\rho_d^u$ was generally established using Burgers circuit (BC). Now to check if there can be a state under the barrier, a constant potential is good enough. It is to be noted that the LHS, that is $\frac{d\theta_R}{e_0\, dU}$ expression for DOS do not explicitly use the tunneling wave functions because its derivation is independent of whether the states are tunneling or propagating in region II. When we match boundary conditions as in Eqs.(3.40) and (3.41) to calculate scattering phase shifts we can just say that we are working with wavelets (Fourier components) of a wave packet with a certain interpretation of probability and currents in quantum mechanics. For constant potentials, we do need the Schrödinger equation in order to establish a relation between incident energy E, asymptotic wave vector k and internal wave vector q. But now for the tunneling states it is unfair to say κ is the internal wave vector. So we would rather say that the LHS is a general formula for ρ_d^u that applies for any potential, derived from Burgers circuit using an infinitesimal change dU, without any knowledge of U. We can also say that θ_R has been calculated by assuming some kind of relation between k and κ that does not destroy the analyticity of θ_R. Besides, phase changes, or change in θ_R, is not determined by the exact relation between k and κ, but is rather determined by the phase singularities and the topology of the complex plane.

The RHS of Eq.(7.20) uses the solutions of Schrödinger equation explicitly, but analytically continued. The RHS expression consisting of 3 terms, in first brackets, are completely different for evanescent modes than that for propagating modes and has to be found by integrating the absolute value of analytically continued wave function in region II with appropriate normalisation constant. So the RHS of Eq.(7.20) is positive definite. Interestingly, the RHS of Eq.(7.20) giving DOS under the barrier has some negative terms signifying there are partial states under the barrier for which counting in real numbers (measure) can yield a negative answer. Noting that ρ_d^u is positive definite, and also $s = \left[\frac{2m_0}{\hbar^2}(U-E)\right]^{\frac{1}{2}}$ is positive, $[e^{2sl_2}-1] \geq 0$ and $[1-e^{-2sl_2}] \leq 0$ the remaining terms on RHS of Eq.(7.20) is also positive. Although the negative terms do not dominate over the positive terms, they do signify presence of processes back in time. However, there is no evidence that such processes can carry signal or information because for that we

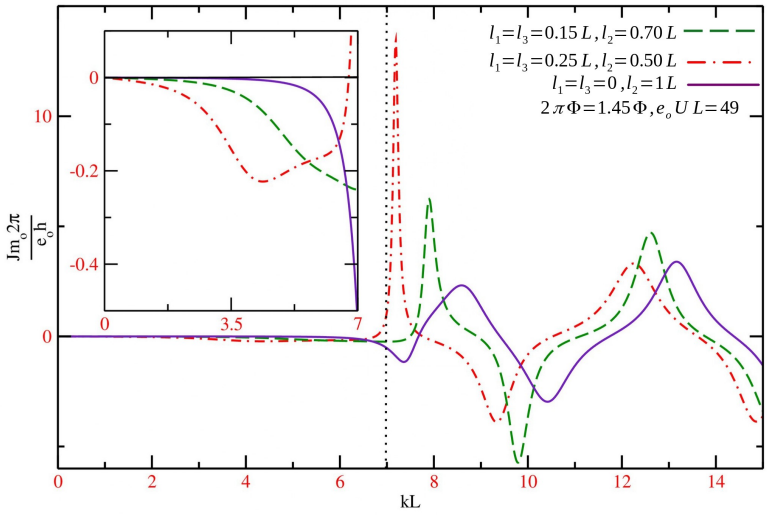

Figure 7.3: Plot of probability current density in region II as a function of wave vector kL as obtained from Eq.(7.15) for three different systems corresponding to different lengths of regions I, II and III for the system shown in figure 7.2. Current conservation implies that the current in region I and II will be the same. Current in region II has to be also obtained from Eq.(7.16) and it confirms this. The vertical dotted line at kL=7 give the crossover point for the parameters used in this figure wherein modes in region II change from evanescent to propagating. We have taken $\hbar = 1$ and $2m_0 = 1$.

need propagating wave packets. We have shown in chapter 6 in [9] that propagating wave packets can carry signal to the past using Fano resonances. Of course if we connect more leads to the ring being discussed now, then there may occur possibilities of transmission zeroes and Fano resonances and then these negative terms can manifest in some way. Below we will numerically check the equality in Eq.(7.20).

One may further say that there are states under the barrier given by Eq.(7.20) consisting of three terms in first brackets. But all three terms are not responsible for carrying current. Only the last term carries current as Eq.(7.15) confirms. An expression like e^{2sl_2} on RHS can grow indefinitely as l_2 is increased and to balance that the current carrying part of DOS that is $(cd^*l_2e^{i\Phi} + dc^*l_2e^{-i\Phi})$ become fewer and fewer. Current propagates only through these partial states. So if these partial states become fewer and fewer, then the electron takes lesser and lesser time to traverse the barrier. Only the electrons in these partial states show up in the Hartman effect but as these states do not constitute a propagating wave packet they cannot transmit a signal.

7.3 Results and discussions

We further proceed to demonstrate that Eq.(7.16) give the same current as Eq.(7.7) and that the equality claimed in Eq.(7.20) is true. As we have discussed in Chapter 3 that one can setup the boundary conditions that lead to a set of simultaneous equations, that can be solved to obtain R, a, b, c, d, f, and g of Eqs.(7.2) to (7.5). One lead is associated

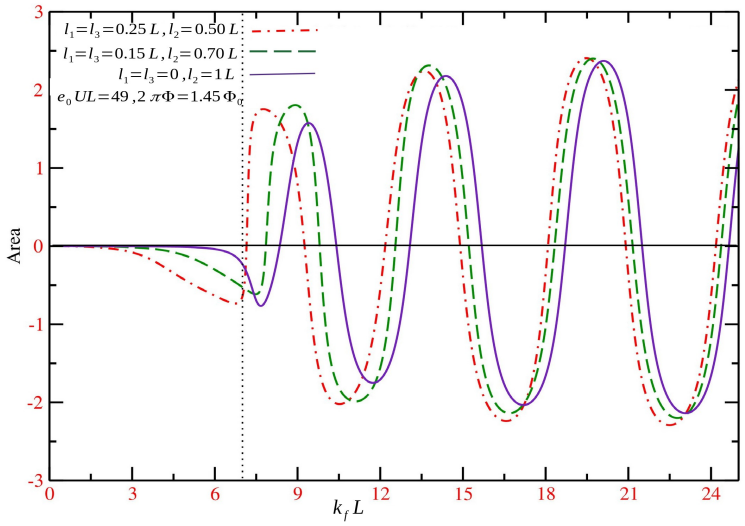

Figure 7.4: Plot of measurable current in region II as a function of Fermi wave vector k_fL as obtained from Eq.(7.17) for the same three different systems considered in figure 7.3. Again, upto $kL = 7$, we have evanescent modes. We have taken $\hbar = 1$ and $2m_0 = 1$.

with ideal 1D quantum ring in figure 7.2. We have derived the current expression and now we will plot current vs k for different set of values for l_1, l_2 and l_3 with fixed value of potential $U = 49$. For satisfying dimensions, we have written $e_0UL = 49$. The total sum (L) of l_1, l_2 and l_3 is 1. By varying these lengths one can see current due to fully or partially evanescent states. With increasing the value of incident energy from zero (or 0) upto $kL = 7$, we get evanescent current and after that you have propagation current. The dotted line in graph shows this. At $kL = 7$, there is no discontinuity that means curve is smooth. One can say, derived evanescent current expression is consistent with propagation current. In the figure 7.3, dot-dashed curve is plotted when $l_1 = l_3 = 0.25L$ and $l_2 = 0.50L$. Dashed curve is plotted when $l_1 = l_3 = 0.15L$ and $l_2 = 0.70L$. And third curve is plotted when $l_1 = l_3 = 0$ and $l_2 = 1$. Upto $kL = 7$, we have evanescent states since potential is $e_0UL = 49$. After $kL = 7$ we have propagation modes. These data are mentioned in figure one can verify. We have enlarged the evanescent states in the inset of figure.

This measurable current plot in figure 7.4 has something interesting about propagation and evanescent current. The length of region I and III is shrinked to zero keeping total length unchanged. For energy $E < e_0\ U$ current in the ring shows a smooth shift from paramagnetic to diamagnetic. The length of region is taken $l_2 = 0.5L$, then current in the ring changes from diamagnetic to paramagnetic at $kL = 6.68$ shown in the figure with dash-dotted curve. Now length of region II, l_2, is increased upto 0.7 then same transition happens at $kL = 7.47$ shown with dashed curve in figure. Now length of region II is increased upto 1, in this case crossover takes place at $kL = 7.67$ in the figure shown with solid line. In evanescent current there is only diamagnetic states no paramagnetic states.

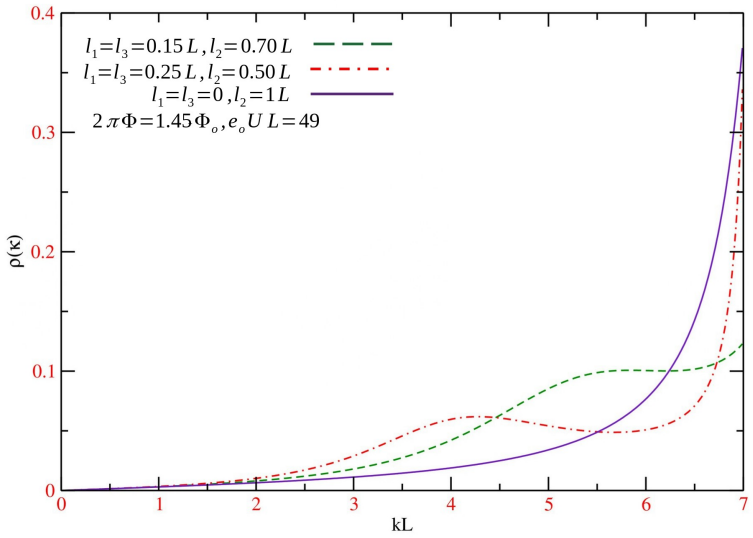

Figure 7.5: Plot of density of states (DOS) vs kL in region II only for the same set of parameter values used in figures 7.3 and 7.4. We have take $\hbar = 1$ and $2m_0 = 1$. One can verify each curve of DOS with the evanescent current curve in figure 7.3.

The property of transition from diamagnetic to paramagnetic current with oscillation is only for energy $E > e_0\ U$. For this regime of energy, we get propagation mode or current. Propagation current has the even odd parity effect but diamagnetic current has no parity effect. Parity effect implies that propagation current is carried by opposite states while evanescent current is carried by single type of state. Evanescent current has no nodes and no transition from diamagnetic to paramagnetic oscillations. Now one may interested in diamagnetic shift due to tunneling region with different scales. So there is no such effective diamagnetic shift after first peak of propagation current till $k_f L = 8.35$. But one can get higher value of energies for evanescent states in the ring which will also show a diamagnetic shift. Such higher energies evanescent modes are only possible with sub-bands due to lateral confinement as higher sub-bands have higher thresholds. This measured current shows comparable magnitude of current with propagation mode. For evanescent current magnitude is ≈ 1 while for propagation mode ≈ 2. It happens because in the presence of partial or full tunneling current is small in magnitude but always diamagnetic resulting in a large area under the curves. Propagating current states alters from paramagnetic to diamagnetic and has a lot of cancellation effect. Generally, response of evanescent states to external fields is stable against phase fluctuations while make them to find a device application.

For a clear picture we have also derived density of states (DOS) using analytical continuation in internal wave function and plotted DOS in figure 7.5 for evanescent states. RHS and LHS of Eq.(7.20) identical to each other for all the mentioned data in figure similar as current and observable plot. Again what plot we get with quantum mechanics approach for DOS, exactly same curve is also given by Larmor clock's approach. One can

look at the DOS curves for all data which show that when current is higher in magnitude under the barrier then DOS is also higher.

In summary, asymptotic theory works for current as well as DOS and has been also used to show that propagation under the barrier is a reality. Propagation under the barrier is not a well defined problem in quantum mechanics and so the asymptotic theory that goes beyond quantum mechanics, uses the idea of physical clocks and analyticity of scattering matrix elements help confirm this. This is referred to as a theoretical experiment but one can also make clean practical experiments to confirm this further. It also provides evidence that time reversed states have a role to play in propagation under the barrier. So there is a lot of merit in trying to address the question of propagation time and superluminality of tunneling particles. In Chapter 5, a signal can be sent back in time is discussed for propagation mode which requires construction of a wave packet. The problem of tunneling time although found to be more complicated, the asymptotic theory can be used to understand currents and thermodynamic properties.

CHAPTER 8

CONCLUSION

Recently, a novel development in mesoscopic physics is the possibility of realizing time travel with present day state of the art technology. It was theoretically shown that a time dependent quantum wave packet can be sent to the past. A proper experiment showing time travel is incomplete unless someone in the past has the technology to receive the signal. However, the principle of the possibility of time travel opens up many avenues of research and technology. In this thesis, we have considered some standard experimental setups that are regularly used in the laboratory and show that such setups can be used to indirectly test time travel or in other words consequences that follow from time travel. We also discuss theoretical experiments in the sense that we can get quantum mechanical results without using quantum mechanics. Although, these experimental setups are very successful in the laboratory, they do not address the issue of measurements which in this case turns out to be a quantum measurement. So in a third setup we show that the issue of quantum measurements can be bypassed to see indirect signatures of time travel.

The first two setups is a standard three probe setup wherein a steady state current flow from a cathode terminal to anode terminal. The third probe is used in two different ways. In the first case the third probe is earthed to intend carry away some of the current to the grounded neutral terminal. In the second case, the third terminal is used a voltage probe that does not carry away any current but still can reduce the coherent current from cathode to anode. So the third probe intends to create loss of coherent current, in the first case loss of actual current and in the second case loss of coherence. One of the primary signatures of evolution in forward time is loss or aging. If we fix parameters at which one can expect time travel then loss actually show up as a gain and coherent current increases.

In the third setup, we consider persistent currents in an open Aharonov-Bohm (AB) ring and argue that the setup can be used to create tunneling currents under the barrier.

Such tunneling currents have some intrinsic theoretical problems. We not only clarify these problems but also show that the theory of tunneling currents do signify processes back in time. Such tunneling persistent currents can be measured classically, thus bypassing the quantum measurement problem.

We covered sample fabrication technique for two-dimensional electron gas (2DEG) in Chapter 2. A detailed description on important fundamental key concepts like Aharonov-Bohm effect, Landauer's formula, importance of leads in mesoscopic systems, electronic wave functions, Feynman path approach, etc. is discussed for open mesoscopic systems in Chapter 3. With the axiomatic approach, we derived current expression for semi-infinite leads at zero and non-zero temperatures which is in accordance with Landauer's formalism. We further proceeded to provide an explicit description of local objects of the hierarchy which is derived by Larmor clock theory with the help of spin precession and Larmor frequency in Chapter 4. We showed that these local objects of hierarchy are observable quantities in quantum systems. We also found that lead indicies exhibit significant role in objects of hierarchy. In realsitic mesoscopic systems, Fano resonances are found frequently that is discussed in Chapter 5. In presence of Fano resonance, availability of local objects in quantum systems is explained with rigorous mathematical concepts in functional analysis such as Burgers circuit, loops and sub-loops in Argand diagram (AD), phase slip of scattering phase shift, etc. to re-interpret our results.

Hopefully, this thesis will give a major contribution for deeper understanding of this new area of mesoscopic world. Local entities can be determined in quantum systems without using axioms of quantum mechanics. As scattering phase shift of an electron can be measured in laboratory, all local objects of the hiearchy can be verified using experimental setups mentioned in this thesis. These local entities can also be negative which may further employ many applications as technological and theoretical perspectives of fundamental physics.

APPENDIX A

SCATTERING PROBLEM FOR Q-1D SYSTEM

Applying boundary conditions

In Section 5.2, I was discussing an analytical calculation of scattering for realistic system shown in figure 5.2. In this appendix, I will show some intermediate steps of this calculation. Due to symmetry of the system, in figure 5.2, applying boundary condition at one junction $x = a$ will give the result at another junction $x = -a$ as well. We apply boundary conditions in figure 5.2 at $x = a$ in Eq.(5.32). After substituting from Eq.(5.27) and Eq.(5.31) into Eq.(5.32), we get

$$\sum_{m=1}^{\infty} \sqrt{\frac{1}{k_m}} \left(\delta_{mm'}(-ik_m)e^{-ik_m a} - s^e_{mm'}(ik_m)e^{ik_m a} \right) \chi_m(y) = \sum_{n=1}^{\infty} c_n \frac{d\zeta^e_n(a,y)}{dx} \tag{A.1}$$

One has to first do the derivative and then substitute $x = a$. Using $\chi_m(y)$ from Eq.(5.15) we get

$$-i \sum_{m=1}^{\infty} \sqrt{\frac{2k_m}{b}} \left(\delta_{mm'} e^{-ik_m a} + s^e_{mm'} e^{ik_m a} \right) \sin \frac{m\pi}{b}(y + \frac{b}{2}) = \sum_{n=1}^{\infty} c_n \frac{d\zeta^e_n(a,y)}{dx} \tag{A.2}$$

Multiplying by $(\sqrt{\frac{2}{b}}) \sin \frac{m''\pi}{b}(y + \frac{b}{2})$ from the left on both sides, integrating and using

$$\int_{-\frac{b}{2}}^{\frac{b}{2}} \sin \frac{m''\pi}{b}(y + \frac{b}{2}) \sin \frac{m\pi}{b}(y + \frac{b}{2}) dy = \frac{b}{2} \delta_{m''m} \tag{A.3}$$

we get

$$-i\sum_{m=1}^{\infty}\sqrt{k_m}\left(\delta_{mm'}e^{-ik_m a}+s^e_{mm'}e^{ik_m a}\right)\delta_{m''m}=\sum_{n=1}^{\infty}c_n\sqrt{\frac{2}{b}}\int_{-\frac{b}{2}}^{\frac{b}{2}}\sin\frac{m''\pi}{b}(y+\frac{b}{2})\frac{d\zeta^e_n(a,y)}{dx}dy \tag{A.4}$$

$$\text{or}\quad -i\sqrt{k_{m''}}\left(\delta_{m''m'}e^{-ik_{m''}a}+s^e_{m''m'}e^{ik_{m''}a}\right)=\sum_{n=1}^{\infty}c_n\sqrt{\frac{2}{b}}\int_{-\frac{b}{2}}^{\frac{b}{2}}\sin\frac{m''\pi}{b}(y+\frac{b}{2})\frac{d\zeta^e_n(a,y)}{dx}dy \tag{A.5}$$

$$\text{Let }\sqrt{\frac{2}{b}}\int_{-\frac{b}{2}}^{\frac{b}{2}}\sin\frac{m''\pi}{b}(y+\frac{b}{2})\frac{d\zeta^e_n(a,y)}{dx}dy=F^e_{m''n}\sqrt{k_{m''}k_n} \tag{A.6}$$

Therefore,

$$-i\sqrt{k_{m''}}\left(\delta_{m''m'}e^{-ik_{m''}a}+s^e_{m''m'}e^{ik_{m''}a}\right)=\sum_{n=1}^{\infty}c_nF^e_{m''n}\sqrt{k_{m''}k_n} \tag{A.7}$$

Now we interchange the indices of the delta function only and change the dummy index on RHS as $n\to m$ as there is no m on LHS.

$$-i\sqrt{k_{m''}}\left(\delta_{m'm''}e^{-ik_{m''}a}+s^e_{m''m'}e^{ik_{m''}a}\right)=\sum_{m=1}^{\infty}c_mF^e_{m''m}\sqrt{k_{m''}k_m} \tag{A.8}$$

Now we apply another boundary condition to match wave functions at $x=a$, we have Eq.(5.35)

$$\psi^e_{m'}(x,y)|_{x=a}=\eta^e_{m'}(x,y)|_{x=a}$$

Substituting from Eqs.(5.27), (5.31), (5.15) into Eq.(5.35)

$$\sum_{m=1}^{\infty}\sqrt{\frac{2}{bk_m}}\left(\delta_{mm'}e^{-ik_m a}-s^e_{mm'}e^{ik_m a}\right)\sin\frac{m\pi}{b}(y+\frac{b}{2})=\sum_{n=1}^{\infty}c_n\zeta^e_n(a,y) \tag{A.9}$$

We multiply $(\sqrt{\frac{2}{b}})\sin\frac{m''\pi}{b}(y+\frac{b}{2})$ on both sides from the left and substitute

$$\zeta^e_n(a,y)=\sqrt{\frac{2}{b}}\sin\frac{n\pi}{b}(y+\frac{b}{2}) \tag{A.10}$$

because the internal and lead wave functions has to match on the dotted line at $x=a$ in

the figure 5.2. After this substitution we integrate both sides and use Eq.(A.3) to get

$$\sum_{m=1}^{\infty}\frac{2}{b\sqrt{k_m}}\left(\delta_{mm'}e^{-ik_m a}-s^e_{mm'}e^{ik_m a}\right)\frac{b}{2}\delta_{m''m}=\sum_{n=1}^{\infty}c_n(\frac{2}{b})(\frac{b}{2})\delta_{m''n} \tag{A.11}$$

or

$$\sum_{m=1}^{\infty}\frac{1}{\sqrt{k_m}}e^{-ik_m a}\delta_{m''m}\delta_{mm'}-\sum_{m=1}^{\infty}\frac{1}{\sqrt{k_m}}\delta_{m''m}s^e_{mm'}e^{ik_m a}=\sum_{n=1}^{\infty}c_n\delta_{m''n} \tag{A.12}$$

$$\text{or}\quad \frac{1}{\sqrt{k_{m''}}}e^{-ik_{m''}a}\delta_{m''m'}-\sum_{m=1}^{\infty}\frac{1}{\sqrt{k_m}}\delta_{m''m}s^e_{mm'}e^{ik_m a}=\sum_{n=1}^{\infty}c_n\delta_{m''n} \tag{A.13}$$

$$\text{or}\quad \frac{1}{\sqrt{k_{m''}}}\left(\delta_{m''m'}e^{-ik_{m''}a}-s^e_{m''m'}e^{ik_{m''}a}\right)=c_{m''} \tag{A.14}$$

Interchanging m'' and m' in the delta function only, in Eq.(A.14)

$$\frac{1}{\sqrt{k_{m''}}}\left(\delta_{m'm''}e^{-ik_{m''}a}-s^e_{m''m'}e^{ik_{m''}a}\right)=c_{m''} \tag{A.15}$$

From Eq.(A.15) with $m^{''}\rightarrow m$

$$\frac{1}{\sqrt{k_m}}\left(\delta_{m'm}e^{-ik_m a}-s^e_{mm'}e^{ik_m a}\right)=c_m \tag{A.16}$$

Substituting this c_m in Eq.(5.34) or (A.8)

$$\begin{aligned}&-i\sqrt{k_{m''}}\left(\delta_{m'm''}e^{-ik_{m''}a}+s^e_{m''m'}e^{ik_{m''}a}\right)\\ &=\sum_{m=1}^{\infty}\frac{1}{\sqrt{k_m}}\left(\delta_{m'm}e^{-ik_m a}-s^e_{mm'}e^{ik_m a}\right)F^e_{m''m}\sqrt{k_{m''}k_m}\end{aligned} \tag{A.17}$$

$$\text{or}\quad \sum_{m=1}^{\infty}(F^e_{m''m}-i\delta_{m''m})e^{ik_m a}s^e_{mm'}=F^e_{m''m'}e^{-ik_{m'}a}+i\delta_{m'm''}e^{-ik_{m''}a} \tag{A.18}$$

Note that the last term on the RHS is a diagonal term (with respect to symmetry) because of the Kronecker delta, there being no sum. So in this last term alone we can interchange m'' and m' and it still remains a diagonal term.

$$\sum_{m=1}^{\infty}(F^e_{m''m}-i\delta_{m''m})e^{ik_m a}s^e_{mm'}=F^e_{m''m'}e^{-ik_{m'}a}+i\delta_{m''m'}e^{-ik_{m'}a} \tag{A.19}$$

or, we get Eq.(5.36) from Eq.(A.19)

$$\sum_{m=1}^{\infty}\left(F^e_{m''m}-i\delta_{m''m}\right)e^{ik_m a}s^e_{mm'}=\left(F^e_{m''m'}+i\delta_{m''m'}\right)e^{-ik_{m'}a} \tag{A.20}$$

This is the equation that we have to solve to find $s^e_{mm'}$. Similarly we will get an equation for $s^o_{mm'}$. Multiplying identical terms on both sides of Eq.(5.36), we get

$$\sum_{n=1}\Big[(F^e-iI)^{-1}\Big]_{nm''}\sum_{m=1}^{\infty}(F^e_{m''m}-i\delta_{m''m})e^{ik_ma}s^e_{mm'} = \sum_{n=1}\Big[(F^e-iI)^{-1}\Big]_{nm''}(F^e_{m''m'}+i\delta_{m''m'})e^{-ik_{m'}a} \tag{A.21}$$

$$\text{or}\quad \sum_{nm}\Big[(F^e-iI)^{-1}\Big]_{nm''}(F^e_{m''m}-i\delta_{m''m})e^{ik_ma}s^e_{mm'} = \sum_{n}\Big[(F^e-iI)^{-1}\Big]_{nm''}\Big[F^e+iI\Big]_{m''m'}e^{-ik_{m'}a} \tag{A.22}$$

$$\text{or}\quad \sum_{nm}\Big[(F^e-iI)^{-1}\Big]_{nm''}\Big[F^e-iI\Big]_{m''m}e^{ik_ma}s^e_{mm'} = \sum_{n}\Big[(F^e-iI)^{-1}\Big]_{nm''}\Big[F^e+iI\Big]_{m''m'}e^{-ik_{m'}a} \tag{A.23}$$

Introducing a sum on both sides

$$\text{or}\quad \sum_{nm}\sum_{m''}\Big[(F^e-iI)^{-1}\Big]_{nm''}\Big[F^e-iI\Big]_{m''m}e^{ik_ma}s^e_{mm'} = \sum_{n}\sum_{m''}\Big[(F^e-iI)^{-1}\Big]_{nm''}\Big[F^e+iI\Big]_{m''m'}e^{-ik_{m'}a} \tag{A.24}$$

In quantum mechanics, a series can be seen as a limit of a finite sum and so we can talk of Eq.(5.36) as a matrix equation. In this particular case the series has a natural truncation because very high k_m values correspond to very high energy states that are not possible in condensed matter systems. The work function of a material provides a natural cut off. Since on LHS, after the sum over m'', we are multiplying matrix elements from two matrices that are inverse to each other, two matrix elements must multiply to give a 0 or a 1.

$$\sum_{nm}\delta_{nm}e^{ik_ma}s^e_{mm'} = \sum_{n}\sum_{m''}\Big[(F^e-iI)^{-1}\Big]_{nm''}\Big[F^e+iI\Big]_{m''m'}e^{-ik_{m'}a} \tag{A.25}$$

$$\text{or}\quad \sum_{n}e^{ik_na}s^e_{nm'} = \sum_{n}\sum_{m''}\Big[(F^e-iI)^{-1}\Big]_{nm''}\Big[F^e+iI\Big]_{m''m'}e^{-ik_{m'}a} \tag{A.26}$$

$$\text{or} \quad \sum_n e^{ik_n a} s^e_{nm'} = \sum_n \Big[(F^e - iI)^{-1}(F^e + iI)\Big]_{nm'} e^{-ik_{m'}a} \tag{A.27}$$

Since this is true for any arbitrary $k_n a$, we can remove the sum from both sides. We get Eq.(5.41)

$$e^{ik_n a} s^e_{nm'} = \Big[(F^e - iI)^{-1}(F^e + iI)\Big]_{nm'} e^{-ik_{m'}a} \tag{A.28}$$

$$\text{or} \quad s^e_{nm'} = e^{-ik_n a}\Big[(F^e - iI)^{-1}(F^e + iI)\Big]_{nm'} e^{-ik_{m'}a}$$

Binomial expansion

Now binomial expansion like procedure can be followed because the identity matrix commutes with any matrix.

$$\begin{aligned}
(F^e - iI)^{-1}(F^e + iI) =& \frac{1}{(F^e - iI)}(F^e + iI) = \frac{1}{i(-iF^e - I)} i(-iF^e + I) \\
&= \frac{1}{(-iF^e - I)}(-iF^e + I) = \frac{-1}{(I + iF^e)}(I - iF^e) \qquad \text{(A.29)} \\
&= -[1 - iF^e + (iF^e)^2 - (iF^e)^3 + ...](1 - iF^e) \\
&= [-1 + iF^e - (iF^e)^2 + (iF^e)^3 ..... \\
&+ iF^e - (iF^e)^2 + (iF^e)^3 - (iF^e)^4 + ...] \\
&= \Big[-1 + 2(iF^e) - 2(iF^e)^2 + 2(iF^e)^3 - 2(iF^e)^4 + ...\Big] \\
&= \Big[1 - 2\Big(1 - (iF^e) + (iF^e)^2 - (iF^e)^3 + (iF^e)^4 + ...\Big)\Big] \\
&= \Big[1 - 2(1 + iF^e)^{-1}\Big] \\
&= 1 - \frac{2}{(1 + iF^e)} = 1 - \frac{2}{i}\frac{1}{(-i + F^e)} \\
&= 1 - \frac{2}{i}(F^e - iI)^{-1} = 1 + 2i(F^e - iI)^{-1} \qquad \text{(A.30)}
\end{aligned}$$

Thus from Eqs.(A.29) and (A.30)

$$(F^e - iI)^{-1}(F^e + iI) = 1 + 2i(F^e - iI)^{-1} \tag{A.31}$$

Therefore from Eq.(5.39), where we drop the superscript e for convenience, which we will bring back after some simplification.

$$s_{nm'} = e^{-ik_n a}\Big[1 + 2i(F - iI)^{-1}\Big]_{nm'} e^{-ik_{m'}a} \tag{A.32}$$

A value

After Eq.(5.46), we continue our calculation. From Eq.(5.45)

$$\begin{bmatrix} F_{oo} - i1 & F_{oc} \\ F_{co} & F_{cc} - i1 \end{bmatrix} \begin{bmatrix} A & B \\ C & D \end{bmatrix} = \begin{bmatrix} 1 & 0 \\ 0 & 1 \end{bmatrix} \tag{A.33}$$

From Eq.(A.33)

$$(F_{oo} - i1)A + F_{oc}C = 1 \tag{A.34}$$

$$(F_{oo} - i1)B + F_{oc}D = 0 \tag{A.35}$$

$$F_{co}A + (F_{cc} - i1)C = 0 \tag{A.36}$$

$$F_{co}B + (F_{cc} - i1)D = 1 \tag{A.37}$$

Therefore from Eq.(A.36)

$$C = -[F_{cc} - iI]^{-1} F_{co}A \tag{A.38}$$

Putting the value of C from Eq.(A.38) into Eq.(A.34)

$$\Big[F_{oo} - iI\Big]A - F_{oc}\Big[F_{cc} - iI\Big]^{-1} F_{co}A = 1 \tag{A.39}$$

$$\text{or} \quad \left(\Big[F_{oo} - iI\Big] - F_{oc}\Big[F_{cc} - iI\Big]^{-1} F_{co}\right)A = 1 \tag{A.40}$$

We get Eq.(5.47)

$$A = \Big(F_{oo} - iI - F_{oc}(F_{cc} - iI)^{-1} F_{co}\Big)^{-1}$$

BIBLIOGRAPHY

[1] Gordon E. Moore, Electronics, **38**, 8 (1965).

[2] S. Datta, Electronic transport in mesoscopic systems, Cambridge University press, 1995, reprinted in 1999.

[3] B. J. van Wees et al. (1988), Phys. Rev. Lett. **60**, 848.

[4] D. A. Wharam, T. J. Thorton, R. Newbury, M. Pepper, H. Ahmed, J. E. F. Frost, D. G. Hasko, D. C. Peacock, D. A. Ritchie, and G. A. C. Jones. One-dimensional transport and the quantization of the ballistic resistance, J. Phys. C, 21:209, 1988.

[5] Imry, Y. (1986). Physics of mesoscopic systems, in: Grinstein, G., Mazenco, G. (eds.), Directions in Condensed Matter Physics (World Scientific, Singapore), pp. 101–163.

[6] Imry, Y. (1997). Introduction to Mesoscopic Physics (Oxford University Press, New York, Oxford).

[7] Aharonov, Y., & Bohm, D. (1959). "Significance of Electromagnetic Potentials in the Quantum Theory." Physical Review, 115(3), 485-491; R.A. Webb, S. Washburn, C. P. Umbach and R. B. Laibowitz. Observations of $\frac{h}{e}$ oscillations in normal metal rings. Phys. Rev. Lett. 24:2696, 1985.

[8] M. Buttiker, Time in quantum mechanics, pg 279 - 303,, Springer (2001).

[9] P. Singha Deo, mesoscopic route to time travel, Springer (2021).

[10] Kanchan Meena, P. Singha Deo Adv Theo Comp Phys 5, ISSN: 2639-010, 858 (2022).

[11] Kanchan Meena and P. Singha Deo, "Multiple manifestations of negative local partial density states", AIP Proceedings, DAE Symposium (2023) (Accepted).

[12] Kanchan Meena and P. Singha Deo, Physica E, **149**, 115680 (2023).

[13] K. Huang, Statistical physics, 3rd edition.

[14] Horacio M. Pastawski Phys. Rev. B, **46**, 4053 (1992).

[15] P. Singha Deo, Phys. Rev. B 53 15447 (1996).

[16] Eugene P. Wigner, Phys. Rev. B, **1** (1955).

[17] Landauer R, Martin Th. Rev Mod Phys 1994;66:217–28. and references therein.

[18] G. Iannaccone, Phys. Rev. B 51, 4727 (1995); G. Iannaccone and B. Pellegrini, Phys. Rev. B 53, 2020 (1996).

[19] A. I. Baz, Sov. J. Nucl. Phys. **4**, 182 (1967).

[20] V.F. Rybachenko, Sov. J. Nucl. Phys., **5**, 635 (1967).

[21] C. R. Leavens and G. C. Aers, Solid State Commun. 63, 1107 (1989); C. R. Leavens and G. C. Aers Phys. Rev. B 40, 5387-5400 (1989).

[22] M. Buttiker, Phys. Rev. B 27, 6178 (1983).

[23] M. Buttikker and R. Landauer, Phys. Rev. Lett. 49, 1739 (1982).

[24] M. Büttiker, J. Phys.: Condensed Matter 5, 9361 (1993); M. Büttiker, H. Thomas, and A. Prêtre, Z. Phys. B 94, 133 (1994); M. Büttiker, A. Prêtre and H. Thomas, Phys. Rev. Lett. 70, 4114 (1993);

[25] M. Büttiker, H. Thomas, and A. Prêtre, Phys. Lett. A 180, 364 (1993); V. Gasparian, T. Christen, and M. Büttiker, Phys. Rev. A 54, 4022 (1996);

[26] T. Gramespacher and M. Buttiker, Phys. Rev. B 56, 13026-13034 (1997); Phys. Rev. B 60, 2375-2390 (1999); Phys. Rev. B 61, 8125-8132 (2000).

[27] R. Schuter et al. (1997) Nature (London) 385, 417-420.

[28] Hu, Yayun; Liu, Haiwen; Jiang, Hua; Xie, X. C. (2017). "Numerical study of universal conductance fluctuations in three-dimensional topological semimetals". Physical Review B. 96 (13): 134201.

[29] K. Kobayashi, H. Aikawa, S. Katsumoto, Y. Iye, Phys. Rev. B 68 235304 (2003); K. Kobayashi, H. Aikawa, A. Sano, S. Katsumoto, Y. Iye, Phys. Rev. B 70 035319, (2004).

[30] E. Tekman and P. F. Bagwell, Phys. Rev. B **48**, 2553 (1993).

[31] W. Porod, Z. Shao, and C. S. Lent, Phys. Rev. B **48**, 8495 (1993).

[32] D. Mailly et al, (1993); B. Reulet et al, (1995); R. Deblock et al, (2002); L. Levy et al, (1990); R. Webb et al, (1985).

[33] P. Singha Deo and U. Satpathi, "Transmitting a signal in negative time", Results in Physics, 12 1506 (2019).

[34] U. Satpathi and P. Singha Deo, "Negative partial density of states in mesoscopic systems", Annals of physics, 375, 491 (2016).

[35] Kubo, Ryogo (1957) J. Phys. Soc. Jpn. 12 (6): 570–586.

[36] Friedel, J. (1952). "XXIII. Sum rule for the scattering of electrons by random configurations of impurities in a metal". Philosophical Magazine. 43 (341): 153–169.

[37] K. Van Klitzing, G. Dorda and M. Pepper, Phys. Rev. Lett 45, 494 (1980).

[38] K. Hirakawa, S. Komiyama, H. Sakaki, and Y. Toyozawa, "Quenching of Quantum Hall Resistance in InGaAs/InAlAs Heterostructures" Physical Review Letters (1985); A. M. Chang, L. N. Pfeiffer, and K. W. West, "Effect of Magnetic Field Quenching on the Quantum Hall Resistance" Physical Review Letters (1987); H. W. Jiang, C. E. Johnson, K. L. Wang, and S. T. Hannahs, "Quenching of the Quantum Hall Effect and Breakdown of the Law of Corresponding States" Physical Review Letters (1990).

[39] R. L. Willett, M. A. Paalanen, R. R. Ruel, K. W. West, and L. N. Pfeiffer, "Possible Observation of $\frac{\Phi_0}{2}$ Period Oscillations in GaAs/AlGaAs Heterostructures" Physical Review Letters, (1997); "Evidence for $\frac{\Phi_0}{2}$ R. L. Willett, R. R. Ruel, M. A. Paalanen, K. W. West, and L. N. Pfeiffer, "Period Oscillations in a Two-Dimensional Electron Gas" by R. L. Willett, R. R. Ruel, M. A. Paalanen, K. W. West, and L. N. Pfeiffer. Published in Physical Review Letters (1999).

[40] Yen, F.; Chen, X.; Wang, R. B.; Zhu, J. M.; Li, J.; Ma, G. T. (2013). "Induced Currents in Closed-Ended Type-II Superconducting Coils". IEEE Trans. Appl. Supercond. 23 (6): 8202005; "Measuring elusive "persistent current" that flows forever". R&D Daily. October 12, 2009.

[41] Akkermans, Eric; Montambaux, Gilles (2007). Mesoscopic Physics of Electrons and Photons. Cambridge University Press. ISBN 978-0-521-85512-9; Büttiker, M.; Imry, Y.; Landauer, R. (1983). "Josephson behaviour in small normal one-dimensional rings". Phys. Lett. A. 96 (7): 365.

[42] A. M. Jayannavar and P. Singha Deo, Phys. Rev. B **51**, 15 (1995).

[43] R. B. Laughlin, "Fractional Quantum Hall Effect: Experiments and Theory", Reviews of Modern Physics in 1983.

[44] Landauer, R. (1957) IBM Journal of Research and Development. 1 (3): 223–231.

[45] Landauer, R. (1970). Electrical resistance of disordered one-dimensional lattices, Phil. Mag. 21, pp. 863–867.

[46] Landauer, R. (1975). Residual Resistivity Dipoles, Z. Phys. B. 21, pp. 247–254.

[47] Büttiker, M. (1990). Scattering theory of thermal and excess noise in open conductors, Phys. Rev. Lett. 65, pp. 2901–2904.

[48] Büttiker, M. (1992). Scattering theory of current and intensity noise correlations in conductors and wave guides, Phys. Rev. B 46, pp. 12485–12507.

[49] Büttiker, M. (1993). Capacitance, admittance, and rectification properties of small conductors, J. Phys. Condensed Matter 5, pp. 9361–9378.

[50] Neil W. Ashcroft and N. David Mermin, Solid State Physics, 1975.

[51] Charles Kittel, Introduction to Solid State Physics, eighth edition, University of California, Berkeley.

[52] Büttiker, M. and Moskalets, M. (2010). From Anderson Localization to Mesoscopic Physics, in: Abrahams, E. (ed.), 50 Years of Anderson localization (World Scientific, Singapore), pp. 169–190.

[53] B.F. Bayman and C.J. Mehoke, Am. J. Phys. 51 (10) 875 (1983).

[54] P. Singha Deo, Phys. Rev. B 75, 235330 (2007).

[55] U. Satpathi and P. Singha Deo, IJMPB 26 1250028 (2012).

[56] O. Kalman, P. Foldi, M.G. Benedict, F.M. Peeters, Physica E 40 567 (2008).

[57] P.F. Bagwell Phys. Rev. B 41 10354 (1991).

[58] T.E. Hartman, J. Appl. Phys. 33 3427 (1962).

[59] T.E. Hartman, J. Appl. Phys. 33 (1962) 3427; J.R. Fletcher, J. Phys. C 18 (1985) L55; V.S. Olkhovsky, E. Recami, Phys. Rep. 214 (1992) 339.

[60] S. Bandopadhyay, A.M. Jayannavar, arXiv:quant-ph/0411161 (2004) and references therein.

[61] A. F. Hebard and M. A. Paalanen, "Electrical and thermal transport in strongly disordered superconductors," Physical Review Letters, vol. 65, no. 7, pp. 927-930, (1990); A. A. Abrikosov and L. P. Gor'kov, "Superconducting alloys at high-resistance impurities," Soviet Physics JETP, vol. 12, no. 6, pp. 1243-1253, (1961).

[62] G. Bonneau et al, Am. J. Phys 69, 322 (2001).

[63] M. Buttiker, Phys. Rev. B 32, 1846(R), (1985).

[64] S. Mukherjee Deo, M. Manninen and P. Singha Deo Physica E 44, 62 (2011).

[65] Hendrik Bluhm, Nicholas C. Koshnick, Julie A. Bert, Martin E. Huber, and Kathryn A. Moler, PRL 102, 136802 (2009).

[66] Mahan, G. D. "Many-Particle Physics", Springer (2000).

[67] Kanchan Meena, P. Singha Deo, and A. M. Jayannvar, "Mesoscopic response: semiclassical versus quantum mechanics", Submitted to ArXiv (2021).

[68] S. Bandhopadhyay and P.S. Deo, Phys. Rev. B **68**, 113301 (2003).

[69] P. Singha Deo, B. C. Gupta, A. M. Jayannavar and F. M. Peeters, Phys. Rev. B, **58**, 10784 (1998).

[70] C.R. Leavens and G.C. Aers, Phys. Rev. B 39, 1202 (1989).

[71] Berry, M. V., J. Mod. Opt. 45, 1845-1858 (1998).

[72] R. Landauer and T. Martin, Rev. Mod. Phys. **66**, 217-228 (1994).

[73] E. Hauge and J. Stovneng, Tunneling times: a critical review, Reviews of Modern Physics **61**, 917 (1989); S. Yusofsani and M. Kolesik, Quantum tunneling time: Insights from an exactly solvable model, Physical Review A **101**, 052121 (2020); D. Sokolovski and E. Akhmatskaya, No time at the end of tunnel, Communications Physics **1**, 1 (2018); G. Muga, R. S. Mayato, and I. Egusquiza, Time in quantum mechanics, Vol. 734 (Springer Science and Business Media, (2007); R. Brunetti, K. Fredenhagen, and M. Hoge, Time in quantum physics: from an external parameter to an intrinsic observable, Foundations of Physics **40**,1368 (2010); D. Sokolovski and E. Akhmatskaya, Tunneling times, Larmor clock, and the elephant in the room, Scientific Reports **11**, 1 (2021); T. Rivlin, E. Pollak, and R. S. Dumont, Determination of the tunneling flight time as the reflected phase time, Physica Review A **103**, 012225 (2021); R. S. Dumont, T. Rivlin, and E. Pollak, The relativistic tunneling flight time may be superluminal, but it does not imply superluminal signaling, New Journal of Physics **22**, 093060 (2020); A. Hernandez-Maldonado, J. Villavicencio, and A. Hernandez-Avina, Delay time and persistent oscillations for a shifted quantum shutter, Physica Scripta **96**, 055213 (2021); D. C. Spierings and A. M. Steinberg, Tunneling takes less time when it's less probable, arXiv preprint arXiv:2101.12309 (2021).

[74] E. Akkermans, A. Auerbach, J. E. Avron, and B. Shapiro, Phys. Rev. Lett. 66, 76 (1991).

[75] Pier A. Mello, Physical review B, **47**, 24 (1993).